Lancaster Environment Centre | Lancaster University

Mitigation and Control of Urban Air Pollution in Beijing

Tabish Umar Ansari
Lancaster Environment Centre
Lancaster University, UK
March 2020

This thesis is submitted to Lancaster University in partial fulfilment of the requirements for the degree of Doctor of Philosophy. It is the work of the author, except where otherwise stated. Excerpts of this thesis have been published in journals, as indicated within.

Abstract

Outdoor air pollution kills more than 4 million people around the world per year and heavy pollution episodes continue to occur especially around large urban centres. In addition to long-term mitigation strategies, short-term emission controls are needed to prevent heavy pollution episodes in megacities such as Beijing. Such controls have been implemented with reasonable success in the past, notably during mega-events, but need to be carefully evaluated to develop a robust mitigation strategy for future. In this work, the 10-day long controls implemented before the APEC summit in Beijing during November 2014 were evaluated for their effectiveness using an online atmospheric chemical transport model WRF-Chem. The controls were found to be only partly responsible for the improvement in air quality during the summit period, while the rest of the improvement was due to favourable meteorology which reduced pollutant levels significantly as compared to the levels before the control period. The controls were found to be insufficient in meeting national air quality standards if applied during periods with more stagnant conditions.

Sensitivity studies were performed to identify temporally-resolved source contributions from various sectors and regions. It was found that controls on local emissions benefit air quality on the same day, controls on regional emissions show peak benefits a day or two after the start of controls and controls on distant emissions show peak benefits three to four days later. Local and regional residential and industry sectors were found to dominate contributions to $PM_{2.5}$ levels in Beijing. A Gaussian statistical technique was used to replace the model behaviour over Beijing with a fast emulator to generate concentration response surfaces for emission reductions across various sectors and regions. These results were utilized to develop an optimal policy for short-term emission controls in Beijing and were implemented in an automatic air quality forecasting and emission prescription system

which runs the model successively with reduced emissions to meet daily air quality targets and outputs the magnitude and timing of controls needed across various sectors and regions to prevent heavy pollution episodes in Beijing. This is a novel application of the popular method called Model Predictive Control often used in the petrochemical industry, to air quality modelling. The framework developed here is for Beijing but can be readily adopted for any other polluted region of the world.

Quote

"Jhonka hawa ka aaj bhi,

zulfein udaata hoga na."

(The gust of wind, even today, must be blowing your hair.)

- Mehboob

Dedication

Dedicated to my late maternal uncle Mohd. Zafar (Zafar Mamu) who, in my childhood, often dropped me off at school on his motorcycle.

Acknowledgements

I want to thank my supervisor Prof. Oliver Wild for his engaged guidance throughout the four years of my PhD studies. We had a total of 173 weekly meetings and exchanged countless emails to shape the work in its current form.

I remain extremely grateful to the Lancaster Environment Centre for financially supporting an overseas student like me with a generous scholarship to carry out PhD in the UK; I'm fully aware that such non-EU international scholarships are rare.

I thank Dr. Edmund Ryan, a former postdoc in our group, now at the University of Manchester, for his help with statistical emulation used in my work. I thank Dr. Doug Lowe of the University of Manchester for his suggestions and recommendations on using the WRF-Chem model.

I thank my thesis appraisal committee members: Dr. Kirsti Ashworth and Dr. Andy Jarvis for keeping me on my toes especially in the final year of my PhD.

I thank my friends Ramin Raeesi and Amer Reza for all the daytrips, hikes, outings, laughter and fun which provided me crucial support in a foreign country and kept me going. I thank Yogang Singh, my friend from IIT Madras, who was in Plymouth for most of my time in Lancaster, for being just a phone call away.

Thanks to my family: Mummy, Papa and Bhaiya for just being there.

Thank you to Agata, for her unwavering belief in me.

Contents

List of Figures

List of Tables

CHAPTER 1

Introduction

Air pollution is a major global environmental problem which is responsible for premature deaths, illness and loss of quality of life for millions of people around the world. It is characterised by high concentrations of pollutants in the air which occur when emission rates exceed the natural assimilative and cleansing capacity of the atmosphere.

In order to support an ever-growing population of 7.7 billion people in terms of food, transport, electricity, and other services, the modern industrial economy primarily relies on burning of fossil fuels such as coal, oil and natural gas. Developing countries in Asia and Africa also rely on solid biofuels like wood and animal waste which are even more polluting than oil and gas. Fossil fuel burning from industrial use, power production, vehicles and household cooking and heating emits harmful pollutants such as carbon dioxide, ozone, carbon monoxide, nitrogen oxides, sulfur oxides, volatile organic compounds and particulate matter. Increasing use of fertilizers in farmlands to achieve higher agricultural productivity in order to feed a growing population emits pollutants such as ammonia which is also a precursor for particulates. These pollutants often exceed safe levels prescribed by the World Health Organization and national governments. Apart from adverse effects on human health, air pollution also damages plant health and reduces crop productivity. High levels of particulate matter reduce visibility, often causing road accidents and delaying trains and flights, and play an important role in climate by modulating regional temperature and precipitation.

Instances of heavy urban smog and acid rain were common in the developed world in the mid-twentieth century. Heavy smog episodes were reported in cities like London and Los

Angeles in the 1950s that claimed many lives. Widespread acid rain in the 1970s led to the acidification of soil, water and forests, harming fragile ecosystems. While emissions of key pollutants have significantly decreased in the developed world in the last few decades, they have had an increasing trend in the developing world, especially Asia. This is because in the last few decades the developed world (North America and Western Europe) transitioned into a cleaner services-based economy (real-estate, banking, finance and insurance, health and social care, information technology and tourism) which consumes little fossil fuel while a large part of the fuel-intensive manufacturing industries shifted to eastern countries like China, South Korea and Taiwan. Since Asia is home to a larger population than the developed world, increasing pollution in this region has increased net per capita exposure to pollutants and led to a total increase in the number of deaths due to outdoor air pollution globally. Therefore there is an acute need to mitigate air pollution, esp. in Asia which adversely affects large populations.

There are a number of ways to reduce human exposure to air pollution including, installation of green infrastructures which may trap or absorb pollutants; moving emission sources away from large population centres; and most importantly, reducing emissions. Reducing emissions without reducing economic growth and production is a long-term transition process which involves technology upgrades in industries and vehicles, along with gradual phasing-out of dirty fossil fuels in exchange of higher grade fossil fuels and cleaner energy alternatives such as wind, solar and nuclear.

Even as these long-term emission reduction strategies are in place, severe pollutant episodes continue to occur frequently, especially in winter months across Asia. Emergency emission-cuts are required in the short-term to prevent air pollution from reaching hazardous levels. Such emergency measures reduce emissions at the expense of economic growth and production for a few days for the sake of human health and well-being. These measures include, limiting industrial production or completely shutting down factories, limiting vehicle use through license plate rules, temporary shutdown of coal- and gas-fired power plants, ban on construction activities, and ban on residential combustion. Such short-term strategies have been tested in many cities, for example traffic restrictions in Paris, Delhi and Beijing.

While the spatial influence of air pollution can be regional (up to hundreds of kilometers), the biggest problems are often concentrated over urban centres, home to large populations and most emission sources. Most vehicular and residential pollution originates from urban centres. Industries and power plants are also generally located near cities. Therefore cities often become the focus of short-term air pollution control efforts.

Current emission control policies to reduce air pollution in the short-term are *ad-hoc* and leave a lot to be desired. Repeating successful short-term control policies of the past does not promise prevention of future episodes. This is because air pollution is strongly controlled by meteorology, and the same meteorology is not guaranteed for all future pollution episodes. Therefore a more modular approach which takes a range of possible meteorological conditions of the region into account is needed.

Atmospheric simulations by means of mathematical models are a great way to assess past emission control policies and prescribe robust control policies for the future. Recent advancements in computational resources and availability of ground-based measurements as well as satellite observations have led to significant improvement in scientific understanding of physical and chemical processes governing air pollution. Sophisticated *science-based* mathematical models of the atmosphere that represent these detailed processes and simulate transport and evolution of pollutants, can be used on conjunction with *data-based* statistical and machine learning techniques to devise tailor made short-term emission control strategies. Such episode-specific policies can guarantee successful abatement of pollution episodes of varying intensities, for a range of different weather conditions.

In this work I explore the possibilities of improving short-term emission controls in the megacity of Beijing, China. Beijing is an ideal city for this kind of study due to its high pollution levels and a very large human exposure as well as the availability of good quality emissions data and ground-based observations which allow accurate modelling of formation and evolution of pollution episodes and evaluation of past emission control policies.

The aims and objectives of this work are: to configure and thoroughly evaluate a state-of-the-art atmospheric chemical transport model for China with a focus on Beijing laying out the strengths and weaknesses of the model in its ability to reproduce real-world atmospheric environment over the study region; simulate a previous emission control period and understand the effectiveness of the short-term emission control policy in context of meteorological conditions and implications for future; to lay out the scope of improvement in existing short-term emission control policies in terms of emission sectors, regions and timing of control by studying source contributions to pollution in Beijing, with a focus on $PM_{2.5}$; to build a reduced-form model trained on the chemical transport model output with the help of statistical techniques; to produce emission-concentration contour plots (response-surfaces) which serve as a quick decision making tool for policymakers in varied weather conditions; to develop an emissions toolkit which generates anthropogenic emissions for the study region based on the user input scalings for various sectors and regions; and create an automatic model running framework with dynamic emissions scaling where

the model is run successively with reduced emissions for each day based on consultation with the response-surfaces until daily healthy air quality standards are met, finally prescribing specific sectoral and regional controls required over the period–all without user intervention.

This thesis is organised into six chapters. Chapter 2 provides a general background on air pollution, air pollution in China and Beijing, and air quality modelling techniques. I use the Weather Research and Forecasting–Chemistry (WRF-Chem) modelling tool for my studies. Chapter 3 describes the model set-up and evaluation and discusses emission controls during the 2014 Asia-Pacific Economic Cooperation (APEC) summit as a case study. Chapter 4 presents sensitivity analysis of different emission sectors and regions to understand source contributions, discusses the lingering effects on 1-day emission cuts on subsequent days, and presents easy-to-use emission-concentration contour plots (response-surfaces) derived from statistical emulation of the science-based model output. Chapter 5 presents dynamic emissions control model runs with automatic iterative emissions scaling based on predicted pollution level guided by response-surfaces, to meet daily healthy air quality targets. Chapter 6 summarises the work and presents the conclusions.

CHAPTER 2

Background and Literature Review

2.1 Air pollution and its sources

Air pollution profoundly impacts human health, visibility, the ecosystem, the weather, and climate (IPCC 2013). Pollutants from both outdoor and indoor sources represent the single largest environmental risk to health globally. As per recent estimates 9 out of 10 people in the world breathe air containing high levels of pollutants (WHO 2016).

The atmosphere is the recipient of many of the products of our technological society (Seinfeld & Pandis 2006). Common air pollutants include trace gases such as carbon dioxide (CO_2), ozone (O_3), carbon monoxide (CO), nitrogen oxides (NO_X), sulfur oxides (SO_X), ammonia (NH_3) and millions of volatile organic compounds (VOCs), and particulate matter (PM) or aerosol which comprises organic and black carbon, sulfates, nitrates, ammonium and chloride salts. Metals such as lead (Pb) and mercury (Hg) may also be present as particulates.

Air pollution primarily arises from combustion processes and evaporation of industrial solvents. Common anthropogenic sources include coal- and gas-powered power stations, manufacturing industries (factories), vehicles, residential cooking, and traditional biomass (wood, dung, crop and waste) burning which involve combustion of fossil fuels. Industrial production of synthetic chemicals such as paint, hair spray, varnish, aerosol sprays is another major source of air pollution esp. volatile organic compounds (VOCs). Fertilized farmlands are a major source of NH_3 and NO_X. Natural sources of air pollution include desert dust, livestock (emits methane), wildfires (CO and PM), and volcanic activity (sul-

phur, chlorine and PM).

Air pollutants can either be *primary* which are directly emitted into the atmosphere, e.g., CO, NO_X, SO_X, NH_3, black carbon etc. or *secondary* which are not directly emitted but formed away from the emission sources as a result of complex chemical reactions of directly emitted species (precursors) in the atmosphere, e.g., tropospheric ozone and secondary aerosols. A significant fraction of aerosols are formed from gaseous precursors and exist in a kinetic and thermodynamic equilibrium with them.

2.2 Urban air pollution: history and status

Big cities have historically been at the receiving end of the worst effects of air pollution. Records exist about health impacts of air pollution in ancient Rome (Hippocratic Corpus, Epistulae Morales CIV) which may have had a population over one million (Brimblecombe et al. 1998). Air pollution surged during the industrial revolution in major European cities with widespread combustion of wood and coal. The first recorded modern smog episode occurred in the Meuse valley in Belgium during 1st–5th December 1930 which led to more than 63 deaths (Firket 1931). Los Angeles had 1 million vehicles as early as in 1940 which doubled to 2 million by 1950 in a post-war booming population and economy. The city experienced many smog episodes in the summer months of the 1940s and 1950s with very high levels of PM and ozone. Major federal, state, and local regulations on vehicle emission control were put in place to control urban smog in Los Angeles (Parrish et al. 2011). The Great Fog of London, 5^{th}–8^{th} December, 1952 was one of the first widely recognised smog episode which resulted from coal burning of domestic heating and power generation and led to extremely high levels of particulate matter and SO_2 (more than 1000 times the safe levels recommended today), resulting in over 4000 premature deaths and 10000 illnesses (Brimblecombe 2006) and its persisting effects caused about 12000 excess deaths by February 1953 (Bell & Davis 2001). The London smog was a classical or sulphurous smog characterised by high levels of SO_2 caused by burning of sulfur-rich fossil fuels, particularly coal. On the other hand, the Los Angeles smog was a photochemical smog caused due to high levels of NO_2 and VOCs in the presence of sunlight (something not very common in London!). The occurrence of these two distinct smogs in two different cities of the world highlights the different sources and chemistry of air pollution.

Much has changed today, at least in the developed world–residential heating in major cities has become centralised, through electricity, and industries have moved far away from city centres which are now generally filled with a dense fleet of vehicles. However,

the modern industrial economy is still powered by coal, oil and gas, which inevitably produce harmful byproducts on burning. Urban air pollution remains one of the greatest environmental challenges facing mankind in the 21st century (WHO 2016, Zhang et al. 2015c). Today, urban air pollutants consist of a complex combination of gases and fine particulate matter, $PM_{2.5}$ (particles with the aerodynamic diameter smaller than 2.5 µm) emanating from vehicles, residential cooking, coal-fired power stations and factories among other sources.

Air pollution affects people in middle-income countries, with fuel-intensive economies, at a much higher rate than those in high-income countries with mature service-based economies. In the recent past, many developing countries, such as China and India, have experienced severe air pollution because of their fast-developing economy and urbanization. Globally, the urbanization trend is projected to continue: 70% of the world population will reside in urban centers by 2050, and there will exist 41 megacities (cities with more than 10 million inhabitants) by 2030 (Zhang et al. 2015c). Many of the world's megacities exceed WHO's guideline levels for air quality by more than five times, representing a major risk to people's health. WHO air quality recommendations call for countries to reduce annual mean values of air pollution to 20 $\mu g\,m^{-3}$ for PM_{10} and 10 $\mu g\,m^{-3}$ for $PM_{2.5}$.

Countries are taking measures to reduce air pollution from particulate matter. For example, the annual median exposure to ambient $PM_{2.5}$ in China was 48.8 $\mu g\,m^{-3}$ in 2016—a 17% reduction from the estimate for 2012, but still almost five times higher than WHO recommendations (Zheng et al. 2018, Cheng et al. 2018). Governments are increasing commitments to monitor and reduce air pollution. The estimated number of air pollution deaths in the region has come down from 2.8 million in 2012 to 2.2 million in 2016 (WHO 2016).

2.3 Health impacts and standards

Polluted air was responsible for 8 million deaths worldwide in 2016: 3.8 million from household air pollution and 4.2 million from ambient air pollution (burden of disease 2016, WHO 2016). Polluted air penetrates deep into their lungs and cardiovascular system and leads to heart disease, stroke, chronic obstructive pulmonary disease, lung cancer, and acute respiratory infections in children. Ambient air pollution accounts for 29% of all deaths and disease from lung cancer, 17% of all deaths and disease from acute lower respiratory infection, 24% of all deaths from stroke, 25% of all deaths and disease from ischaemic heart disease, and 43% of all deaths and disease from chronic obstructive pulmonary disease

Table 2.1: Healthy standards for criteria pollutants prescribed by World Health Organization.

Pollutant	Annual mean	24h mean	8h mean	1h mean	10 minute mean
$PM_{2.5}$	10	25	–	–	–
PM_{10}	20	50	–	–	–
O_3	–	–	100	–	–
NO_2	40	–	–	200	–
SO_2	–	20	–	–	500

All units are in $\mu g\,m^{-3}$.

(burden of disease 2016). While mortality is the most important health effect of severe ambient air pollution and has been studied the longest (Anderson 2009), sustained exposure to milder levels of air pollution can also cause respiratory symptoms, pulmonary disease, and other human annoyance effects (WHO 2016, State of Global Air 2018).

The World Health Organization has set guideline values for pollutants which have the strongest evidence for public health concern. These are $10\,\mu g\,m^{-3}$ annual mean and $25\,\mu g\,m^{-3}$ 24-hour mean for fine particulate matter ($PM_{2.5}$), $20\,\mu g\,m^{-3}$ annual mean and $50\,\mu g\,m^{-3}$ 24-hour mean for coarse particulate matter (PM_{10}), $100\,\mu g\,m^{-3}$ 8-hour mean for ozone, $40\,\mu g\,m^{-3}$ annual mean and $200\,\mu g\,m^{-3}$ 1-hour mean for NO_2, and $20\,\mu g\,m^{-3}$ 24-hour mean and $500\,\mu g\,m^{-3}$ 10-minute mean for SO_2. These standards are summarized in Table 2.1.

2.4 Air pollution meteorology

Meteorological processes occurring close to the earth's surface are central to understanding air pollution. Weather parameters such as temperature, moisture, wind speed and direction can greatly influence regional air pollution levels. Some key meteorological processes that affect air quality are: solar radiation (determines photolytic reaction rates), horizontal wind speed (determines the extent of advection of pollutants), turbulence (affects vertical mixing and dilution of pollutants), clouds and precipitation (scavenge pollutant species), temperature and humidity (determine the kinetic and thermodynamic equilibrium of several pollutant species).

Fronts are boundaries between air masses where a meteorological variable changes rapidly across a small horizontal distance and divides air masses. Passage of fronts over a region can cause rapid change in air quality. Enhanced *convection* can lead to improvement in air quality through vertical dilution of air pollutants. Temperature *inversions* suppress vertical dispersion of pollutants and trap them near the surface thereby exacerbating air

quality.

Air pollution levels can be low despite high emissions if they are efficiently transported high up in the atmosphere, thereby lowering surface pollution levels. In this context, it is important to understand the concept of *Atmospheric Stability*. Stability classes (or states of the atmosphere) are defined based on the behaviour of air parcels once they are displaced from their initial position. Positive stability implies that a displaced air parcel will return to its initial position, neutral stability implies that a displaced air parcel will remain at its new position, and negative stability or instability means that a displaced air parcel will continue to accelerate away from its rest position. Positive, neutral and negative stability classes are associated with high, moderate and low air pollution respectively. This is because, under unstable conditions, even upon slight disturbance an air parcel at the surface will keep moving away from its initial position, i.e., higher up in the atmosphere and will carry the surface pollutants along with it. On the other hand, under stable conditions, an air parcel at the surface will remain at the surface for a long time, thereby leading to build-up of pollutants.

Horizontal transport at various scales (local, regional and synoptic) is also a key factor in determining air quality for a given location. High pollutant concentration upwind can be transported to a different region causing substantial increases in air pollution levels than would otherwise occur.

Air pollution meteorology includes the effect of meteorology on air pollutants as described above as well as the effect of pollutants on meteorology. This often leads to a positive feedback loop where unfavourable meteorology (low temperatures, milder winds, high RH) increases pollution levels which then make the meteorology even more unfavourable.

Some common air pollutants are also greenhouse gases (e.g., CO_2, O_3). While their surface concentrations are determined by various meteorological parameters discussed above, they trap outgoing infrared radiation thereby leading to an increase in temperature - which further affects these and other pollutants. Particulate matter such as black carbon can dim the light entering the earth's surface and convert it into heat. It can also indirectly lead to sooty clouds which absorb more light. Other forms of particulates such as sulfates may have the opposite effect as they are lighter in color and can reflect some of the incoming solar radiation away from earth's surface. Such effects modulate meteorological parameters which can in turn affect air quality. Therefore, a sound understanding of these two-way feedback effects is central to understanding air pollution.

2.5 Air pollution in China

Air pollution levels remain dangerously high in many parts of Asia and around 2.2 million of the world's 6.4 million premature deaths each year from household (indoor) and ambient (outdoor) air pollution are in East and South-East Asia–home to one quarter of the world's population (WHO 2016, State of Global Air 2018).

China has had rapid economic growth for the past three decades and became the world's second largest economy in terms of gross domestic product (GDP) in 2010 and was the world's biggest energy consumer in 2009. In 2012, China's total energy consumption reached 2·43 billion tonnes oil equivalent, and its per-capita GDP energy consumption was 1·4 times the world average (Chen et al. 2013b). In 2012 coal consumption in China accounted for 67% of the country's total energy consumption and 50% of world's total coal consumption. The number of on-road civilian vehicles in China increased from 16·09 million in 2000 to 93·56 million in 2011. China's heavy chemical and petrochemical industries have been growing robustly over the past years. The country's current cement and crude steel production capacity total 1·7 billion tonnes and more than 1 billion tonnes, respectively. China's extensive industrial development, substantial coal-dependent energy consumption, and increasing number of vehicles have led to a significant rise in emissions of air pollutants and carbon dioxide (Chen et al. 2013b). The Global Burden of Disease Study 2010 found that $PM_{2.5}$ has become the fourth biggest threat to the health of the Chinese people. In addition, the death rate from lung cancer has soared since 1970, and is now the leading cause of death from malignant tumours in the country.

Since 1978 in China, increasing numbers of workers have migrated from the countryside to the urban areas, particularly to large and developed cities for better job opportunities. From 1980 to 2005, the urban population in China increased from 19.6 to 40.5%. The number of cities increased to over 660, and more than 170 cities had over 1 million permanent residents in 2004. These metropolises generated 65.5% of the GDP, but at the expense of the environment (*China Statistical Yearbook 2005, 2006* n.d.). Megacities, which are conventionally defined as cities with populations over 10 million, emerged in the 1990s in China and city clusters were developed in the proximity of the mega cities during the last decade (*Urban Statistical Yearbook of China 2005, 2006* n.d.). This urbanization trend is likely to continue in the future (Liu & Diamond 2005, Shao et al. 2006).

Total emissions in China for all key pollutants rose swiftly during the last few decades (Hoesly et al. 2018) with significant increases in urban clusters (Lin & Zhu 2018). As of 2015, 65% of Chinese cities did not meet the secondary national air quality standards for

PM_10; 18.4% of the cities did not meet the secondary standards for NO_2; and 3.3% of the cities did not meet the secondary standards for SO_2 (Lin & Zhu 2018). Severe winter haze days (days with daily mean $PM_{2.5}$ exceeding $150\,\mu g\,m^{-3}$) have consistently increased in the Beijing–Tianjin–Hebei region from 1985 to 2017 with an average increase of 4.5 days per decade and a corresponding increase of $13.5\,\mu g\,m^{-3}$ in $PM_{2.5}$ averaged over the haze days (Dang & Liao 2019). Chang et al. (2009) reported consistent reduction in visibility in Beijing, Chengdu, Guangzhou, Shanghai, and Xi'an during 1973–2007.

The National Plan on Air Pollution Control was launched by the Chinese Government in 2010 during the 12^{th} Five-Year Plan (2011–15) that set out strict targets and measures to prevent and control air pollution in thirteen key regions across China. Further, in 2013, the National Action Plan on Air Pollution Prevention and Control (2013–17) was rolled out which required PM_{10} in cities at or above the prefecture level to be reduced by over 10% by 2017 compared with the 2012 level, and that the number of blue-sky days should grow every year. This plan also identified three key regions, namely, Beijing-Tianjin-Hebei (BTH) Area, Yangtze River Delta (YRD), and Pearl River Delta (PRD) requiring the annual mean $PM_{2.5}$ level to be reduced by over 25%, 20% and 15% respectively, by 2017 compared with 2012 levels, and that the annual mean $PM_{2.5}$ level in Beijing should be controlled at $60\,\mu g\,m^{-3}$ in 2017. A budget of US$ 277·5 billion was set for this five year plan. The National Health and Family Planning Commission of China initiated the development of an air pollution and health effects monitoring system in October 2013. The Chinese Academy for Environmental Planning claimed that these measures will prevent 200,000 premature deaths each year if the annual level of PM_{10} in Chinese cities reaches the first level standard of $40\,\mu g\,m^{-3}$, as set out in the newly revised China National Ambient Air Quality Standards (Chen et al. 2013b). Emissions decreased by 62% for SO2, 17% for NO_X, 27% for CO, 38% for PM_{10}, 35% for $PM_{2.5}$, 27% for Black Carbon (BC), and 35% for Organic carbon (OC) from 2010 to 2017. However, there was an increase of 11% for non-methane volatile organic compounds (NMVOCs) and 1% for NH3 during the same period (Zheng et al. 2018).

While the long-term action plan has been effective to bring down annual mean pollution levels and may improve the overall air-quality substantially, it does not avert the extreme pollution episodes, esp. haze episodes during the winter months which generally have a 3–5 day span and are mostly caused due to unfavourable weather conditions such as low temperature, high relative humidity and low wind speeds. Therefore, more radical short-term emission controls are needed especially during winter months in order to avoid extreme haze episodes which cause severe health damage to citizens as short-term exposures

to $PM_{2.5}$ are found to be significantly associated with increased risk of mortality (Di et al. 2017).

Figure 2.1: A picture of Tiananmen square in Beijing during a haze episode.

The first concerted attempt at short-term controls in China were made during the Beijing Olympics in 2008. Test studies were conducted prior to the event which revealed that controlling only local sources in Beijing would not be sufficient to attain the healthy air quality goal and that Hebei province can contribute to 50-70% of $PM_{2.5}$ in Beijing (Streets et al. 2008). The controls were implemented in phases. While the event spanned 8–24 August 2008, partial controls started even before 20 July. Heavy industrial polluters (e.g. the Capital Steel Company) were relocated, and 50% of government cars were forbidden to drive in Beijing after 23 June. During the full-scale control (20 July to 19 September), the odd-even license plate number rule was applied on personal vehicles in Beijing; stricter control was applied on vehicles entering Beijing; and the production of high-emitting factories was limited or stopped. Another 20% of government cars were forbidden to drive in Beijing (70% total reduction), some outdoor constructions were stopped, and usage of coal-burning facilities were restricted during 8–24 August (Olympic Games period) and 7–19 September (Paralympics period) (Gao et al. 2011). Estimated emissions of aerosol precursors during the Olympic Games were reduced by about 40–60% compared with those in June 2008 (Wang et al. 2010a, Zhou et al. 2010).

On-road concentrations of NO_X, SO_2, CO and BC were reduced by 41%, 70%, 54% and 12% respectively and the mean daytime O_3 concentration was reduced by 15 ppbv during the Olympics as compared to those of the pre-control period (Wang et al. 2010a). Modelling and data analysis studies found that favourable meteorology during the control period contributed to at least 16% reduction in $PM_{2.5}$ levels while emission controls contributed

to at least 43% reduction (Yang et al. 2011). Also, despite overall reduction in $PM_{2.5}$ levels during the control period, unfavourable weather conditions associated with southwesterly flow led to occasional high $PM_{2.5}$ concentrations (higher than $150\,\mu g\,m^{-3}$) during the control period (Gao et al. 2011).

Since then similar short-term emission control efforts have been made to ensure satisfactory air quality for many other special events such as the 41st Shanghai World Expo in 2010 (Huang et al. 2012, *SEPB: Shanghai Environmental Protection Bureau* 2010), the 16th Guangzhou Asian Games and Asian Para Games in 2010 (*GEPB: Guangzhou Environmental Protection Bureau* 2009, Liu et al. 2013), the Chengdu Fortune Forum 2013 (*CEPB: Chengdu Environmental Protection Bureau* 2013) and more recently the Asia-Pacific Economic Cooperation (APEC) summit 2014 and the 2015 China Victory Day Parade(Liang et al. 2017). Since most of these short-term controls have been a first such initiative for most regions except Beijing, they tend do be based on *ad-hoc* decisions. However, Beijing has seen multiple short-term controls which should allow us to build enough scientific knowledge to inform smarter controls for future. There is ample scope of improvement in short-term emission control policies in urban Beijing esp. because it has a good network of ground-based observations all around the city and also a representative meteorological station at the airport, along with other observations available from tower measurements from various scientific campaigns.

Although air pollution in China has been extensively studied through ground measurements, modelling, satellite observations, and long-term data analysis, some key research gaps remain. Firstly, the duration of controls need to be optimized by investigating temporal nature of reductions in pollutant concentrations for a wide range of weather conditions. Secondly, while many studies advocate for wider controls (Gao et al. 2011, Wang et al. 2016b, Chang et al. 2018), few have evaluated contributions from far-away sources outside of Beijing–Tianjin–Heibei region to Beijing. Furthermore, changes in relative contributions from the near and far regions of control need to be understood in terms of their temporal effect as well as dominant sources for varying meteorological conditions.

2.6 Atmospheric chemical transport models

The processes controlling the formation and fate of air pollution can be explored in detail using chemical transport models. Atmospheric Chemical Transport Models (ACTMs) are weather forecast models which include emissions, and chemical and deposition processes needed to represent air pollution. The general objective of ACTMs is to simulate the

evolution of interacting chemicals in the atmosphere (Brasseur & Jacob 2017). This is done by solving a coupled system of continuity equations that represent conservation of mass.

$$\frac{\partial C_i}{\partial t} = -v \cdot \nabla C_i + P_i(C) - L_i(C)(i = 1, ...n) \tag{2.1}$$

Here, v is the 3-D wind vector, and P_i and L_i are total production and loss rates for species i which involve contributions from chemical reactions (coupling to other species), emissions, and deposition. $(\partial C_i/\partial t)$ is the change in mixing ratio with time which is expressed as the sum of inflow minus outflow (flux divergence term v $\cdot\nabla C_i$) within a grid point and net local production (P_i – L_i). The solution of equation 2.1 depends on meteorological variables through the 3-D wind vector v. The production and loss terms may also depend on meteorological variables.

Offline ACTMs borrow 3-D time-dependent data (e.g., winds, humidity, temperature etc.) from an external meteorological model which must define a mass-conserving airflow with consistent values for different variables that affect transport, production, and loss terms in eqn 2.1. Various independently developed offline ACTMs have been successfully used to study air pollution events in China, e.g., CMAQ (developed by the US Environment Protection Agency) (Chang et al. 2018, Hu et al. 2016, Zhang et al. 2017, 2016b), NAQPMS (developed at FRSGC, Yokohama, Japan) (Li et al. 2014, Chen et al. 2015a, Wang et al. 2017b, Chen et al. 2019a) and CAMx (developed at Ramboll Environment and Health, US) (Li et al. 2015, Zhang et al. 2018).

Online ACTMs generate their own meteorological environment where continuity equations for chemical species are solved together with the meteorological equations for conservation of air mass, momentum, heat, and water. Online ACTMs, while more computationally expensive than the offline ACTMs, offer several advantages over the latter: they enable studying feedback effects of pollutants (e.g.,O3, aerosols) on meteorology, they avoid the need for separate high-resolution meteorological archives to study air pollution, and they are not subject to time-averaging errors associated with the use of offline meteorological fields (Brasseur & Jacob 2017). Two-way coupled WRF-CMAQ (Wong et al. 2012), WRF-Chem (Grell et al. 2005), GEOS-Chem (Bey et al. 2001), UKCA (Morgenstern et al. 2008) and ECHAM-HAM (Zhang et al. 2012) are some examples of online ACTMs.

ACTMs can be global (e.g., ECHAM, GEOS-Chem, UKCA) which simulate the atmosphere of the entire globe or regional (e.g., CMAQ, WRF-Chem, NAQPMS) which simulate only the region of interest. Regional ACTMs are also called Limited-Area Models (LAMs). Global ACTMs have a coarser horizontal resolution (larger grid sizes) and are traditionally

used to study global change in atmospheric composition, for example in Wild et al. (2004), Strode et al. (2019).

It is common to use a higher resolution of the model over a region of interest without the computational expense of high resolution at other regions. *Nesting* is a process where a model runs at a finer resolution by borrowing initial and boundary conditions about the physical and chemical state of the atmosphere from the output of its coarser version and both versions proceed ahead in time simultaneously with either one-way or two-way exchange of information. In one-way nesting, the coarser version of the model supplies information about the state of the atmosphere at the boundaries of the region of interest which is being simulated at a higher resolution. In two-way nesting, the coarser version provides this information to the finer version which then also provides aggregated information back to the coarser version and both versions evolve simultaneously in time, benefiting from higher resolution geographic and emissions data and a finer representation of wind flow, turbulence and convective processes.

Recent studies have used global models at finer resolutions to study smaller target regions such as the North China Plain and Seoul with or without nesting (see Wang et al. 2014b, Lee et al. 2017). However, if we are not interested in studying global change, it makes less sense to use our computational resources to simulate the entire globe. Regional ACTMs only simulate a limited area of the globe so that most of the computational resources are exploited in modelling the region of interest, while relying on external global model output (easily downloadable for free) for meteorological and chemical initial and boundary conditions. Therefore, regional ACTMs have become an attractive choice to model city- and district-level pollution episodes in sufficient detail without worrying about the state of pollution farther away. I have chosen the well-tested regional ACTM, WRF-Chem for my studies which is described in the next section.

2.7 The WRF-Chem model

The Weather Research and Forecasting model with chemistry (WRF-Chem) is an online ACTM where the meteorological component and chemistry component share the same transport scheme, grid, physics schemes for subgrid-scale transport, and time-step.

The meteorological component WRF features an advanced numerical solver–an iterative procedure to find approximate solutions to ordinary differential equations–for solving continuity equations for mass and water vapour, (thermodynamic) energy conservation equations to relate air temperature to heating and cooling processes, 3-D Navier-Stokes

equation for momentum conservation, and the ideal gas law to relate pressure to air density and temperature. WRF features a mass-based terrain-following coordinate and allows for two-way nesting with multiple nests and nest levels, flexible vertical grid spacing for better representation of boundary layer processes and inversion, multiple map projections (polar, conic, cylindrical etc.) to represent a limited-area across any part of the globe with minimal map distortion, a selection of different advection schemes with mass and scalar conservation, and parameterized representations for land-surface, planetary boundary layer, atmospheric and surface radiation, cloud microphysics and cumulus convection. For a detailed description of governing equations, the numerical solver, treatment of initial and boundary conditions, nesting, and representation of boundary layer turbulence, land surface processes, radiation, cloud processes and convection, see Skamarock et al. (2008).

The chemistry component Chem consists of a variety of independently developed chemical mechanisms for gas-phase pollutants and aerosols. The user can select simpler or complex gas-phase and aerosol representations based on their research question and availability of computational resources. The chemistry component also features sophisticated atmospheric processes such as dry deposition, wet deposition and scavenging, cloud chemistry, and photolysis (Grell et al. 2005). Figure 2.2 shows a simple schematic diagram of the modelling framework. The user supplies geographic data (land use and topography), emissions (anthropogenic, biogenic and biomass burning), meteorological reanalysis (global model output assimilated with observations) for lateral boundary conditions, and global ACTM output for chemical initial and boundary conditions which are preprocessed to a gridded form on a user-selected map projection. The preprocessing system prepares the initial meteorological and chemical state of the atmosphere on the required grid focusing on the study region. The model is then run forward in time which performs numerical integration of various ordinary differential equations as mentioned in section 2.6 and produces a range of different 3D and 4D fields of both meteorology and pollutants at finer spatial and temporal scales representing the evolution of the atmosphere over the study period.

WRF-Chem is a well-tested model in the atmospheric pollution modelling community and offers some excellent options which other models do not. Its meteorological component features fully compressible nonhydrostatic equations with hydrostatic option (Ooyama 1990), an accurate and efficient numerical solver (Skamarock & Klemp 2008) with mass-based terrain-following coordinate (Laprise 1992), variable vertical grid spacing, 2-way nesting, full physics options for land-surface, planetary boundary layer, atmospheric and surface radiation, cloud microphysics and cumulus convection, and the chemistry component features two-way coupling with simultaneous evolution of meteorology and chemistry,

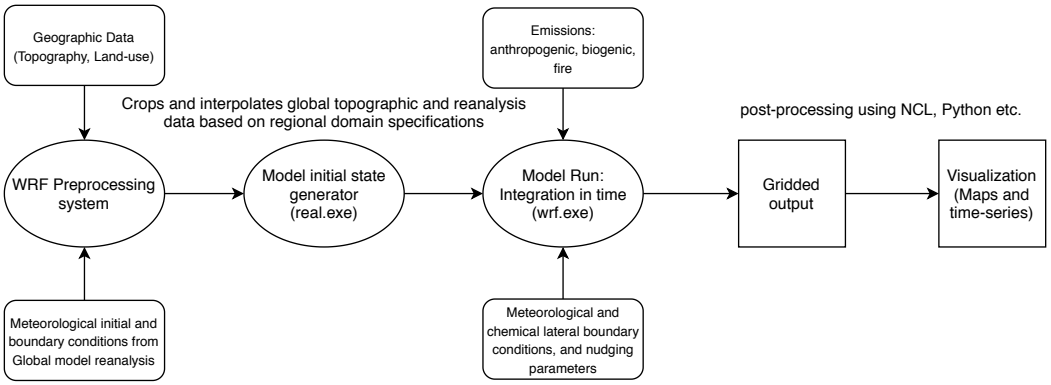

Figure 2.2: A simple schematic diagram of the WRF-Chem model running framework

a range of choices of various gas-phase and aerosol chemical mechanisms including interaction of aerosols with gases (e.g., gas-to-particle conversion), scattering and absorption of both solar and terrestrial radiation by aerosols, and aerosol effects on cloud formation–something still lacking in other models. It also allows for data assimilation–a technique of nudging the model results towards available observations to improve overall prediction. WRF-Chem has been used extensively to study trace gases (Zhang et al. 2009, Wang et al. 2010b, Chen et al. 2013a, Ansari et al. 2016, Sharma et al. 2016, Mu et al. 2017) and aerosols (Luo & Yu 2011, Saide et al. 2012, He et al. 2014, Ansari et al. 2015, Ma et al. 2018) and has been thoroughly evaluated at multiple scales for various parts of the world including China (Misenis & Zhang 2010, Kuik et al. 2016, Banks et al. 2016, Zhong et al. 2016, Flaounas et al. 2017, Crippa et al. 2017, Yahya et al. 2017, Pithani et al. 2018). It is therefore a great choice for air pollution studies over Beijing as it has a good well-tested representation of key atmospheric processes for investigation of haze episodes. Choosing a well-tested model helps us to build over existing knowledge while also aiding in reproducibility of previous results over the same region thereby strengthening our confidence in a consistent theoretical understanding of pollution events.

The WRF-Chem model code is written in FORTRAN90 and relies on several other libraries such as NetCDF, GRIB, zlib, szip and MPI. WRF-Chem code is modular and allows for serial or parallel build, i.e., the model may be ported onto a single-processor machine (serial), a shared-memory machine or a distributed *cluster* (parallel mode). Modelling of atmospheric chemistry is a grand computational challenge which requires solving a large system of 4-D partial differential equations, therefore it is practical to port the model on to large distributed *clusters* or *supercomputers*. For this research, WRF-Chem was ported on to the Lancaster HEC distributed cluster and up to 64 processors were were used in parallel to conduct the simulations. Other tools for emissions and boundary

conditions preprocessing were also installed.

Several tests were performed to select the best-suited model parameters for the study region and period. Firstly, to select the optimal time-stepping of meteorological and chemical solvers, the model was run with various combinations of meteorological time step and chemical time step: (90s,90s), (150s,150s) and (150s,30m). Finally a meteorological time step of 150 s and a chemical time step of 10 m was selected as a good compromise between numerical accuracy and computational efficiency. Then, with these time steps, further tests were performed to obtain a good vertical representation of the atmosphere over the study region–mainly by testing several combinations of model top, number of vertical levels, and the boundary layer scheme with and without data assimilation of key meteorological parameters. Ultimately, 31 vertical levels with a model top of 50 hPa and the Yonsei University boundary layer scheme were selected along with grid nudging of moisture, heat and winds outside the boundary layer, based on a realistic spatial and temporal representation of boundary layer height and other pollutants. Results from some of these tests are shown in Appendix D.

2.8 Modelling approaches

Although WRF-Chem has been used extensively in the last decade to study air pollution events all across the world, its application has been rather conventional, i.e., running the model during a pollution episode, comparing the model output against observations and explaining the differences. There is tremendous scope for novel application techniques of the model to gain further insight into formation mechanisms and source attribution of air pollution.

Several studies also miss the crucial step of meteorological evaluation prior to the chemical evaluation. In atmospheric modelling, simulated results often match anticipated/observed values due to various intermediate parameters having an offsetting effect on each other–right answers for the wrong reasons. For example, a model may have a lower chemical production of a chemical species than reality but also a shallower boundary layer which leads to reduced vertical mixing and more chemical accumulation at the surface, finally matching the levels of observations. Similarly, an emission inventory (emission input data) that is read by the model might have a wrong location of an emission source of a precursor species, say, slightly upwind of its real location, but the model may underestimate temperature in the region leading to a slower chemical production of secondary species thereby forming further downwind in the model than it should, ultimately matching

the ground-based observations due to offsetting effect of chemistry and transport. Higher emission rates or chemical production can also be compensated by higher removal rates (dry and wet deposition, chemical destruction) in the model which may not be the same as real atmosphere but ultimately lead to the same levels of pollutant accumulation in the atmosphere at a given time. Such results can lead to an incorrect understanding of atmospheric processes, and formulation of a flawed a control policy. Therefore careful evaluation is required at each step of prediction, and the uncertainties have to be recognized. A thorough meteorological evaluation highlighting the strengths and weaknesses of the model across all domains (if nesting is used) is necessary before making claims about the chemical prediction skill of the model. The causes of better or worse model performance in certain regions or at certain times have to be explained. This helps us better interpret the pollutant predictions and identify the inadequacies within the model in context of a particular research question.

Source apportionment (identifying sources of pollution for a given receptor) is a key exercise in formulating smarter emission-control policies. Source attribution can be performed through sensitivity analysis or through 'tagging' of emissions. Sensitivity analysis involves running the model with reduced emissions from a particular source to obtain pollutant concentrations at the receptor which are then compared with concentrations from the baseline emissions run. The difference gives us the contribution from the considered source to the receptor. Multiple simulations are needed to identify contributions from different sources. Therefore the sensitivity analysis method can become very tedious if several sources are considered. The tagging method overcomes the problem of multiple simulations by treating emissions of a given species from different regions as completely independent species in the model such that the model simulates their emission, transport and removal independently. In such a model run, the tagged species are reported as separate variables. Simulations with several tagged species can be much more computationally expensive than individual simulations of the brute-force method but may still be a more efficient choice overall depending on the computational resources available. The biggest problem of tagging method is that it cannot attribute secondary pollutants accurately–as they do not originate from primary emission sources but are formed on the way. $PM_{2.5}$ episodes in Beijing are dominated by secondary aerosols (Sun et al. 2016a,b, Tao et al. 2017, Li et al. 2017, Chen et al. 2015b, Huang et al. 2019), therefore tagging is not an attractive method to investigate their sources. Sensitivity analysis can attribute secondary pollutants to considered sources and has been used extensively in modelling studies for source attribution (Burr & Zhang 2011, Han et al. 2016, Zhang et al. 2017). However, the

sensitivity analysis method can only be used to attribute secondary pollutants to individual emission sources by removing one source at a time and does not take into account the interactions of various sources and non-linear response of secondary pollutant concentrations towards emissions. To fully understand source contributions, the nonlinearity of pollution response to reductions in various emission sources has to be understood in detail. Ideally, hundreds of thousands of simulations are needed with different sets of perturbations to all emission sources in order to sufficiently capture the interactions between different sources. Such a large number of runs with a computationally expensive ACTM is impractical.

Statistical and machine learning (ML) techniques are useful in learning the underlying behavior of a system from a set of training data without a prior knowledge about the nature of the relationships between the data (Lary et al. 2016). ML-based techniques are particularly useful in: classification problems; when there is no deterministic model for the system; and when the system's deterministic model is computationally expensive (Lary et al. 2016). The problem of source attribution corresponds to the third case here due to the large number of simulations involved.

Gaussian Process Emulation is an attractive statistical technique to study source attribution of pollution. Here, the computationally expensive ACTM (simulator) is replaced by an emulator trained on the input-output relationships derived from a sufficient number of perturbation runs of the simulator such that enough parameter space is covered. The emulator, being computationally efficient, can then be run thousands of times with a lot more perturbations in the input parameters (here, emission strengths of different sources) to calculate the Global Sensitivity Indices of each input parameter; this is the sensitivity of each emission source towards pollution levels at the receptor, averaged over all possible values of other sources. Global sensitivity indices present a more holistic information about source attribution than simple one-at-a-time sensitivity studies–this is because the latter attribute contributions to a given source while all other sources remain fixed at their nominal values while Global Sensitivity Indices represent a mean response to changes in strength of a given source averaged over all possible changes in other sources.

Apart from computing Global Sensitivity Indices, Gaussian Process Emulation can also be used to create response surfaces which relate emission strength of various sources to resulting concentration at the receptor. Response surfaces can be utilized to work out the most optimal reductions needed across various sectors and regions to meet a certain pollution target at the receptor which can be implemented back in the simulator to test the results. These set of reductions can either be constant in time during a pollution episode (linear controls) or variable in time. The latter method can lead to a more dynamic policy

framework which updates daily and controls emissions by just the right amount to meet daily targets. This method of optimizing a multivariable system is called Model Predictive Control (MPC) and has been used in several applications such as industrial processes, self-driving cars and guided missiles.

MPC is a feedback control algorithm that uses a model to make predictions about future outputs of a process. MPC can handle multi-input multi-output systems that might have interactions between their inputs and outputs. MPC can handle constraints and incorporate future reference information into the control problem thereby acquiring preview capabilities. In a control problem, the goal of a controller is to calculate the input to the system (here, the ACTM) such that the system output follows a desired reference. MPC uses a simplified model of the system to make predictions about the future of the system output behaviour. It also uses an optimizer which ensures that the predicted future system output tracks the desired reference. The MPC controller simulates multiple future scenarios of the system for a given prediction horizon. These predictions are not done in a random way but in a systematic way by means of the optimizer which solves an error minimization problem. While solving this optimization problem it is also made sure that the prediction stays within prescribed limits or constraints. The optimized prediction is then implemented to the system and predictions are made for the next prediction horizon with updated conditions. An MPC-based approach is developed in this work by means of gaussian process emulation to guide the WRF-Chem model towards the desired output: the national standard for daily mean $PM_{2.5}$ concentration in Beijing.

This work presents a comprehensive model study of pollution episodes in Northern China with a focus on Beijing using a state-of-the-art high-resolution atmospheric chemical transport model WRF-Chem. A past short-term emission control policy in Beijing is evaluated for its robustness and temporally-resolved source contributions from various sectors and regions to $PM_{2.5}$ levels are investigated. Furthermore, novel use of computationally cheap statistical emulation is demonstrated to identify nonlinearities in pollution response to emission cuts, and response surface charts are produced for informing short-term emission control policy. An automatic model running framework is developed with dynamically changing emissions guided by response surfaces in order to meet daily healthy air quality targets. This is one of the first studies to emulate an air quality model, and the first to build a dynamic emission scaling framework based on emulated results.

CHAPTER 3

Effectiveness of short-term air quality emission controls: a high-resolution model study of Beijing during the Asia-Pacific Economic Cooperation (APEC) summit period

Tabish Umar Ansari[1], Oliver Wild[1], Jie Li[2], Ting Yang[2], Weiqi Xu[2,3], Yele Sun[2,3,4], and Zifa Wang[2]

[1]Lancaster Environment Centre, Lancaster University, Lancaster, UK

[2]State Key Laboratory of Atmospheric Boundary Layer Physics and Atmospheric Chemistry, Institute of Atmospheric Physics, Chinese Academy of Sciences, Beijing, China

[3]College of Earth Sciences, University of Chinese Academy of Sciences, Beijing, China

[4]Center for Excellence in Regional Atmospheric Environment, Institute of Urban Environment, Chinese Academy of Sciences, Xiamen, China

(This chapter is reproduced from a published paper in Atmospheric Chemistry and Physics. `https://www.atmos-chem-phys.net/19/8651/2019/`)

Author contributions: TUA, OW, and ZW designed this study, and TUA performed the model simulations and analysis. JL provided emission data and expertise on the model set-up; TY provided the lidar data and guidance on deriving PBLH height; and YS, WX, and ZW provided measurement data from IAP tower. TUA and OW prepared the paper, with input from all co-authors.

3.1 Abstract

We explore the impacts of short-term emission controls on haze events in Beijing in October–November 2014 using high resolution WRF-Chem simulations. The model reproduces surface temperature and relative humidity profiles over the period well and captures the observed variations in key atmospheric pollutants. We highlight the sensitivity of simulated pollutant levels to meteorological variables and model resolution, and in particular to treatment of turbulent mixing in the planetary boundary layer. We note that simulating particle composition in the region remains a challenge, and we overpredict NH_4 and NO_3 at the expense of SO_4. We find that the emission controls implemented for the APEC Summit period made a relatively small contribution to improved air quality (20–26%), highlighting the important role played by favourable meteorological conditions over this period. We demonstrate that the same controls applied under less favourable meteorological conditions would have been insufficient in reducing pollutant levels to meet the required standards. Continued application of these controls over the 6-week period considered would only have reduced the number of haze days when daily mean fine particulate matter exceeds $75\,\mu g\,m^{-3}$ from 15 to 13 days. Our study highlights the limitations of current emission controls and the need for more stringent measures over a wider region during meteorologically stagnant weather.

3.2 Introduction

Air pollution poses serious health risks to urban residents and is one of the most important environmental problems facing cities around the world (Liang et al. 2017). Fine particulate matter with a diameter less than 2.5 µm ($PM_{2.5}$) is a major air pollutant that often exceeds safe limits during haze episodes which are a common occurrence in many developing megacities over the past decade. It has been estimated that outdoor air pollution, mostly by $PM_{2.5}$, leads to 3.3 million premature deaths per year worldwide, predominantly in Asia (Lelieveld et al. 2015). $PM_{2.5}$ also reduces visibility and has important impacts on regional climate (Westervelt et al. 2016). Beijing is the capital and political and cultural centre of China and is among the most polluted cities in the country (Batterman et al. 2016). The population of Beijing municipality increased from 14.2 million in 2002 to 21.2 million in 2013 (Jiantang et al. 2014), and this has been accompanied by an increase in anthropogenic emissions across the region. High $PM_{2.5}$ concentrations are frequently reported in city clusters in the Beijing–Tianjin–Hebei, Yangtze River Delta, and Pearl River Delta

regions in China. Haze episodes are particularly common during winter months and have attracted substantial scientific attention (Gao et al. 2017). Independent observational (Gao et al. 2016a, Zhong et al. 2018, Shang et al. 2018, Chen et al. 2015b, Sun et al. 2016a), modelling (Matsui et al. 2009, Kajino et al. 2017, Gao et al. 2015a, Chen et al. 2016e) and long-term data analysis studies (Chen et al. 2016, Liu et al. 2016d, Chen et al. 2015c, Yan et al. 2018) have investigated the sources, evolution and fate of $PM_{2.5}$ in Beijing, but many uncertainties remain, and improved understanding is required in order to inform sound, evidence-based emission control policies. Strict short-term emission controls have been applied effectively to improve air quality in Beijing during the Beijing Olympics in 2008 (Gao et al. 2011, Yang et al. 2011) and more recently for major events such as the Asia-Pacific Economic Cooperation (APEC) summit in November 2014 (Li et al. 2017d, Wang et al. 2016c) and the China Victory Day Parade in 2015 (Liang et al. 2017, Liu et al. 2016c, Zhao et al. 2016). Real-world emission controls provide an ideal opportunity for testing current scientific understanding of the sources and processing of air pollution as represented in models in a robust way. With improved confidence in model performance over a focus region we can explore the impact of alternative control options to aid formulation of more effective policies for emission reduction.

A number of previous studies investigated the effect of emission controls during the APEC period in November 2014 using surface observations (Sun et al. 2016b, Xu et al. 2015, Wang et al. 2016c, Li et al. 2017d, Zhou et al. 2017) and atmospheric chemical transport models (Zhang et al. 2016a, Guo et al. 2016, Wang et al. 2017a, Gao et al. 2017) and found that $PM_{2.5}$ concentrations were much lower than during the preceding weeks. Many of these studies attributed this improved air quality largely to the emission controls that were applied without thoroughly evaluating the role of meteorological variations. Comparison with observations in preceding weeks or over similar time periods in earlier years does not adequately account for the role of meteorology in governing haze episodes. Model studies with and without emission controls are insufficient to evaluate the contribution of meteorological processes if they focus on the control period alone, without evaluating the model performance outside the control period. Gao et al. (2017) found that the emission controls reduced $PM_{2.5}$ levels by about $18\,\mu g\,m^{-3}$ during APEC with about half the reduction being due to emission controls in surrounding districts outside Beijing. However, the study involved coarse-resolution (27 km) model simulations which may be insufficient in capturing regional and city-level atmospheric events well and lacked component-level analysis of aerosols. Other studies have noted the role of meteorology during the period but have not quantified it, attributing the benefits mostly to emission controls.

In this study we investigate the effectiveness of short-term emission controls and how meteorological processes influence this, using the APEC period as an example. We use a nested version of the Weather Research and Forecasting model with Chemistry (WRF-Chem) over China with a specific focus on the Beijing–Tianjin–Hebei region. WRF-Chem has been used successfully at coarser resolution in previous studies investigating haze formation over Beijing (Matsui et al. 2009, Tie et al. 2014, Zhang et al. 2015b, Chen et al. 2016e). We describe the model set-up, emissions, and observations in Section 5.3. In section 3.4 we present a thorough meteorological and chemical evaluation of the model simulations against surface observations and tower measurements, including aerosol composition, and we assess the strengths and weaknesses of the model. We present sensitivity studies to key physical and chemical processes in section 3.5. In section 3.6 we investigate the impact of emission controls over the APEC period and compare these with the same controls over a period two weeks earlier to demonstrate the important role of meteorological conditions in governing their effectiveness.

3.3 Model configuration and the APEC period

We use the WRF-Chem model (Grell et al. 2005, Fast et al. 2006) version 3.7.1 to simulate the meteorology and air quality over northern China. Previous studies have shown that WRF-Chem is capable of reproducing air quality in China relatively well (Gao et al. 2015a, 2016b, Guo et al. 2016, Chen et al. 2016e). We use the Carbon Bond Mechanism version Z (CBMZ) chemistry scheme coupled with the Model for Simulating Aerosol Interactions and Chemistry (MOSAIC) aerosol module (Zaveri et al. 2008). CBMZ explicitly treats 67 species with 164 gas-phase, heterogeneous and aqueous reactions, and provides a suitable compromise between chemical complexity and computational efficiency. MOSAIC uses a sectional approach with eight aerosol size bins and treats the key aerosol species, including sulfate, nitrate, chloride, ammonium, sodium, black carbon (BC), primary organic mass, liquid water and other inorganic mass. Secondary organic aerosol (SOA) formation is not included in the chemical mechanism used here. Current SOA schemes are poorly parameterized for Chinese conditions and significantly underpredict SOA (Gao et al. 2016b, 2015b). SOA contributed only 17–23% of total ground-level fine particulate matter in Beijing during the period investigated here, while secondary inorganic aerosols contributed up to 62% by mass (Sun et al. 2016b). We consider the lack of SOA formation in the model in drawing our conclusions. Further details of the model configuration used in this study are given in Table 3.1.

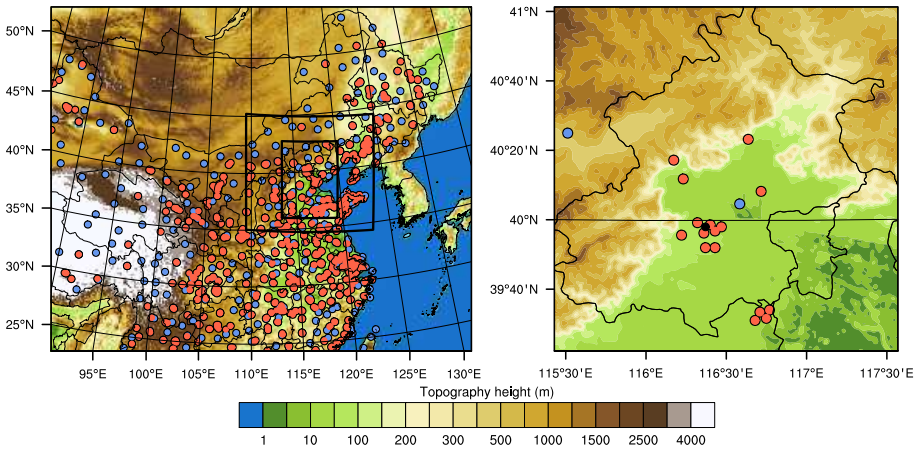

Figure 3.1: Map of the model domain (left) showing nests over northern China and the North China Plain, and map of Beijing municipality (right) showing the location of IAP (black) and measurement stations for meteorology (blue) and air quality (red).

We perform two-way coupled simulations with three nested domains that include China as the parent domain (D01) at 27 km horizontal resolution, northern China as a nest (D02) at 9 km resolution and the North China Plain as an innermost nest (D03) at 3 km resolution, as shown in Fig. 3.1. The model is nudged to meteorological reanalysis data above the boundary layer every six hours for winds, temperature and moisture to permit direct comparison of the simulations with observed pollutant concentrations under comparable conditions.

We use anthropogenic emissions from the Multi-resolution Emission Inventory for China (MEIC) for the year 2010 (Li et al. 2017c). This provides emissions of major air pollutants including NO_x, CO, non-methane volatile organic compounds (NMVOCs), SO_2, NH_3, $PM_{2.5}$, PM_{10}, black carbon (BC) and organic carbon (OC) from five major emission sectors that include residential, traffic, industry, power and agricultural sources, and it has been used in a number of previous modelling studies (Li et al. 2015, Gao et al. 2015a, Zhang et al. 2015b, Chen et al. 2015a, 2016e). Emissions were provided at the native resolution of each domain, i.e., at 27 km, 9 km and 3 km. We impose a vertical profile for these emissions over the lowest eight model levels to account for the effective source height distribution for each sector based on the distribution used for EMEP emissions (Bieser et al. 2011, Mailler et al. 2013), and impose a diurnal cycle for each sector. SO_2 emissions over the Beijing–Tianjin–Hebei region were reduced by 50% to account for strong emission reductions between 2010 and our focus year of 2014 (Zheng et al. 2018, Krotkov et al. 2016). We assume that 6% by mass of SO_2 is emitted as primary SO_4 to account for the discrepancy between high observed concentrations of SO_4 and low secondary production in the model (Gao et al.

Table 3.1: Model configuration used in this study

Configuration	Description
Horizontal resolution	27 km, 9 km, 3 km (three domains)
Vertical levels	31 with model top at 50 hPa
Aerosol scheme	MOSAIC with eight bins (Zaveri et al. 2008)
Photolysis scheme	FAST-J photolysis (Wild et al. 2000)
Gas-phase chemistry	CBMZ (Zaveri & Peters 1999)
Cumulus parameterization	Grell 3-D scheme
Shortwave radiation	RRTMG shortwave scheme (Clough et al. 2005)
Longwave radiation	RRTMG longwave scheme (Mlawer et al. 1997)
Cloud microphysics	Lin scheme (Lin, Yuh-Lang, Richard D. Farley 1983)
Land surface scheme	NOAH LSM (Chen & Dudhia 2001)
Land-use data	MODIS 20 category at 30 arcseconds
Surface layer scheme	Monin–Obukhov scheme (Monin & Obukhov 1954)
Boundary layer scheme	YSU (Hong et al. 2006)
Meteorological conditions	ECMWF 6-hourly data
Chemical boundary conditions	MOZART (Emmons et al. 2010)

2015a, Chen et al. 2016e, Li et al. 2017a). Biogenic emissions are based on the Model of Emissions of Gases and Aerosols from Nature (MEGAN, Guenther et al., 2012). These are calculated online in the model based on canopy and emission factors and factors for leaf age, soil moisture, the leaf area index, light dependence and temperature responses. Hourly fire emissions are included from the Fire Emissions INventory from NCAR (FINN; Wiedinmyer et al., 2011) to represent biomass burning, although this is not a major source in the region at this time of year.

To evaluate the model, meteorological observations were obtained from the National Climatic Data Center (NCDC) hourly integrated surface database `http://www.ncdc.noaa.gov/data-access/` for all of China. These sites are shown in Fig. 3.1. We focus on 2 m temperature and relative humidity, 10 m wind speed, and direction for model evaluation. Vertical profiles of meteorological variables were obtained from the 325 m high observational tower located at the Institute of Atmospheric Physics (IAP), Chinese Academy of Sciences, Beijing (39°58′28″ N, 116°22′16″ E). This provides independent measurements of temperature, relative humidity, wind speed and wind direction at 17 different height levels. Measurements of boundary layer mixing height were retrieved from aerosol lidar profiles at IAP (Yang et al. 2017), providing a valuable additional test of model meteorological processes. Hourly concentrations of NO_2, CO, SO_2, O_3, $PM_{2.5}$ and PM_{10} are available from the national monitoring network run by the China National Environmental Monitoring Center (CNEMC). In addition, detailed measurements of atmospheric pollutants and aerosol composition were made from the IAP tower over the October-November 2014 period. These include measurements of NH_4, NO_3, SO_4, and OC from an Aerodyne

Table 3.2: Comparison of observed and simulated meteorological variables using FNL and ECMWF fields

	Obs. avg.	Sim. avg.		Bias		RMSE		r	
		FNL	ECMWF	FNL	ECMWF	FNL	ECMWF	FNL	ECMWF
2-m Temperature (°C)									
Beijing	9.68	11.52	11.44	1.84	1.76	3.28	3.36	0.88	0.87
North China Plain	8.91	8.98	8.95	0.07	0.04	2.47	2.46	0.94	0.94
2-m Relative Humidity (%)									
Beijing	54.7	34.1	39.1	-20.6	-15.6	26.9	22.4	0.77	0.81
North China Plain	54.9	44.8	48.9	-10.1	-6.0	19.6	16.7	0.75	0.78
10-m Wind Speed ($m s^{-1}$)									
Beijing	5.41	2.27	2.24	-3.14	-3.17	4.98	5.09	0.72	0.69
North China Plain	5.73	3.26	3.20	-2.47	-2.53	4.60	4.65	0.62	0.61
10-m Wind Direction (°)									
Beijing	197.5	214.2	191.0	16.7	-6.6	73.9	73.9	0.79	0.80
North China Plain	215.1	210.0	206.5	-6.9	-8.6	62.7	63.4	0.78	0.78

Hourly values are taken from 1 station in Beijing and 30 stations over the North China Plain from 12 October to 19 November 2014. Where observation data are missing, model values were removed to ensure that sampling was consistent.

Aerosol Chemical Speciation Monitor (ACSM) instrument at 260 m altitude (Sun et al. 2016b) and from a high-resolution aerosol mass spectrometer (HR-AMS) instrument at the surface (Xu et al. 2015), and BC at the surface was measured with an aethalometer. The size-segregated samples collected at the two heights were analysed for water-soluble ions. Detailed procedures for the data analysis are described in Ng et al. (2011) and Sun et al. (2012).

3.4 Model evaluation

To investigate the strengths and weaknesses of the model in representing air quality in China, the model was evaluated against meteorological and pollutant measurements across all three domains and at the IAP tower site in Beijing.

3.4.1 Meteorology

We test the model performance using two sets of meteorological fields: final reanalysis data (FNL) from the National Centers for Environmental Prediction (NCEP) and ERA-Interim data from the European Centre for Medium-Range Weather Forecasts (ECMWF). Table 3.2 presents a comparison of the performance of the model against ground-based observations from the NCDC dataset for Beijing and the North China Plain. For a detailed evaluation over each model domain, please see Table A.1 in the supplement. The average 2 m temperature is reproduced well over the North China Plain but is overpredicted at the single Beijing site. This is located at the airport on the outskirts of the city, and may not be representative of the wider region. The surface relative humidity is underpredicted for all domains with both sets of fields, although the biases are smaller and correlation is better

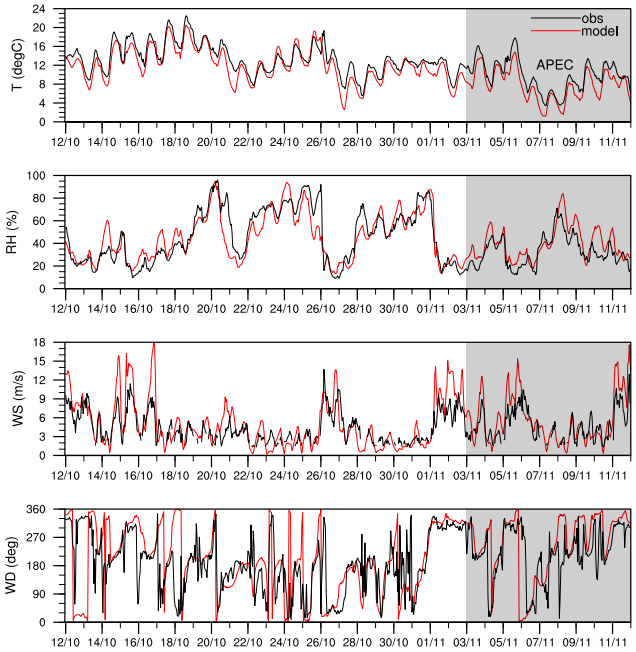

Figure 3.2: Comparison of meteorological measurements at 190–310 m on the IAP tower in Beijing with model simulations using ECMWF meteorological fields between 12 October and 12 November 2014. The period with emission controls is shaded.

with ECMWF data. The humidity is underpredicted by about 15% at the Beijing site and this may have implications for heterogeneous reactions and the hygroscopic growth of secondary aerosols. The 10 m wind speed is substantially underpredicted using both sets of fields, and this is most notable for the Beijing site. However, the correlation at this site is reasonably good suggesting that the hourly variability in wind speeds is captured adequately. The 10 m wind direction and its variability are also reproduced relatively well. Based on these comparisons, and on subsequent comparison of pollutant concentrations, we find that the model performs marginally better using the ECMWF meteorological fields. With these fields the model captures the timing of pollution episodes better, leading to more realistic pollutant behaviour, and we have therefore chosen to use ECMWF fields for our model studies.

Figure 3.2 presents an evaluation of meteorological variables with measurements from the IAP tower. We evaluate the model against measurements at 190–310 m (model level 4) to minimize the effects of buildings surrounding the site, which are not adequately resolved in the model. The daily maxima and minima in temperature are reproduced reasonably well with a small underestimation that averages less than 2 °C. The diurnal variations and averages for relative humidity, wind speed and wind direction are also captured well. The mean bias in relative humidity is 0.9% and the large underprediction seen at the airport meteorological station is not evident here, suggesting that it may be a surface-level

feature or reflect overestimation of temperature at that location. Over the height of the tower (five model levels, Figure A.2) the diurnal variation in humidity drops by more than a factor of 2, very similar to the reduction seen in the observations. The wind speed is slightly overestimated during windier periods, with a mean bias of $0.54\,\mathrm{m\,s^{-1}}$. This suggests that the underestimation of 10 m wind speeds at meteorological stations seen in Table 3.2 is a surface feature in the model–and does not represent a systematic bias throughout the boundary layer. The synoptic patterns in all four variables are captured very well, highlighting the quality of the ECMWF meteorological data, and there is only one occasion on 20–21 October when substantial deviations in temperature and humidity are evident. There are some marked differences in meteorological conditions between the APEC period (3–12 Nov) and the period preceding it. These include a gradual temperature drop of 7 °C associated with the changing seasons which is accompanied by a drop in relative humidity. There is an increase in the frequency of northwesterly flow with higher wind speeds, and this contrasts strongly with the lighter wind speeds and more frequent southerly flow in October. These changes are captured well by the model. A more detailed comparison of the meteorological conditions is given in Table A.2 in the supplement.

3.4.2 Air quality

We ran the model from 10 October to 19 November 2014 using ECMWF meteorology, and the first two days were set aside as model spin-up. A comparison of hourly modelled pollutants for Beijing and the North China Plain against measurements from the CNEMC network is presented for October in Table 3.3 and the mean spatial distribution of $PM_{2.5}$ during October is shown in Fig. 3.3. We do not include the November period here because emission controls were implemented across Beijing and surrounding provinces from the beginning of November. A more detailed comparison of concentrations on an hourly and daily basis over all model domains is given in Table A.3.

The model overpredicts average surface $PM_{2.5}$ over the period by 5–18% across the three model domains. The correlation for hourly $PM_{2.5}$ improves with resolution, from r=0.47 for domain 1 to 0.63 for domain 3 and 0.68 for the 12 Beijing sites. The model underestimates PM_{10}, although the biases are relatively small (<10%) over Beijing. This may be attributed to neglect of mineral dust sources in the model, which play a relatively small role over Beijing at this time of year. CO is underestimated over much of China, suggesting that the emissions in the inventory are too low, but the biases are relatively small over Beijing, and the variability is captured well. A similar effect is seen for NO_2,

Table 3.3: Comparison of hourly pollutant concentrations with network measurements over the period 12–31 October 2014

	Stations	Obs	Sim	Bias	RMSE	r	slope
$PM_{2.5}$ ($\mu g\,m^{-3}$)							
Beijing stations	12	108.3	126.2	17.9	86.7	0.68	0.83
North China Plain	137	92.6	109.3	16.7	72.2	0.63	0.71
PM_{10} ($\mu g\,m^{-3}$)							
Beijing stations	12	155.4	141.5	-13.9	96.5	0.65	0.79
North China Plain	137	165.7	122.9	-42.8	104.0	0.57	0.50
CO (ppm)							
Beijing stations	12	1.11	0.94	-0.17	0.63	0.60	0.46
North China Plain	137	1.17	0.83	-0.34	0.87	0.29	0.21
NO_2 (ppb)							
Beijing stations	12	39.09	36.09	-3.00	19.33	0.62	0.66
North China Plain	137	29.75	25.88	-3.87	18.95	0.47	0.45
SO_2 (ppb)							
Beijing stations	12	3.92	12.27	8.35	11.88	0.27	0.68
North China Plain	137	13.28	14.47	1.19	13.66	0.21	0.22
O_3 (ppb)							
Beijing stations	12	12.53	12.19	-0.34	13.92	0.47	0.44
North China Plain	137	17.76	18.75	0.99	15.96	0.45	0.43

Where observation data are missing, model values were removed to ensure consistent sampling.

which is underestimated by as much as 45% over parts of China, but by only 8% over the Beijing sites. This may partly reflect better representation of the emission distribution for this shorter-lived pollutant on a finer grid. SO_2 is underestimated by 13% over most of China but is overestimated over Beijing by a factor of 3. The large overestimation for Beijing can be attributed to the recent rapid reduction in emissions in the region between 2010 and 2014 that are not represented in the 2010 inventory (Zheng et al. 2018). Ozone is reproduced well over Beijing, but is overestimated over much of China; this may reflect the bias in NO_2 concentrations, and is likely to be influenced by the urban locations of most of the air quality stations.

For most pollutants, the correlation and slope improve substantially with resolution, and are better on a daily mean basis than at hourly resolution. This suggests that the day-to-day variability driven largely by regional meteorological processes is captured better than the diurnal variations driven by chemistry and local boundary layer mixing, as expected. This is particularly noticeable for ozone, although concentrations of this pollutant remain low at this time of year. Daily mean concentrations are typically used for most metrics of pollutant impacts on human health, and the reasonable model performance for daily averaged data suggests that it is suitable for assessment of these policy-relevant metrics.

The spatial distribution of mean $PM_{2.5}$ concentrations over 12–31 October is shown

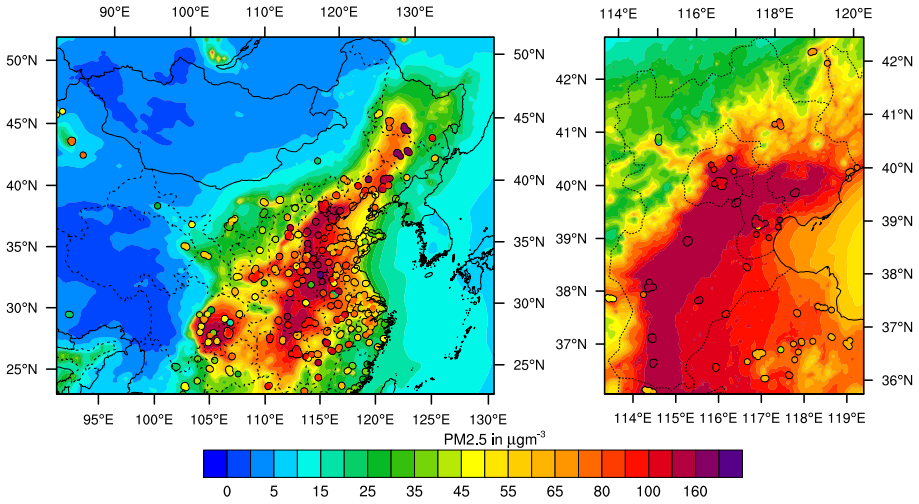

Figure 3.3: Average spatial distribution of $PM_{2.5}$ over the period 12–31 October 2014 for model Domain 1 (China, left) and Domain 3 (North China Plain, right) along with observations shown in circles.

in Fig. 3.3. The distribution is captured reasonably well by the model, with the western parts of China showing clean air with concentrations less than 10 $\mu g\,m^{-3}$) while the eastern, more populous parts of the country show average concentrations of 70–150 $\mu g\,m^{-3}$. Key hotspots over the North China Plain, central China and the Sichuan Basin are reproduced, and concentrations in coastal regions are notably lower, matching observations. The North China Plain is one of the most densely populated parts of the country, incorporating major cities such as Beijing, Tianjin, and Shijiazhuang, and frequently experiences heavy haze episodes with high levels of particulate matter (Wang et al. 2014a, Gao et al. 2015a). The highest concentrations of $PM_{2.5}$ occur on the western side of the North China Plain, where they are trapped by southeasterly winds against the Taihang Mountains, and this is reproduced well by the model. There is a notable east–west gradient as concentrations drop off eastwards towards the coast. Over the mountains to the northwest of Beijing concentrations are much lower, being typically less than 40 $\mu g\,m^{-3}$.

Figure 3.4 shows the time series of key gas-phase and particulate pollutants averaged over the 12 network sites in Beijing. The general synoptic and diurnal patterns of $PM_{2.5}$, PM_{10}, CO, NO_2 and O_3 are reproduced well by the model, including the magnitude of daily maxima and minima. SO_2 is greatly overestimated in October, reflecting recent rapid emission reductions in Beijing (Zheng et al. 2018), and this is consistent with the findings of previous studies (Chen et al. 2016e, Gao et al. 2015a, Guo et al. 2016). However, we note that SO_2 is reproduced much better from 15 November onwards, following the start of the heating season, highlighting the continuing major importance of this source. The observations show that the region experiences clear synoptic patterns of pollutant

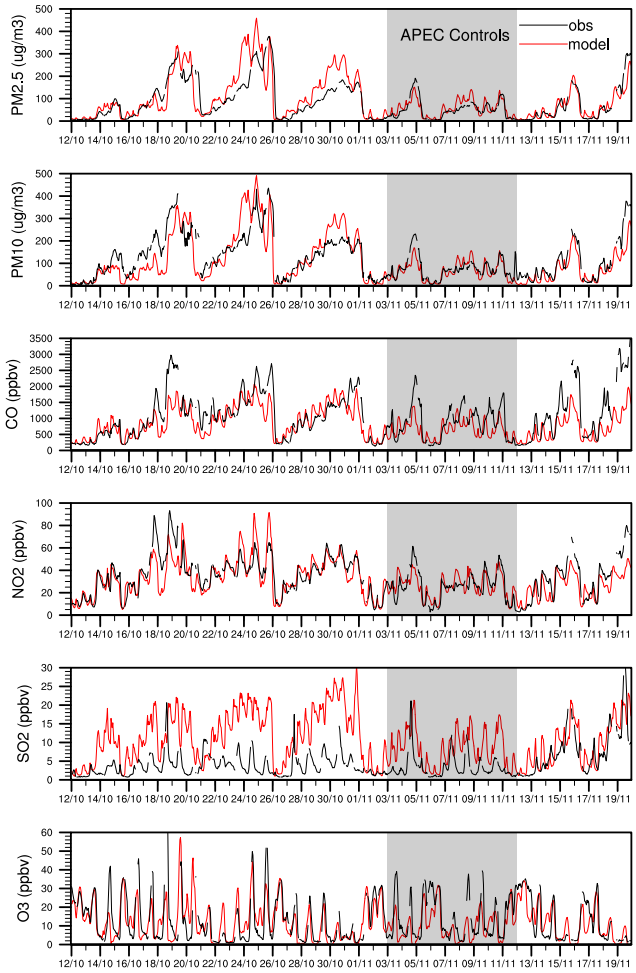

Figure 3.4: Mean time-series of surface pollutants over the 12 air quality stations in Beijing. Model values are with baseline emissions at all times including during the APEC period (shaded).

build-up over 4–5 days followed by sudden clean-out which is typically associated with frontal passage from the northwest (Guo et al. 2014). These synoptic patterns are seen more clearly for particulate matter than for gas-phase pollutants like NO_2 and CO which exhibit a stronger diurnal signal reflecting chemical and dynamical processes. With the exception of SO_2, key pollutants and their variation over this period are reproduced well.

Comparison of aerosol composition with measurements at IAP over this period provides a more critical test of model performance–see Fig. 3.5. The model overestimates BC, NO_3 and NH_4 and underpredicts OC and SO_4 during the three episodes in October. Overestimation of BC likely reflects the reduction in emissions between 2010 and 2014, but may also indicate insufficient removal in the model. The overprediction of NO_3 and NH_4 may be due to uncertainty in NO_2 and NH_3 emissions or to overestimated gas to particle conversion in the model. In particular, secondary production of NO_3 and NH_4 may be overestimated during stagnant conditions during pollution episodes–but matches

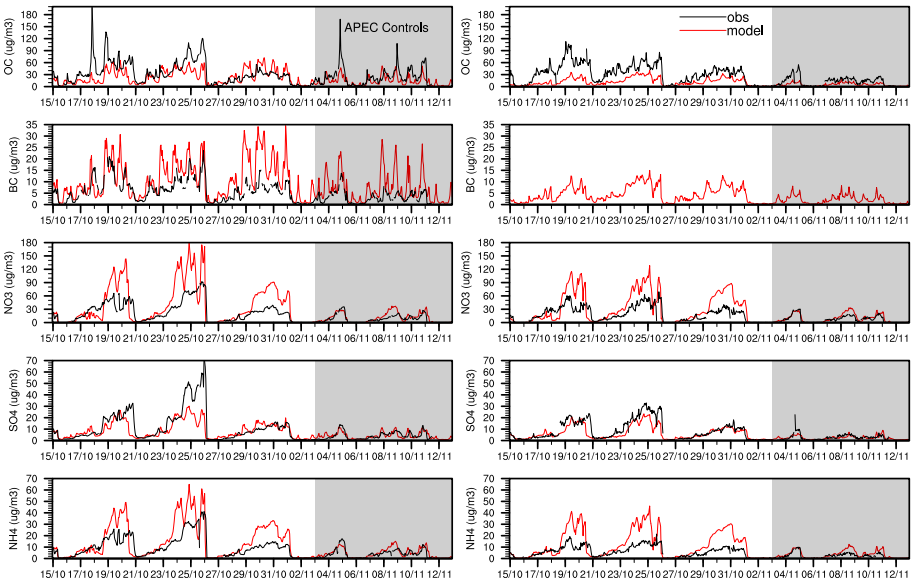

Figure 3.5: Measured and simulated aerosol components at the surface (left) and 260 m (right) on the IAP tower in Beijing. Model values are with baseline emissions at all times including during the APEC period (shaded).

better in November when conditions are less stagnant. The underestimation of SO_4 occurs despite an overestimation of gas-phase SO_2, highlighting insufficient formation of SO_4 in the model. This may also contribute to the overestimation of NO_3 as a decrease in SO_4 frees up ammonia to react with nitric acid and transfers it into the aerosol phase (Seinfeld & Pandis 2006). The underestimation of OC can be explained by the absence of secondary organic aerosol in our studies.

The model captures the vertical gradients of NO_3 and SO_4 well, with drops of 10–15% and 30% between the surface and 260 m, respectively, similar to the drops seen in the observations. However, the model shows a weaker vertical gradient than that observed (22% vs. 33% drop) for NH_4 which can be attributed to higher secondary production of NH_4 in the model. For OC, the model shows a stronger vertical gradient than that observed (53% vs. 12% drop) which reflects the lack of secondary production at elevated levels in the model.

3.5 Investigating model weaknesses

While the baseline model simulation with ECMWF meteorological fields reproduces observed pollutant levels reasonably well, the comparisons have highlighted uncertainties associated with resolution, vertical mixing processes, and aerosol composition. We explore the sensitivity of our results to these factors here.

Table 3.4: Impacts of model resolution on simulation of hourly $PM_{2.5}$ concentrations in ($\mu g\,m^{-3}$) in Beijing over 12–31 October 2014

	Obs mean	Sim mean	Mean Bias	RMSE	r	slope
D03 (3-km)	108.4	126.2	17.8	86.7	0.68	0.83
D02 (9-km)	108.4	128.7	20.3	87.4	0.69	0.85
D01 (27-km)	108.4	123.1	14.7	86.1	0.68	0.81
D01 (no nest)	108.4	99.2	-9.2	83.2	0.59	0.55

3.5.1 Model resolution

To investigate the benefits of high spatial resolution, we sample all three model domains at the 12 Beijing stations and compare the results with observations. To eliminate the influence of two-way nesting, where results from nested domains feed back to the parent domain, we perform an additional simulation at 27 km resolution over the parent domain only. Table 3.4 shows a comparison of modelled $PM_{2.5}$ over Beijing for the different resolutions with measurements in October. In the nested simulation, $PM_{2.5}$ is overestimated by 14% for domain 1, 19% for domain 2 and 16% for domain 3, but is underestimated by 8% for the domain 1 simulation without nesting. Although the mean biases do not improve with higher resolution, reflecting the two-way nesting, there is a substantial improvement in the correlation coefficient (0.59 to 0.68) and slope (0.55 to 0.83) for $PM_{2.5}$ when nesting is used, and this occurs for other pollutants too (see Table A.4). For many variables the results sampled at 9 km resolution (Domain 2) are slightly better than those sampled at 3-km resolution (Domain 3). Results at 27 km resolution without nesting are substantially less good than those with two-way nesting, highlighting the important contribution of the coupling. We conclude that it is worth performing simulations at higher horizontal resolution as it gives a better representation of urban pollution levels.

3.5.2 Boundary layer mixing

Representing turbulent mixing processes in the boundary layer well is critical for simulating surface air quality. The nighttime boundary layer under stable meteorological conditions is particularly difficult to model, and we find that the mixing height is often severely underpredicted (as low as 20 m on some occasions), causing pollutant concentrations to reach unrealistically high levels. Nudging meteorological fields to ECMWF reanalysis data reduces this bias but does not remove it. After testing a number of different boundary layer algorithms we selected the Yonsei University (YSU) scheme (Hong et al. 2006), as it provides the best overall match to lidar-derived observations of boundary layer height. However, stable conditions remain a challenge for this scheme, and we therefore explore

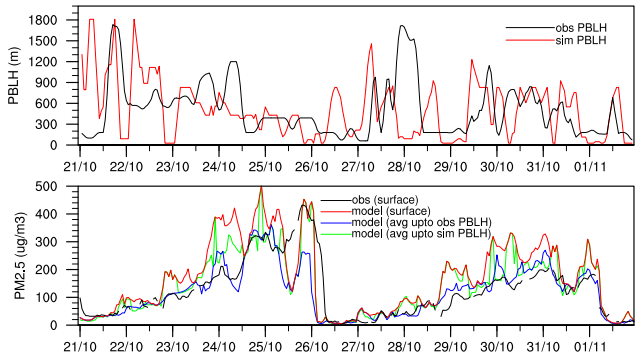

Figure 3.6: Simulated and observed boundary layer mixing height in metres (top) and simulated and observed $PM_{2.5}$ in $\mu g\,m^{-3}$ showing the effect of mixing up to the PBL height in the model (bottom) between 21 October and 1 November 2014.

the sensitivity of simulated surface concentrations to boundary layer mixing under these conditions.

Figure 3.6 shows the time series of simulated and observed planetary boundary layer (PBL) height. The observed PBL height was derived from lidar extinction profiles at IAP using the cubic root gradient method of Yang et al. (2017). The simulated PBL height was diagnosed using the maximum decrease in the modelled $PM_{2.5}$ profile to ensure a consistent definition. We compare the observed PBL height with the simulated height at IAP, and use $PM_{2.5}$ measurements from the surface pollutant station at Aotizhongxin, the closest station to the IAP site (within 2 km) to assess the effect on $PM_{2.5}$ concentrations. The PBL height shows highly variable behaviour over the day and from day to day. While the average model PBL height (514 m) is similar to the average observed PBLH height (509 m) over the haze episodes shown, the nighttime PBL height is severely underpredicted on a number of occasions. Assuming that the PBL height reflects the efficiency of mixing in the boundary layer, we expect the model to overpredict surface pollutant concentrations under these stable nighttime conditions, and this is seen in the time series of $PM_{2.5}$ in Fig. 3.6. To account for misrepresentation of local boundary layer mixing, we post-process the model results by vertically mixing $PM_{2.5}$ up to the simulated mixing height, to eliminate the effect of underestimated mixing, and up to the observed mixing height, to provide a direct comparison against $PM_{2.5}$ observations. Averaging up to the observed PBL height gives a substantial improvement in $PM_{2.5}$ levels compared to observations, particularly for the episodes of 21–25 October and 27 October–1 November when the model underestimates the PBL height. The simulated mean surface $PM_{2.5}$ concentration during the period is reduced from 169 to 118 $\mu g\,m^{-3}$ (the observed mean is 129 $\mu g\,m^{-3}$) and the root-mean-square-error (RMSE) is reduced from 94 to 65 $\mu g\,m^{-3}$; and the biases in NO_3, NH_4 and

BC are significantly reduced. For a more detailed analysis of component-level sensitivity to boundary layer mixing see Figure A.1 and Table A.5 in the supplement.

These results highlight the importance of representing PBL mixing well for accurate reproduction of surface pollutant levels. We note a steady decline in PBL height over the pollution episode during 21–25 October, and $PM_{2.5}$ shows a consistent build-up over this period. This provides observational evidence for the radiative feedback between aerosol concentrations and mixing height, and this appears to be captured relatively well by the model, as shown in previous studies (Gao et al. 2015b). Further improvement in simulation of surface pollutant concentrations requires additional research on representation of PBL mixing processes in urban environments. Profiles of aerosol and meteorological variables from high-resolution lidar measurements provide an important aid to such investigations.

3.5.3 Regional NH_3 emissions

The aerosol components NO_3 and NH_4 are overestimated in these simulations, as shown in Fig. 3.5. These components are governed by secondary production from their gaseous precursors NO_2 and NH_3. Since the concentration of NO_2 is close to that observed, we perform a short sensitivity study over the pollution episode from 21–25 October with NH_3 emissions over the North China Plain reduced by 50% to explore the response of NO_3 and NH_4 to ammonia emissions in the model. We find that the reduction in NH_3 emissions reduces NH_4 and NO_3 concentrations substantially and brings them closer to observations (see Table 3.5 and Figure A.3). This is likely because NH_3 is the limiting reactant in the formation of NH_4NO_3 that directly controls the concentration of both NH_4 and NO_3 aerosols in the North China Plain (Gao et al. 2016b, Chen et al. 2016e). However, reduction in SO_4 concentrations is small ($1\,\mu g\,m^{-3}$) because SO_4 formation is only indirectly associated with NH_3 availability (Tsimpidi et al. 2007). Total $PM_{2.5}$ concentrations are reduced by approximately 26% bringing them closer to observed concentrations. Ammonia emissions were reported to be 1574 kt/yr over the Beijing–Tianjin–Hebei region in 2010 (Zhou et al. 2015) while those in the MEIC emission inventory used here are only 540 kt/yr. Given that our NH_3 emissions are already low compared with other studies (Kang et al. 2016), we do not reduce them further in this study. However, we have demonstrated that $PM_{2.5}$ concentrations during this period are highly sensitive to NH_3 emissions, consistent with the findings of other studies (Zhang et al. 2016a), and highlight this issue for further investigation.

Table 3.5: Mean concentrations (in $\mu g\,m^{-3}$) at IAP during 21–25 October 2014

Species	Control run	Reduced NH_3 run	Observations
$PM_{2.5}$	210.8	154.9	157.5
NO_3	61.28	36.60	33.81
NH_4	23.11	15.24	15.03
SO_4	12.70	11.59	20.40

Table 3.6: Emission controls during APEC period

Emission sector	Emission reduction (%)	
	Beijing	Other districts
Industry	50	35
Power	50	35
Agriculture	40	30
Residential	40	30
Transport	40	30
PM coarse (all sectors)	80	–

APEC1: Beijing, Langfang, Baoding, Shijiazhuang, Xingtai, Handan; APEC2: APEC1 + Tangshan, Tianjin, Cangzhou, Hengshui, Dezhou, Binzhou, Dongying, Zibo, Jinan and Liaocheng

3.6 APEC emission controls

The Asia-Pacific Economic Cooperation (APEC) summit was held from 10–12 November 2014 in Beijing, and was the focus of short-term emission controls to ensure good air quality over the period. Emission controls were applied in Beijing and surrounding regions including Tianjin, the provinces of Hebei, Shanxi, and Shandong; and Inner Mongolia Autonomous Region. More than 460 businesses with high emissions in Beijing were required to limit or stop their production during 3–12 November 2014 (Tang et al. 2015, Wang et al. 2016a, Guo et al. 2016). The number of private vehicles in operation over this period was reduced by about 50% through odd-even license-plate restrictions. Furthermore, 9300 enterprises were suspended, 3900 enterprises were ordered to limit production, and more than 40,000 construction sites were shut down across the northern China region (Wang et al. 2016c, Tang et al. 2015). The start-up of municipal winter heating systems was delayed until 15 November, after the summit. Previous studies report that implementation of these emission controls resulted in significant impacts on regional pollutant transport and local pollutant contributions (Meng et al. 2014, Sun et al. 2016b, Gao et al. 2017).

Previous model studies of the APEC period have adopted different estimates of the emission reductions imposed (Guo et al. 2016, Gao et al. 2017, Wen et al. 2016, Liu et al. 2017, Wang et al. 2017a). The most detailed study of emission reductions considered

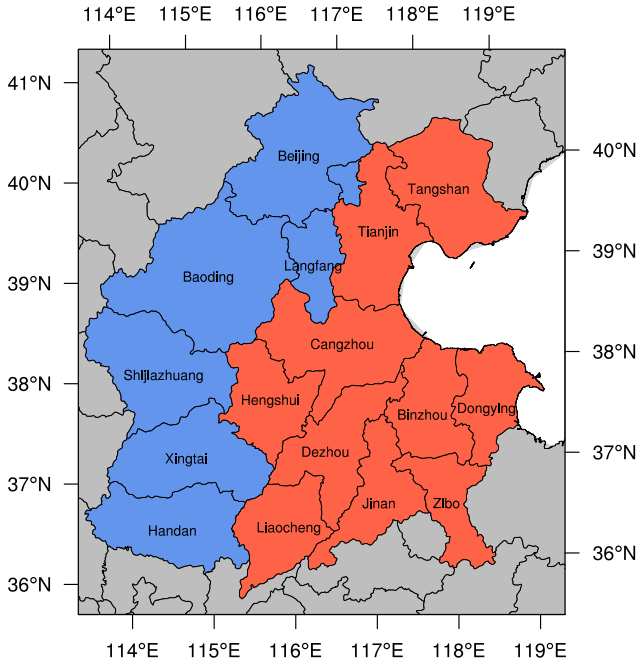

Figure 3.7: Map of districts where major emissions controls were implemented during the APEC period. During phase 1 emissions were focused on Beijing and western Hebei (blue) and in phase 2 additional controls were applied over other parts of the North China Plain (red).

application of controls in two distinct phases (Wen et al. 2016), and we have chosen to implement these controls in our study, as the emission reductions applied are consistent with observation-based assessments of regional emission controls (Li et al. 2017d). During the initial phase (APEC1; 3–5 November), emission controls were implemented in Beijing and the western side of the North China Plain. In a subsequent phase (APEC2; 6–12 November) controls were applied over a wider region including eastern Hebei and parts of Shandong. We represent these controls in the model over the districts shown in Fig. 3.7, following Li et al. (2017d), and neglect smaller changes in emissions in other districts and more distant provinces. Controls were applied across different activity sectors following Wen et al. (2016) and Li et al. (2017d), see Table 3.6.

Figure 3.8 shows the effect of these controls on key pollutants over the period 3–12 November. There is a minor pollution episode over 4–5 November, and the model underestimates $PM_{2.5}$ levels over this period even without emission controls. This may partly reflect an underestimation of OC as the simulation of secondary inorganic aerosol for these two days is good (see Fig. 3.5). $PM_{2.5}$ levels are very well matched in the period 6–9 November leading up to the summit when emission controls are applied. PM_{10} levels are underestimated in the simulations, but this is influenced by what may be a minor dust episode on 11–12 November, when coarse particles were high but $PM_{2.5}$ remained very

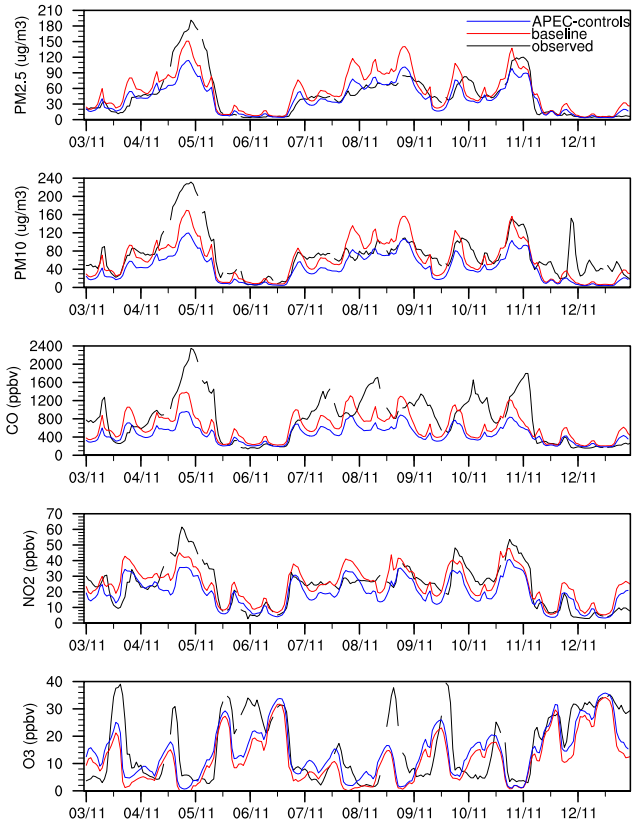

Figure 3.8: Time series of surface pollutants averaged over the 12 measurement stations in Beijing during the APEC period.

low. Overall, the controls had a notable effect, reducing concentrations by 20–30% for all pollutants except O_3, which showed a small increase as expected with reduced levels of NO. Over the critical 10–12 November meeting period, $PM_{2.5}$, PM_{10}, CO and NO_2 were reduced by 21%, 26%, 22% and 22%, respectively (see Table 3.7). The reduction in $PM_{2.5}$ is very similar to the 22% reduction found in previous studies (Gao et al. 2017). However, the absolute improvement in air quality over the meeting period was small, averaging less than $10\,\mu g\,m^{-3}$ for $PM_{2.5}$, reflecting the relatively clean conditions over the period. Average $PM_{2.5}$ in the baseline simulation was $39\,\mu g\,m^{-3}$, close to the observed $36\,\mu g\,m^{-3}$. Under these conditions the key air quality standard, a 24-hour averaged $PM_{2.5}$ of $75\,\mu g\,m^{-3}$, corresponding to a Chinese Air Quality Index (AQI) value of 100, would have been met in the model simulation even without the controls.

To explore the importance of meteorological conditions in contributing to favourable air quality during the APEC period, we apply the same magnitude, location and duration of emission controls to the major pollution episode at the end of October. Fig 3.9 shows the effect of these controls on key pollutants over 16–25 October. The controls reduced pollutant concentrations by a larger amount than during the APEC period, but the relative improvements of 23–38% were very similar. The absolute pollutant concentrations were

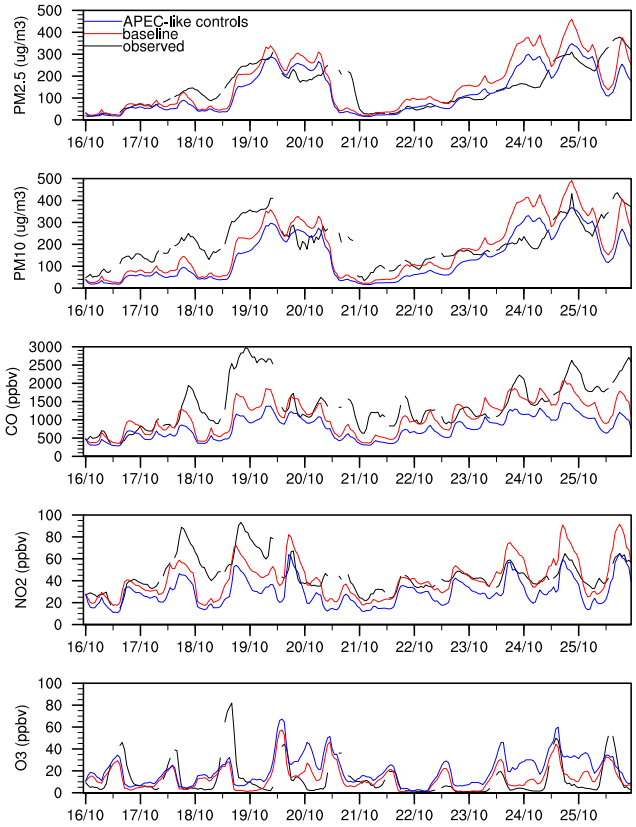

Figure 3.9: Time series of surface pollutants averaged over the 12 measurement stations in Beijing during 16–25 October 2014.

much higher than in November. This can be attributed to lower wind speeds and to winds from the south and east bringing air from across the North China Plain, in contrast to the APEC period which experienced higher wind speeds and more frequent air from the clean northwest sector (see Figure 3.2). The 3-day baseline average concentrations over 23–25 October for $PM_{2.5}$, PM_{10}, CO, and NO_2 were 279 $\mu g\,m^{-3}$,310 $\mu g\,m^{-3}$, 1.48 ppm, and 53 ppb, respectively, substantially exceeding air quality standards. The difference in baseline $PM_{2.5}$ concentrations between the October and November periods without emission controls, 279 vs. 39 $\mu g\,m^{-3}$, highlights the dominant role played by meteorology in bringing clean air during APEC. The emission controls have a much larger absolute effect during the October episode than in the APEC period, with reductions in $PM_{2.5}$ of 65 $\mu g\,m^{-3}$ for 23–25 October, bringing average $PM_{2.5}$ levels down to 214 $\mu g\,m^{-3}$. However, this is insufficient in meeting the standard needed for clean air of 75 $\mu g\,m^{-3}$. This indicates that the same emission control policies applied would have failed to produce the desired results if the meeting had been held at the end of October.

Table 3.8 presents the effect on aerosol components and gas-phase pollutants at the IAP tower. During the emission controls in both the polluted October and cleaner November periods, primary components were reduced by 31–34% while secondary components were

reduced by only 3–17%. This suggests that pollution episodes dominated by primary aerosols may be more easily controlled and has serious implications for winter haze episodes over the North China Plain because much of the increase in aerosol loading is contributed by regional secondary aerosols (see Sun et al. 2016b). The percentage reduction in SO_4 (14–17%) may be overestimated as some fraction of SO_4 mass for which chemical formation pathway remains unknown is treated as primary aerosol in the model. Similarly, the percentage reduction in OC may be overestimated because all OC is primary in the model.

To investigate the feasibility of meeting air quality standards during pollution episodes such as that on 21–25 October, we ran the model with all anthropogenic emissions removed over the North China Plain from 16–25 October. The 3-day average concentrations over 23–25 October showed substantial reductions: 83% for $PM_{2.5}$, 82% for PM_{10}, 79% for CO, 99% for NO_2 and 88% for SO_2. Average $PM_{2.5}$ concentrations were reduced from 279 $\mu g\,m^{-3}$ to 48 $\mu g\,m^{-3}$, demonstrating that air quality standards can be met on highly polluted days, at least in theory, under the most stringent emission controls. From this simulation, and accounting for nonlinearity in secondary aerosol formation, we estimate that a 92% emission reduction over the 10 day period would have been needed to keep the average concentrations for 23–25th October below 75 $\mu g\,m^{-3}$. Even accounting for model overestimation of average $PM_{2.5}$ during this period, driven principally by the positive bias on 24 October, we find that an 85% emission reduction would be required, which is substantially more than what is feasible realistically. It is clear from this analysis that emission controls would need to be applied over a much wider area over neighbouring provinces if the air quality standards in Beijing are to be met.

Finally, we analyse the full simulation period (12 October–19 November) to investigate how many days would meet the "blue-sky" criteria of 24-hour average $PM_{2.5}$ concentrations less than 75 $\mu g\,m^{-3}$ with and without APEC-like controls. We conducted another simulation with APEC2 controls implemented over the full period and found a reduction in daily average $PM_{2.5}$ of $26 \pm 6\%$, and a reduction of $23 \pm 4\%$ for haze days with daily mean $PM_{2.5}$ $>75\,\mu g\,m^{-3}$. Since primary and secondary aerosol components can respond differently to emission controls, we use component-level fractional reductions from the model and apply them to the observed component concentrations to find the reduction in total PM. This is approximately 22% for both October and November periods based on our APEC control runs, suggesting that this scaling is appropriate and robust to uncertainties in model aerosol composition. To generate an emission controls scenario over the full period, we reduce daily mean observed $PM_{2.5}$ concentrations by 22% for all days except 3–12 November when controls were actually in place. For this 3–12 November period we

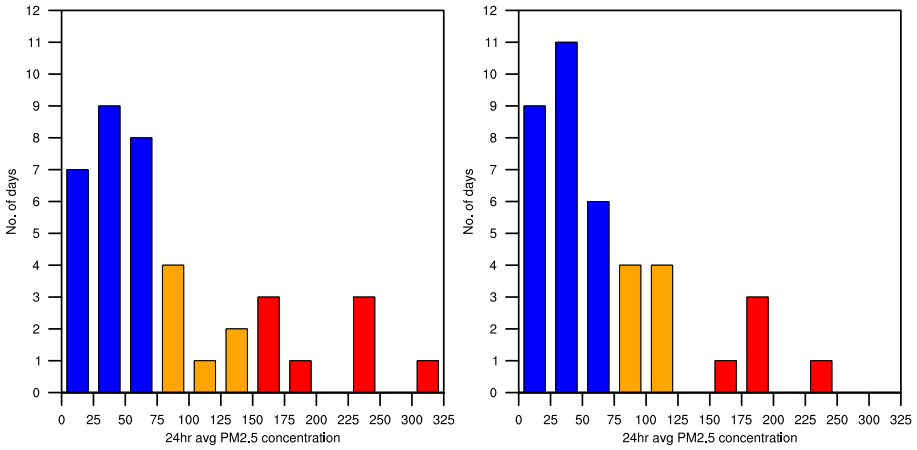

Figure 3.10: Frequency distribution of daily average $PM_{2.5}$ over 12 October–19 November 2014 showing the number of days meeting thresholds of 75 µg m^{-3} (blue) and 150 µg m^{-3} (blue plus orange) without (left panel) and with (right panel) emission controls.

apply an increase of 16–33% based on the APEC controls run to represent conditions with no controls. With these scenarios we find that 15 of the 39 days considered failed to meet the blue-sky criteria of daily average $PM_{2.5}$ concentrations less than 75 µg m^{-3} without controls, and this fell to 13 days when the controls were implemented, a modest decrease of 2 days, see Fig. 3.10. However, if we choose a higher threshold of 150 µg m^{-3} (AQI of 200), the emission controls appear more effective, reducing the number of exceedances from 8 days to 5 days, and with a threshold of 200 µg m^{-3} (AQI of 250) the number of exceedances falls from 4 days to 1 day.

To organize a three-day meeting such as APEC successfully, all three days must individually meet the chosen air quality criteria. We find that without emission controls, only 9 out of 37 possible three-day time slots in our simulation period meet the criteria, including only 3 out of the 8 available during the APEC period of 3–12 November. Under the emission controls, the meeting could have been organized on 14 out of the 37 slots, including all 8 during early November. This suggests that the emission controls were only sufficient to provide an additional 5 time slots to hold a three-day event meeting the criteria. Interestingly, these all occur during the APEC period, highlighting that while favourable weather conditions were vital for meeting the air quality criteria, the emission controls provided critical support in achieving the 75 µg m^{-3} threshold needed to realize blue-sky conditions. Specifically, in the absence of emission controls the first day of the APEC meeting (10 November) would have exceeded the air quality standards. In this respect, it is reasonable to claim that the APEC emission controls were a success. However, it is clear that favourable meteorology was essential in making it possible for the emission

Table 3.7: Influence of emission controls averaged over Beijing air quality stations in October and November

Species	Observed	Model		
	Mean	Baseline	Controls	Improvement
APEC period (10–12 November)				
$PM_{2.5}$ ($\mu g\,m^{-3}$)	36.1	39.3	31.1	8.2 (21%)
PM_{10} ($\mu g\,m^{-3}$)	65.3	43.9	32.5	11.4 (26%)
CO (ppm)	0.64	0.48	0.38	0.11 (22%)
NO_2 (ppb)	19.0	20.6	16.0	4.6 (22%)
SO_2 (ppb)	2.1	6.1	4.2	1.9 (30%)
O_3 (ppb)	20.0	16.5	19.0	-2.5 (-15%)
October period (23–25 October)				
$PM_{2.5}$ ($\mu g\,m^{-3}$)	216.1	278.8	213.7	65.1 (23%)
PM_{10} ($\mu g\,m^{-3}$)	263.8	309.6	236.4	73.2 (24%)
CO (ppm)	1.77	1.48	1.05	0.44 (30%)
NO_2 (ppb)	46.3	53.2	34.9	18.3 (34%)
SO_2 (ppb)	4.0	18.6	11.6	7.0 (38%)
O_3 (ppb)	11.4	15.2	26.7	-11.5 (-76%)

controls to produce the marginal improvements needed to meet the air quality standards.

It should be noted that 23 out of the 37 possible three-day time periods (more than 60%) would not have met the standards even under the emission controls applied. It is therefore clear that much more stringent controls are needed in future to counter the effect of unfavourable meteorological conditions. While greater reductions in the magnitude of emissions are required, it is important that these are applied over a much larger area, including in the neighbouring provinces that surround the North China Plain.

3.7 Conclusions

We have demonstrated that using a high-resolution nested air quality model we can reproduce the observed hourly variation of major pollutants in Beijing during October–November 2014 reasonably well. We capture the synoptic drivers of air quality well, including the build-up of pollutants during pollution episodes and the subsequent cleaning effect of winds from the northwest. The concentrations of $PM_{2.5}$, the dominant pollutant in this season, are reproduced well, and we show that where the model is biased high, typically during nighttime, underlying weaknesses in the treatment of turbulent mixing in the planetary boundary layer are often responsible. We show that use of two-way nesting to high resolution brings a substantial benefit in reproducing observed pollutant concentrations, even when comparing at the coarsest resolution used. Thorough evaluation against aerosol composition measurements over the period highlights some weaknesses in repre-

Table 3.8: Influence of emission controls at the IAP site in October and November

Species	Observed	Model		
	Mean	Baseline	Controls	Improvement
APEC period (10–12 November)				
OC ($\mu g\,m^{-3}$)	30.6	9.8	6.8	3.1 (31%)
BC ($\mu g\,m^{-3}$)	3.4	4.8	3.2	1.6 (34%)
NO_3 ($\mu g\,m^{-3}$)	10.9	8.6	8.3	0.3 (3%)
NH_4 ($\mu g\,m^{-3}$)	5.0	3.8	3.5	0.3 (8%)
SO_4 ($\mu g\,m^{-3}$)	4.8	3.5	2.9	0.6 (17%)
CO (ppm)	2.60	0.68	0.52	0.16 (24%)
NO_2 (ppb)	17.2	30.2	22.9	7.4 (24%)
SO_2 (ppb)	10.4	9.4	6.3	3.1 (33%)
O_3 (ppb)	3.5	17.6	21.6	-4.0 (-23%)
October period (23–25 October)				
OC ($\mu g\,m^{-3}$)	60.5	39.5	26.7	12.8 (32%)
BC ($\mu g\,m^{-3}$)	10.2	16.5	11.0	5.5 (33%)
NO_3 ($\mu g\,m^{-3}$)	51.3	95.0	79.7	15.3 (16%)
NH_4 ($\mu g\,m^{-3}$)	21.1	35.2	29.9	5.4 (15%)
SO_4 ($\mu g\,m^{-3}$)	31.2	18.4	15.8	2.5 (14%)
CO (ppm)	2.92	2.03	1.43	0.60 (30%)
NO_2 (ppb)	44.2	78.1	57.8	20.3 (26%)
SO_2 (ppb)	18.4	26.5	16.5	9.9 (37%)
O_3 (ppb)	5.9	10.3	22.1	-11.8 (-115%)

sentation of key aerosol components, particularly the balance between SO_4, NO_3 and NH_3 which requires more detailed analysis.

We show that short-term emission controls played a valuable role in improving air quality over the APEC period, but that their overall contribution was relatively small, with average reductions of 20–26% for key pollutants. Without the controls, average $PM_{2.5}$ levels are likely to have exceeded the national standard of $75\,\mu g\,m^{-3}$ on 10 November, the first day of the APEC meeting, but the effects were largely incremental, highlighting the important role played by favourable meteorology during the period. If the APEC meeting had been held at a different time, particularly at the end of October, air quality standards would not have been achieved with the emission controls applied. We find that the relative effect of the controls during the pollution episodes of late October is very similar to that during the clean APEC period, averaging 23% for $PM_{2.5}$. Much greater emission reductions of at least 85% would have been needed over the North China Plain region to bring pollutant levels down to meet air quality standards. It is clear that under the stable meteorological conditions present during these pollution episodes, much more stringent emission controls are needed than those that were applied and that these need to be implemented over a much wider region of northern China. Our study demonstrates

the value of short-term emission controls but highlights that long-term, sustained emission reductions on a regional scale are required to bring blue skies to Beijing.

APPENDIX A

Supplementary material for chapter 3

The contents shown in this appendix were submitted as supplementary material for (Ansari et al. 2019a) to Atmospheric Chemistry and Physics. A comprehensive domain-based statistical evaluation of hourly model output is performed against hourly observations from 324 meteorological stations and 1312 pollutant stations across China. Meteorological evaluation is performed for both FNL- and ECMWF-driven model runs (Figure A.1). The distinct meteorology during pre-APEC and APEC period is highlighted in Figure A.2. For air quality evaluation, separate statistical metrics are provided for hourly and daily mean model performance (Figure A.3). Increase in signal through increase in model resolution is presented for all pollutants by sampling model output corresponding to Beijing stations from each domain (Figure A.4). Effect of turbulent mixing up to the model level corresponding to the observed boundary layer height is shown in Figure A.1 and compared with observations in Table A.5. Meteorological evaluation for the bottom five model levels against IAP tower measurements is shown in Figure A.2. Effect of NH_3 emission reduction on inorganic aerosol components is shown in Figure A.3

Tables A.1,A.3 and A.4 were originally part of the manuscript but were asked to be moved to supplement by one of the reviewers.

Table A.1: Comparison of observed and simulated meteorological variables for the entire period using FNL and ECMWF fields

	Number of Stations	Obs. avg.	Sim avg		Bias		RMSE		r	
			FNL	ECMWF	FNL	ECMWF	FNL	ECMWF	FNL	ECMWF
2-m Temperature (°C)										
Beijing	1	9.68	11.52	11.44	1.84	1.76	3.28	3.36	0.88	0.87
D03	30	8.91	8.98	8.95	0.07	0.04	2.47	2.46	0.94	0.94
D02	77	7.87	7.53	7.55	-0.34	-0.32	2.39	2.35	0.95	0.95
D01	324	9.62	7.77	7.79	-1.85	-1.83	3.23	3.23	0.94	0.94
2-m Relative Humidity (%)										
Beijing	1	54.7	34.1	39.1	-20.6	-15.6	26.9	22.4	0.77	0.81
D03	30	54.9	44.8	48.9	-10.1	-6.0	19.6	16.7	0.75	0.78
D02	77	54.4	47.8	51.1	-6.6	-3.3	17.4	15.2	0.74	0.78
D01	324	62.8	60.4	62.6	-2.4	-0.2	16.8	15.6	0.73	0.76
10-m Wind Speed ($m s^{-1}$)										
Beijing	1	5.41	2.27	2.24	-3.14	-3.17	4.98	5.09	0.72	0.69
D03	30	5.73	3.26	3.20	-2.47	-2.53	4.60	4.65	0.62	0.61
D02	77	6.18	3.60	3.55	-2.58	-2.63	4.52	4.55	0.67	0.66
D01	324	5.67	3.38	3.36	-2.29	-2.31	4.29	4.30	0.60	0.61
10-m Wind Direction (°)										
Beijing	1	197.5	214.2	191.0	16.7	-6.6	73.9	73.9	0.79	0.80
D03	30	215.1	210.0	206.5	-6.9	-8.6	62.7	63.4	0.78	0.78
D02	77	214.4	212.2	208.9	-2.8	-5.5	65.4	65.4	0.76	0.76
D01	324	206.5	193.4	188.4	-13.1	-18.0	71.9	72.2	0.74	0.74

Table A.2: Meteorological performance over Beijing during pre-APEC and APEC period

	Obs. avg.	Sim. avg.	Mean bias	RMSE	R
2 m Temperature (°C)					
Episode 1	14.63	16.84	2.21	3.79	0.79
Episode 2	12.15	14.47	2.32	3.28	0.74
Episode 3	11.35	11.76	0.41	1.78	0.86
APEC period	7.14	9.14	2.00	3.76	0.82
Relative Humidity (%)					
Episode 1	61.9	41.4	-20.6	26.6	0.76
Episode 2	74.3	52.7	-21.5	26.0	0.74
Episode 3	55.6	41.3	-14.3	19.5	0.89
APEC period	47.0	34.4	-12.6	21.2	0.82
Wind Speed ($m s^{-1}$)					
Episode 1	5.30	2.45	-2.85	4.86	0.74
Episode 2	3.50	1.82	-1.68	2.76	0.56
Episode 3	5.46	2.07	-3.39	5.35	0.79
APEC period	6.50	2.56	-3.94	6.06	0.67
Wind Direction (°)					
Episode 1	176.9	172.9	-4.1	63.5	0.78
Episode 2	148.6	141.4	-7.3	74.9	0.85
Episode 3	143.6	163.4	19.7	62.1	0.88
APEC period	257.3	220.8	-36.5	69.4	0.79

Table A.3: Comparison of pollutant concentrations with network measurements over the period 12–31 October 2014

	Number of Stations	Obs	Sim	Bias	RMSE hourly/daily	r hourly/daily	slope hourly/daily
$PM_{2.5}$ ($\mu g\,m^{-3}$)							
Beijing stations	12	108.3	126.2	17.9	86.7/66.7	0.68/0.78	0.83/0.93
D03	137	92.6	109.3	16.7	72.2/52.2	0.63/0.74	0.71/0.80
D02	375	75.8	87.9	12.1	63.9/48.6	0.60/0.69	0.65/0.71
D01	1312	71.1	74.8	3.7	61.1/50.2	0.47/0.53	0.48/0.54
PM_{10} ($\mu g\,m^{-3}$)							
Beijing stations	12	155.4	141.5	-13.9	96.5/74.0	0.65/0.77	0.79/0.98
D03	137	165.7	122.9	-42.8	104.0/82.1	0.57/0.68	0.50/0.58
D02	375	138.0	98.6	-39.4	94.3/75.8	0.54/0.65	0.44/0.52
D01	1312	121.0	82.2	-38.8	89.0/76.7	0.42/0.47	0.32/0.37
CO (ppm)							
Beijing stations	12	1.11	0.94	-0.17	0.63/0.43	0.60/0.75	0.46/0.61
D03	137	1.17	0.83	-0.34	0.87/0.72	0.29/0.34	0.21/0.22
D02	375	1.14	0.66	-0.48	0.88/0.79	0.33/0.37	0.20/0.20
D01	1312	1.00	0.50	-0.50	0.79/0.73	0.32/0.34	0.13/0.14
NO_2 (ppb)							
Beijing stations	12	39.09	36.09	-3.00	19.33/11.10	0.62/0.80	0.66/0.83
D03	137	29.75	25.88	-3.87	18.95/14.32	0.47/0.54	0.45/0.51
D02	375	24.86	19.45	-5.41	16.99/13.21	0.49/0.55	0.44/0.50
D01	1312	22.73	12.45	-10.28	18.33/15.44	0.42/0.47	0.30/0.36
SO_2 (ppb)							
Beijing stations	12	3.92	12.27	8.35	11.88/10.55	0.27/0.52	0.68/1.74
D03	137	13.28	14.47	1.19	13.66/9.66	0.21/0.31	0.22/0.24
D02	375	12.23	13.21	0.98	13.19/9.01	0.24/0.34	0.26/0.28
D01	1312	10.27	8.93	-1.34	11.17/8.54	0.19/0.28	0.18/0.24
O_3 (ppb)							
Beijing stations	12	12.53	12.19	-0.34	13.92/6.49	0.47/0.67	0.44/0.82
D03	137	17.76	18.75	0.99	15.96/10.88	0.45/0.49	0.43/0.50
D02	375	21.23	23.08	1.85	17.19/12.80	0.42/0.43	0.37/0.40
D01	1312	21.44	32.29	10.85	22.44/17.03	0.29/0.27	0.27/0.25

Table A.4: Impacts of model resolution on simulation of hourly pollutant concentrations in Beijing over 12–31 October 2014

	N points	Obs mean	Sim mean	Mean Bias	RMSE	r	slope
$PM_{2.5}$ ($\mu g\,m^{-3}$)							
D03 (3-km)	3171	108.4	126.2	17.8	86.7	0.68	0.83
D02 (9-km)	3171	108.4	128.7	20.3	87.4	0.69	0.85
D01 (27-km)	3171	108.4	123.1	14.7	86.1	0.68	0.81
D01 (no nest)	3171	108.4	99.2	-9.2	83.2	0.59	0.55
PM_{10} ($\mu g\,m^{-3}$)							
D03	2670	155.4	141.5	-13.9	96.5	0.65	0.79
D02	2670	155.4	143.6	-11.8	96.6	0.65	0.80
D01	2670	155.4	137.9	-17.5	96.6	0.65	0.79
D01 (no nest)	2670	155.4	111.2	-44.2	99.8	0.58	0.54
CO (ppm)							
D03	3074	1.11	0.94	-0.17	0.63	0.60	0.46
D02	3074	1.11	0.95	-0.16	0.61	0.61	0.47
D01	3074	1.11	0.88	-0.23	0.61	0.64	0.44
D01 (no nest)	3074	1.11	0.68	-0.43	0.73	0.62	0.31
NO_2 (ppb)							
D03	3080	39.09	36.09	-3.00	19.33	0.62	0.66
D02	3080	39.09	35.55	-3.54	19.34	0.62	0.64
D01	3080	39.09	31.92	-7.17	18.33	0.67	0.62
D01 (no nest)	3080	39.09	21.81	-17.28	24.74	0.60	0.48
SO_2 (ppb)							
D03	3074	3.92	12.27	8.35	11.88	0.27	0.68
D02	3074	3.92	12.15	8.23	11.64	0.27	0.66
D01	3074	3.92	10.91	6.99	9.82	0.32	0.69
D01 (no nest)	3074	3.92	6.47	2.55	5.57	0.29	0.40
O_3 (ppb)							
D03	3046	12.56	12.19	-0.37	13.92	0.47	0.44
D02	3046	12.56	12.71	0.15	13.94	0.47	0.43
D01	3046	12.56	14.96	2.40	13.53	0.49	0.44
D01 (no nest)	3046	12.56	17.59	5.03	14.08	0.51	0.45

Table A.5: Comparison of simulated aerosol components in $\mu g\,m^{-3}$ with and without mixing up to observed boundary layer height against surface observations at IAP site

	Obs. avg.	Sim avg		Mean Bias		RMSE	
Components		surface	mixed	surface	mixed	surface	mixed
OC	31.08	23.24	12.86	-7.84	-18.22	21.43	27.30
BC	6.13	10.19	4.96	4.06	-1.16	5.96	3.27
NO3	23.30	36.73	29.42	13.44	6.12	25.47	18.00
SO4	13.16	8.12	6.27	-5.03	-6.89	12.05	13.67
NH4	10.36	14.16	11.12	3.80	0.78	8.05	6.40

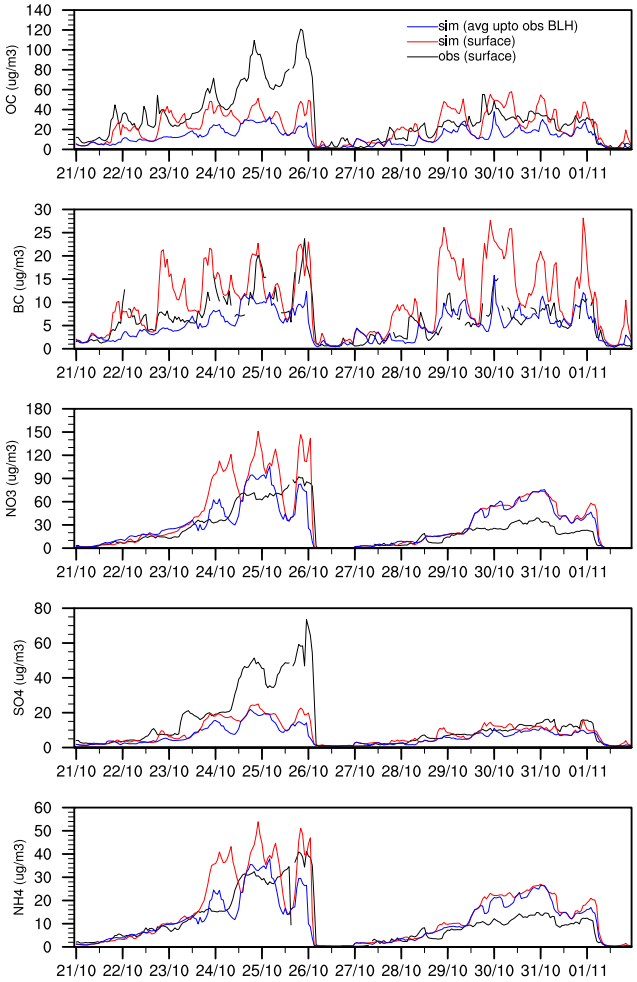

Figure A.1: Time-series of simulated aerosol components with and without averaging up to observed boundary layer height against surface observations at the IAP site.

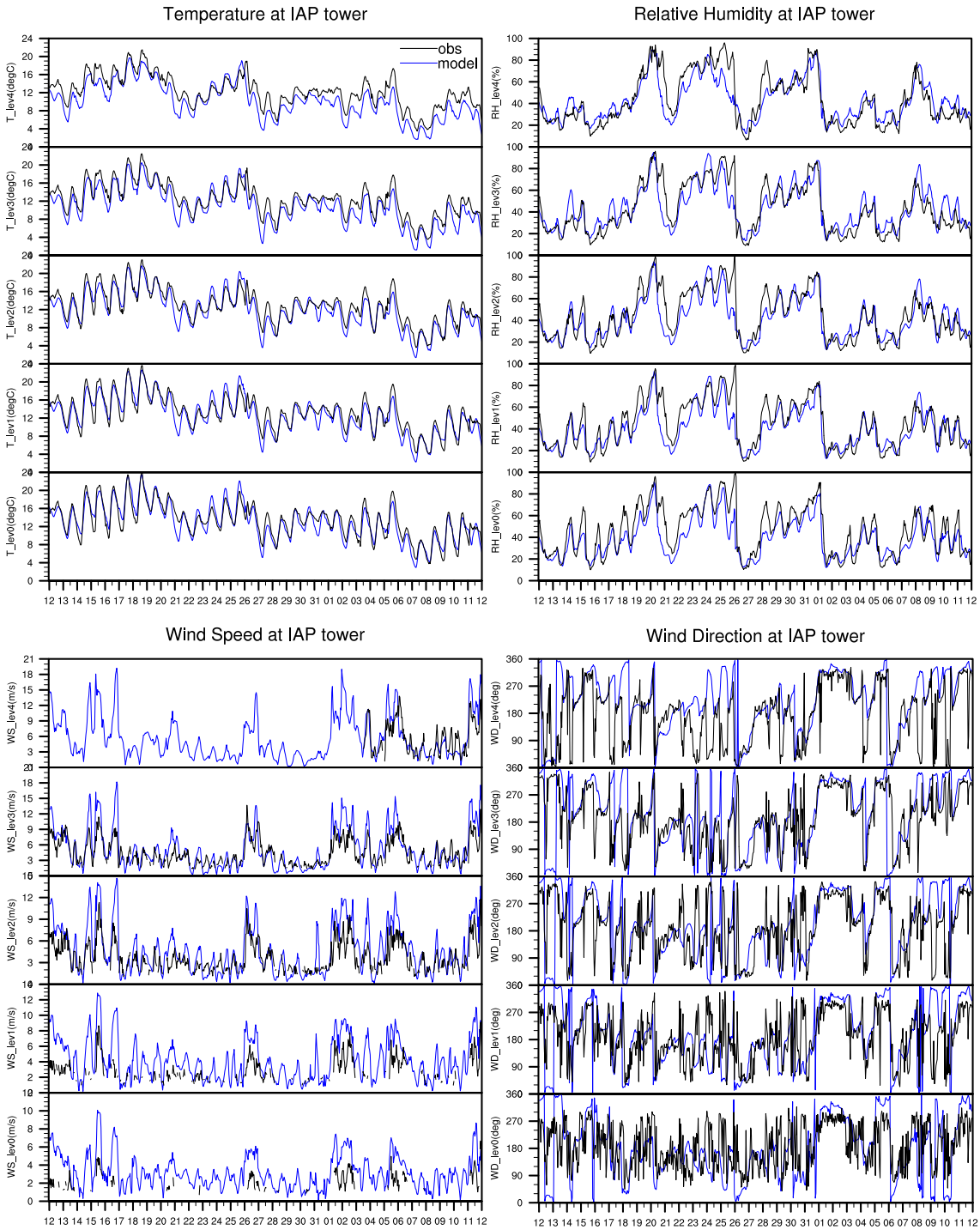

Figure A.2: Meteorological evaluation against IAP tower measurements for bottom 5 model levels. lev 0: 0–27 m, lev 1: 27–90 m, lev 2: 90–178 m, lev 3: 178–289 m, lev 4: 289–429 m.

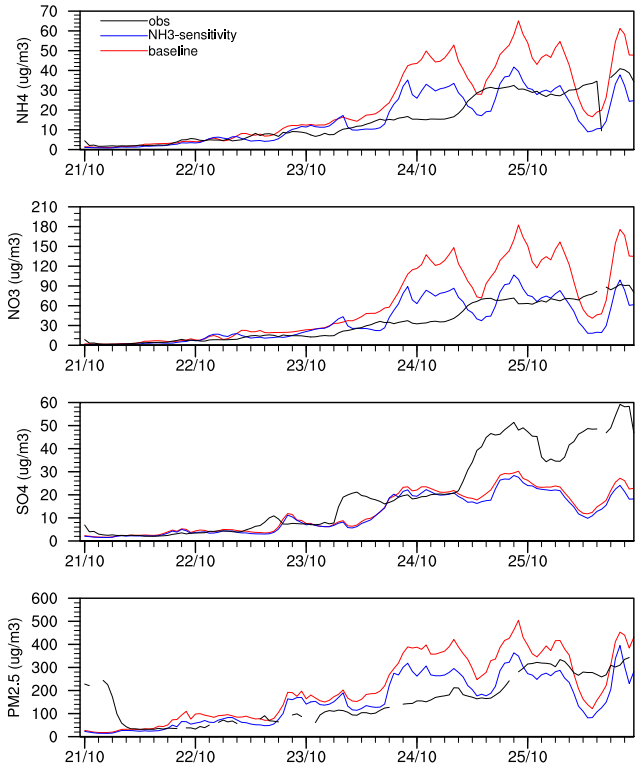

Figure A.3: Time-series of aerosol components NH_4, NO_3 and SO_4 at the IAP site and $PM_{2.5}$ at Aotizhongxin showing simulated concentrations (in $\mu g\,m^{-3}$) from the baseline model run and reduced NH_3 emissions run compared to observations.

APPENDIX B

Additional information on model setup

This appendix provides additional information on the model setup used for the simulations presented in chapter 3, in particular the method used to determine vertical distribution of emission sources and the diurnal cycle applied to various emission sectors, and also describes the aqueous phase chemistry used in the model. Emission maps of key species for the three model domains are presented and total emissions per domain are summarized.

B.1 Emissions: Vertical and temporal profiles

MEIC emissions were initially obtained as 2D arrays for each emission sector for chemical species based on the CB05 chemical mechanism. They were first respeciated by merging or separating to conform to CBMZ-MOSAIC chemistry scheme used in the study. Simulations performed with these emissions generally overestimated surface pollutant concentrations for all species as compared to ground observations. To get a more realistic representation of emissions in the model, the emission inventory was modified by prescribing a vertical distribution to various species based on emission sector and also a diurnal cycle was applied.

The vertical profile for emissions was based on the methodology of Mailler et al. (2013) where they distributed emissions into the bottom 7 model layers (0–20 m, 20–92, m, 92–184 m, 184–324 m, 324–522 m, 522–781 m, 781–1106 m) differently for the 10 different Standard Nomenclature of sources of Air Pollution (SNAP) sectors namely, combustion in energy and transformation industries (SNAP 1), non-industrial combustion plants (SNAP 2), combustion in manufacturing industry (SNAP 3), production processes (SNAP 4), extraction of fossil fuels (SNAP 5), solvent use and other product use (SNAP 6), road transport

Table B.1: Vertical profile of emissions for different sectors

Model level	Height span (m)	Industry-VOCs (%)	Industry (%)	Power (%)	Residential (%)	Transport (%)	Agriculture (%)
0	0–28	71.64	14	0	100	100	100
1	28–95	13.40	40.6	0	0	0	0
2	95–187	13.14	39.85	0.3	0	0	0
3	187–305	1.60	4.89	38.2	0	0	0
4	305–453	0.22	0.66	36.8	0	0	0
5	453–643	0	0	22.3	0	0	0
6	643–877	0	0	2.2	0	0	0
7	877–1115	0	0	0.2	0	0	0

(SNAP 7), other mobile sources and machinery (SNAP 8), waste treatment and disposal (SNAP 9), and agriculture (SNAP 10). See Table 1 in Mailler et al. (2013) for more details. Emissions sectors were represented differently in the MEIC inventory - in five broad sectors namely, industry, power, residential, agriculture and transport. Therefore, the vertical profiles of the 10 SNAP sectors were adapted to suit the five emission sectors used in this modelling setup.

SNAP 1 profile was used for all species in the power sector, an average profile was derived from SNAP (2, 3, 4, 5 and 9) sectors for all species of the industry sectors except for NMVOCs which were assumed to be sourced 67% from SNAP 6 and 33% from SNAP (2, 3, 4, 5 and 9) (Qi et al. 2017, Zheng et al. 2018, Bieser et al. 2011) and a weighted average of these vertical profiles were calculated accordingly for all the NMVOCs within the industry sector. The thickness of model levels in Mailler et al. (2013) was different from the WRF model setup of this study. Here, the bottommost eight model layers approximately corresponded to the height of the bottommost seven model layers in Mailler et al. (2013). Therefore the derived vertical profiles for all species and sectors were then modified accordingly to apportion the emissions into eight parts for the WRF model using volumetric interpolation. The emissions of all species within the residential, agriculture and transport sector were completely allocated at the lowest model level. The final percentage allocations to the bottommost eight model levels are described in Table B.1.

The 2D MEIC emissions that were acquired from Tsinghua University came along with a temporal profile for each sector. These profiles were retained even after vertically distributing the emissions. Hourly sectoral scalings were used for all the species within a sector (see, Table B.1). The model uses two 12-hourly emission files for each domain which are supplied in Universal Time Coordinates (UTC). The temporal profile was shifted eight hours behind to transform from Beijing local time to UTC.

Table B.2 summarises total emissions for each model domain for the months of October and November. October emissions are higher than November emissions for all species.

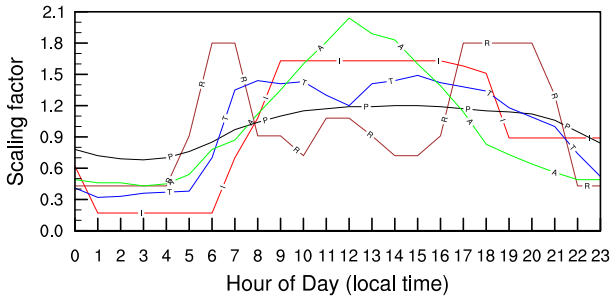

Figure B.1: Temporal profiles applied to emissions of all species for different sectors. I, P, T, R and A refer to industry, power, transport, residential and agriculture sectors respectively.

Figures B.2-B.7 show time-averaged spatial distribution of emissions of CO, NO, SO_2, NMVOCs, NH_3 and total aerosols respectively for the three model domains at 27, 9 and 3 km resolutions. CO and aerosol emissions show clear hotspots near cities and residential clusters. The 3 km resolution domain maps (panels c and f) also show highways and roads. NO emissions are more sparsely distributed than CO and aerosol emissions and show clearer streets and roads in the finest resolution highlighting the transportation sector as a major source and much less emissions from the residential sector. NMVOCs show a similar spatial profile to NO but with slightly less pronounced transportation sources and more pronounced industrial sources particularly from solvent use. SO_2 does not show hotspots corresponding to residential clusters or cities but shows strong sources in the second domain, outside of Beijin–Tianjin–Hebei region, corresponding to coal-fired power plants. NH_3 shows a significantly different spatial profile reflecting the rural areas instead of cities, industries or roads as strongest sources. This is because most of the NH_3 is emitted from fertilizer use in agricultural areas.

B.2 Aqueous-phase chemistry

Production of secondary sulphate aerosol has multiple pathways. The gas-phase oxidation of SO_2 by the OH radical dominates near the surface. However, higher-up in the atmosphere, aqueous-phase oxidation of SO_2 by photochemical oxidants such as H_2O_2 and O_3 can dominate under cloudy conditions (Seigneur & Saxena 1988). The WRF-Chem setup used in this study contains a size-resolved description of aqueous-phase oxidation of SO_2 based on the Variable Size Resolved Model (Fahey & Pandis 2003). A size-resolved description is more accurate than a bulk description because of the pH-dependent oxidation pathways involved in the aqueous-phase oxidation of SO_2, as cloud droplet-pH levels vary with their size. Even though the aqueous pathways of sulphate production are more im-

Table B.2: Total emissions for each species per domain. I and J refer to Aitken and accumulation mode aerosols respectively.

Species	Description	Domain 1		Domain 2		Domain 3	
		Oct	Nov	Oct	Nov	Oct	Nov
Gas-phase species ($mol\,h^{-1}$)							
CO	Carbon monoxide	6.78e+08	6.04e+08	2.29e+08	1.99e+08	1.08e+08	9.11e+07
NO	Nitric oxide	5.69e+07	4.94e+07	2.00e+07	1.73e+07	8.73e+06	7.49e+06
NO2	Nitric oxide	5.81e+06	5.05e+06	2.04e+06	1.77e+06	8.93e+05	7.66e+05
SO2	Sulphur dioxide	4.52e+07	3.77e+07	1.50e+07	1.25e+07	4.94e+06	4.10e+06
NH3	Ammonia	5.34e+07	5.28e+07	1.26e+07	1.24e+07	5.49e+06	5.42e+06
HCHO	Formaldehyde	1.90e+06	1.81e+06	5.59e+05	5.30e+05	2.31e+05	2.17e+05
ALD	Other Aldehydes	7.22e+05	6.58e+05	2.20e+05	1.99e+05	9.80e+04	8.78e+04
CH3OH	Methanol	8.87e+05	8.62e+05	2.68e+05	2.55e+05	1.12e+05	1.05e+05
C2H5OH	Ethanol	5.41e+05	4.24e+05	1.68e+05	1.32e+05	8.24e+04	6.47e+04
TOL	Toluene	3.32e+06	2.48e+06	1.02e+06	7.66e+05	5.16e+05	3.83e+05
OL2	Ethene	4.49e+06	3.89e+06	1.61e+06	1.37e+06	6.87e+05	5.76e+05
OLT	Terminal olefins	1.80e+06	1.55e+06	5.91e+05	5.03e+05	2.62e+05	2.19e+05
OLI	Internal olefins	4.69e+05	3.88e+05	1.48e+05	1.22e+05	6.96e+04	5.63e+04
KET	Ketones	9.65e+05	8.81e+05	2.94e+05	2.66e+05	1.31e+05	1.17e+05
ETH	Ethane	2.99e+06	2.44e+06	9.54e+05	7.89e+05	3.92e+05	3.20e+05
HC3	3-carbon alkanes	3.50e+06	2.81e+06	1.19e+06	9.44e+05	5.60e+05	4.42e+05
HC5	5-carbon alkanes	3.50e+06	2.81e+06	1.19e+06	9.44e+05	5.60e+05	4.42e+05
HC8	8-carbon alkanes	3.50e+06	2.81e+06	1.19e+06	9.44e+05	5.60e+05	4.42e+05
XYL	Xylene	2.12e+06	1.66e+06	6.55e+05	5.16e+05	3.20e+05	2.48e+05
Aerosols ($g\,h^{-1}$)							
ECI	Elemental carbon I	4.09e+07	3.71e+07	1.35e+07	1.20e+07	5.69e+06	4.99e+06
ECJ	Elemental carbon J	1.64e+08	1.49e+08	5.40e+07	4.78e+07	2.27e+07	2.00e+07
ORGI	Organic matter I	1.28e+08	1.23e+08	3.79e+07	3.54e+07	1.51e+07	1.40e+07
ORGJ	Organic matter J	5.13e+08	4.91e+08	1.52e+08	1.42e+08	6.05e+07	5.62e+07
SO4I	Sulphate I	5.20e+07	4.34e+07	1.72e+07	1.44e+07	5.69e+06	4.72e+06
SO4J	Sulphate J	2.08e+08	1.74e+08	6.89e+07	5.77e+07	2.28e+07	1.89e+07
PM25I	PM2.5 other I	1.40e+08	1.13e+08	4.94e+07	3.93e+07	2.20e+07	1.72e+07
PM25J	PM2.5 other J	5.61e+08	4.50e+08	1.97e+08	1.57e+08	8.79e+07	6.88e+07
PM10	PM coarse	4.71e+08	3.70e+08	1.55e+08	1.21e+08	7.02e+07	5.40e+07

portant at the altitude of clouds, sulphate formed through these pathways can reach the surface via downdrafts or turbulent mixing. Currently, aqueous-phase chemistry is only available for resolved (not parameterized) clouds in the model. Despite the representation of both gas-phase and aqueous-phase oxidation of SO_2 within the model, the sulphate aerosol was underpredicted for the haze events in late October. To bridge this gap, there is emerging science coming up suggesting new aqueous-phase pathways for near-surface sulphate aerosol formation based on reactive nitrogen chemistry in the presence of aerosol water under hazy conditions when photochemical activity is weak (Cheng et al. 2016).

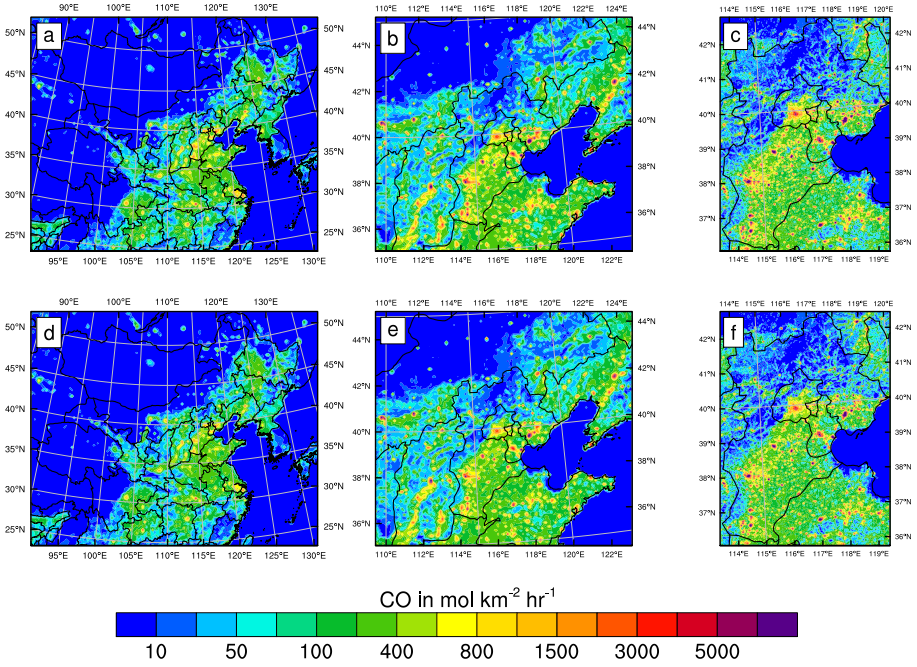

Figure B.2: Vertically integrated and 24 hour averaged emissions of carbon monoxide for October (a, b and c) and November (d, e and f) for the three model domains.

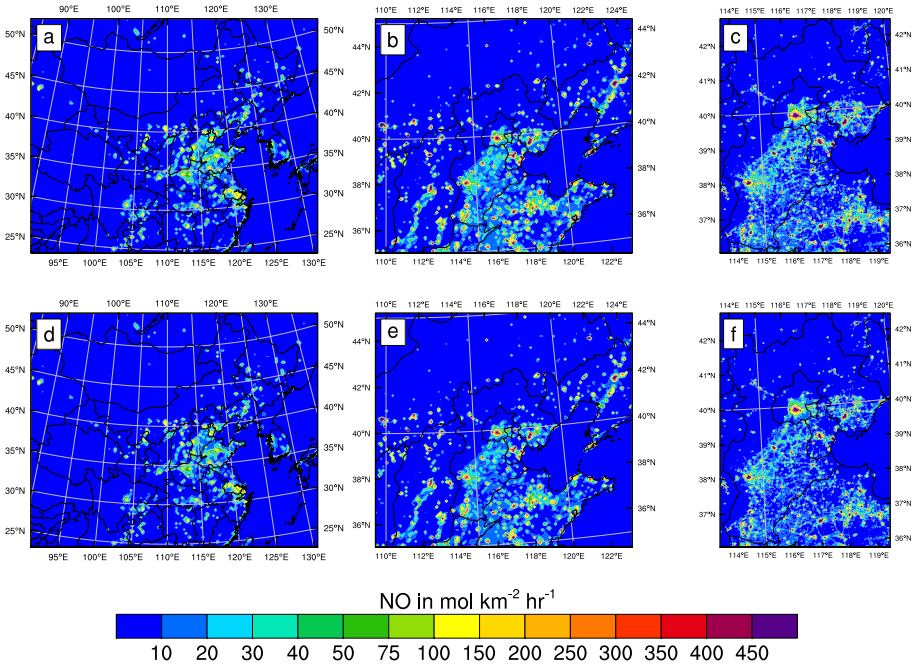

Figure B.3: Vertically integrated and 24 hour averaged emissions of nitric oxide for October (a, b and c) and November (d, e and f) for the three model domains.

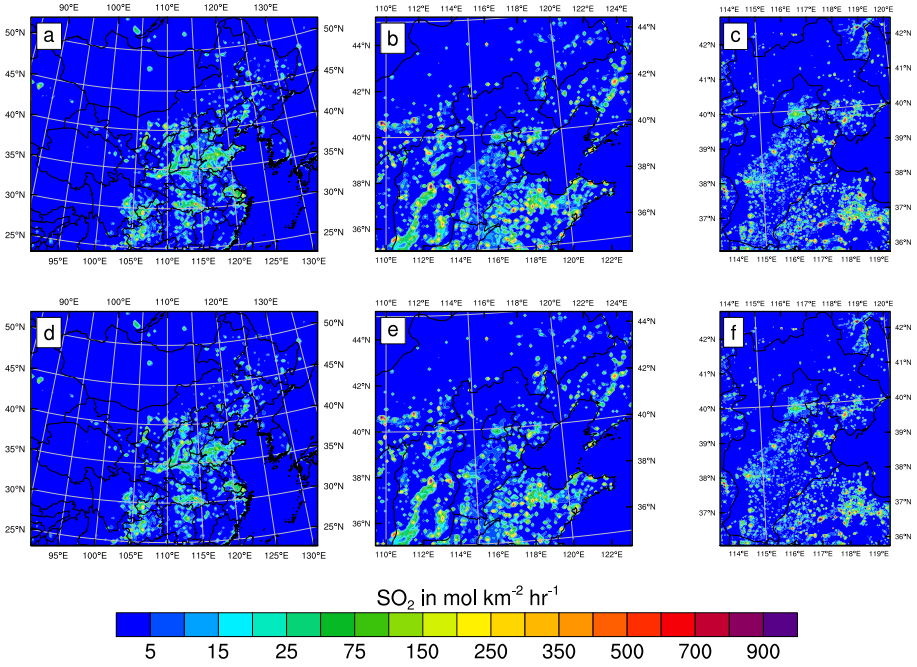

Figure B.4: Vertically integrated and 24 hour averaged emissions of sulphur dioxide for October (a, b and c) and November (d, e and f) for the three model domains.

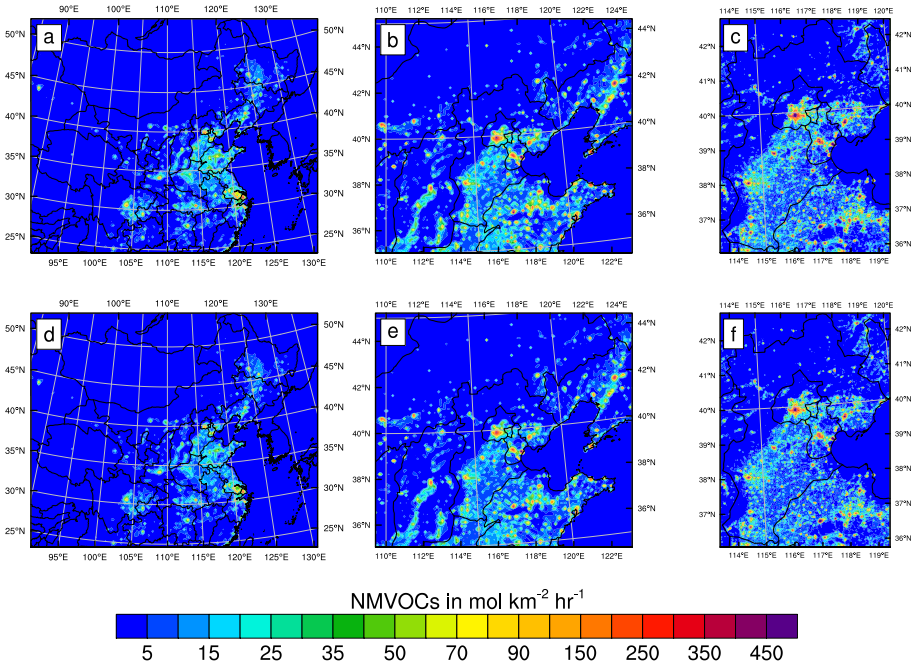

Figure B.5: Vertically integrated and 24 hour averaged emissions of non-methane volatile organic compounds for October (a, b and c) and November (d, e and f) for the three model domains.

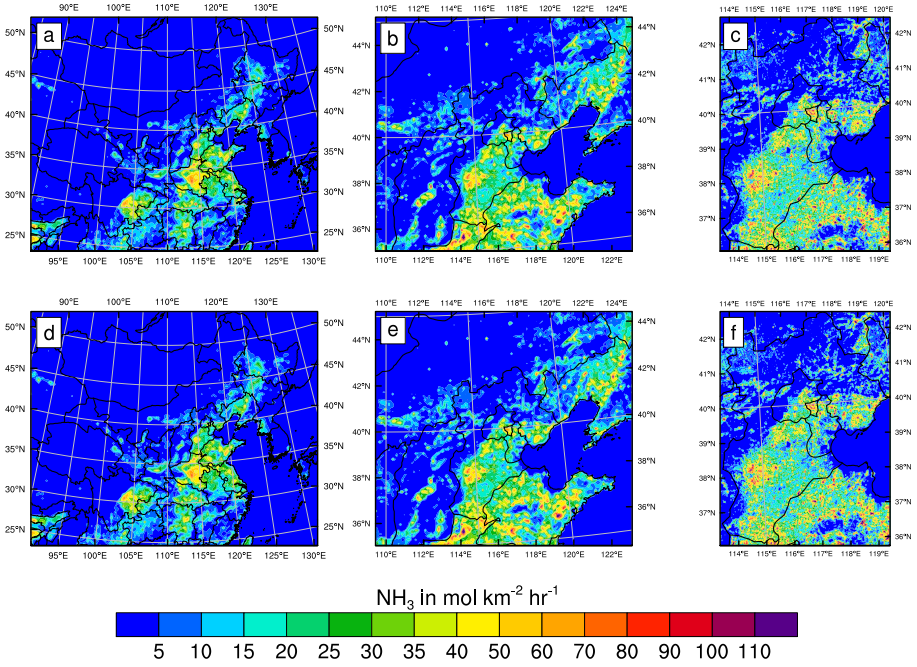

Figure B.6: Vertically integrated and 24 hour averaged emissions of ammonia for October (a, b and c) and November (d, e and f) for the three model domains.

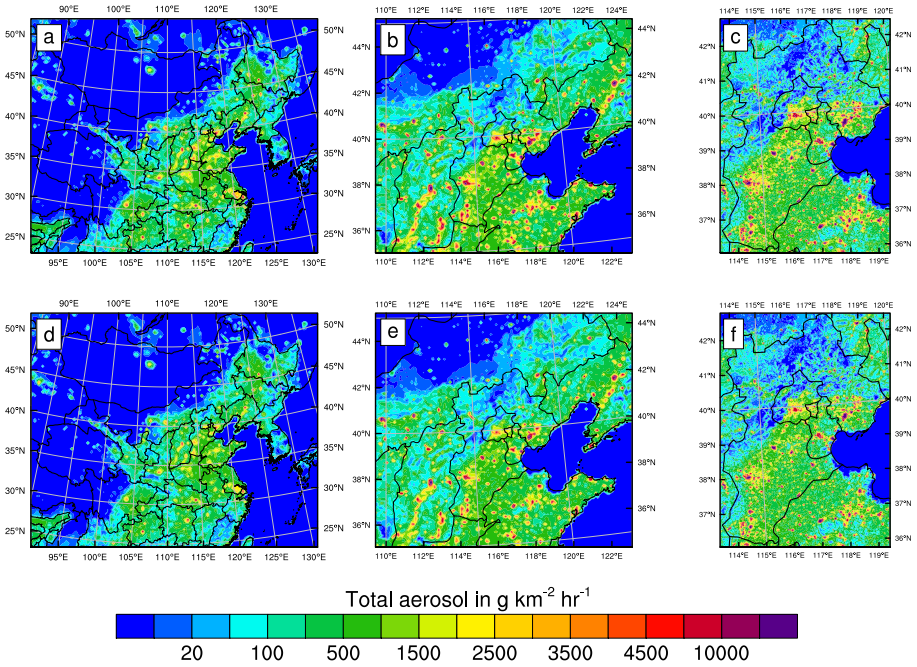

Figure B.7: Vertically integrated and 24 hour averaged emissions of all aerosol species for October (a, b and c) and November (d, e and f) for the three model domains.

CHAPTER 4

Improving short-term emission controls in Beijing: temporal, regional and sectoral source contributions

Tabish Umar Ansari[1], Oliver Wild[1], Edmund Ryan[2], Ying Chen[1], Jie Li[3] and Zifa Wang[3]

[1]Lancaster Environment Centre, Lancaster University, Lancaster, UK

[2]School of Mathematics, University of Manchester, Manchester, UK

[3]State Key Laboratory of Atmospheric Boundary Layer Physics and Atmospheric Chemistry, Institute of Atmospheric Physics, Chinese Academy of Sciences, Beijing, China

(This chapter is the final draft of a manuscript prepared for submission in Atmospheric Chemistry and Physics)

Author contributions: TA, OW and ZW designed this study, and TA performed the model simulations and analysis. JL provided emissions data and expertise on the model configuration. ER generated code for emulating the model output. YC provided scientific expertise on back trajectories and critical support on model restarts. TA and OW prepared the manuscript with input from all coauthors.

4.1 Abstract

We investigate the contributions of major local and regional emission sources to air quality in Beijing to inform short-term emission controls aimed at mitigating major pollution episodes. We use a well-evaluated version of the WRF-Chem model at 3 km horizontal resolution to explore the temporal contribution of local and regional emission sources to

air quality in Beijing under a range of meteorological conditions. Considering feasible emission reductions of 40–50% across industry, power, residential and transport sectors we find that the effect of local emission cuts is greatest (up to 38%) on the day of control, but that they still make a small contribution (up to 8%) five days later under stagnant conditions. Emission controls in surrounding regions have greatest effect (up to 18%) on the second day but may be negligible under northwesterly flow when local emissions dominate. To determine the effect of different emission sectors and regions, we consider the four main emission sectors over local (Beijing), near-neighbourhood (North China Plain) and far-neighbourhood (North China) regions. Using simple one-at-a-time sensitivity studies over a 11-day period that encompasses a range of differing meteorological conditions, we found that residential and industry sectors from neighbouring provinces dominate $PM_{2.5}$ levels in Beijing on polluted days however local residential as well as industry and residential emissions from farther provinces can also contribute significantly during some episodes. We then apply a novel Gaussian Process Emulation approach to build pollutant response surfaces over this period, and use these surfaces to identify the short-term emission controls needed to meet the national air quality target of daily average $PM_{2.5}$ less than $75\,\mu g\,m^{-3}$ for various intensities of episodes. We found that for heavy pollution days with daily mean $PM_{2.5}$ higher than $225\,\mu g\,m^{-3}$, 90% reduction is needed across all four sectors for all three source regions considered in order to reduce it to less than $75\,\mu g\,m^{-3}$, which is much more stringent than what has been implemented in the past.

4.2 Introduction

Beijing, located at the foot of the Yanshan mountains on the northern edge of the heavily-populated North China Plain, has consistently been named among the most polluted capital cities in the world (State of Global Air 2018, WHO 2016). While recent emission controls have brought substantial improvements in air quality (Ma et al. 2018, Cheng et al. 2018), the city continues to experience high levels of $PM_{2.5}$ (atmospheric particulate matter with diameter less than 2.5 µm) especially in winter when frequent haze episodes pose risks to human health, visibility and climate (Lelieveld et al. 2015, Luan et al. 2018, WMO 2011). In 2013, the State Council of China launched the Air Pollution Prevention and Control Action Plan (APPCAP) setting targets to reduce $PM_{2.5}$ concentrations over the Beijing–Tianjin–Hebei region by 25% by 2017, and to reduce annual mean $PM_{2.5}$ concentrations in Beijing to $60\,\mu g\,m^{-3}$ (Zheng et al. 2018, WEI et al. 2017). During 2013–2017, the air quality in Beijing significantly improved following the implementation of local and

regional emission control measures, and the annual mean $PM_{2.5}$ concentration decreased from 89.5 $\mu g\,m^{-3}$ in 2013 to 58 $\mu g\,m^{-3}$ in 2017 (Ma et al. 2018, Cheng et al. 2018, Zheng et al. 2018). These long-term mitigation strategies included measures such as gradual phase-out of residential biofuel use, changes in industrial technology, improved vehicle fuel standards and relocation of coal-fired power plants.

Despite these long-term pollution mitigation strategies, $PM_{2.5}$ concentrations in excess of 500 $\mu g\,m^{-3}$, twenty times the WHO 24 h standard, are common in many Chinese cities during periods of heavy pollution (Sheehan et al. 2014). Additional, short-term emission-control measures, generally lasting 3–7 days, are necessary to prevent these extreme pollution episodes, especially during winter when stable meteorological conditions are conducive to formation and accumulation of very high levels of particulate matter. Such short-term controls have been tested, with some success, during special events such as the 2008 Beijing Olympics, 2014 Asia-Pacific Economic Cooperation (APEC) meeting and 2015 China Victory Day Parade (Zhang et al. 2015a, Xu et al. 2019, 2017). However, these successful outcomes have often been helped by favourable weather conditions (Liu et al. 2017, Liang et al. 2017, Gao et al. 2017) and studies have shown that these control strategies would fail under less favourable meteorological conditions (Ansari et al. 2019a). Previous studies have advocated application of emission controls over a wider geographical region (Guo et al. 2016, Wen et al. 2016, Ansari et al. 2019a) but have not identified the spatial or temporal scales needed for successful policy implementation, or proposed any general framework to devise future mitigation strategies that account for differing meteorological conditions. In this study we use a range of new modelling approaches, including 1-day emission cuts and Gaussian Process emulation, to gain a detailed understanding of the magnitude and timing of local and regional source contributions to $PM_{2.5}$ in Beijing under varying meteorological conditions. We develop easy-to-use pollutant response surfaces based on these different emission sectors and regions, and demonstrate how they can be used to guide the development of future short-term emission control policies in the city.

4.3 Modelling Approaches

We use the Weather Research and Forecasting–Chemistry model (WRF-Chem) version 3.7.1 at a horizontal resolution of 27 km over China with nested domains over Northern China at 9 km and the North China Plain at 3 km resolution. Gas-phase chemistry in the model is represented by the Carbon Bond mechanism version Z (CBMZ) which is coupled with the Model for Simulating Aerosol Interactions and Chemistry (MOSAIC)

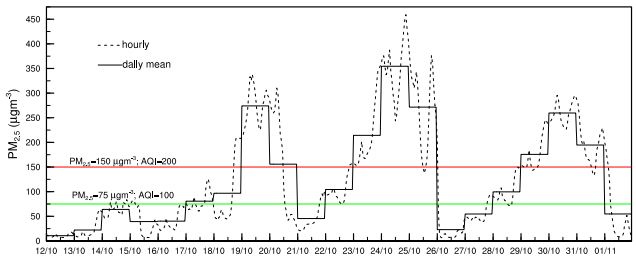

Figure 4.1: Average simulated hourly and daily mean $PM_{2.5}$ in Beijing in October 2014. The national air quality standard for 24 hr average $PM_{2.5}$ of 75 $\mu g\,m^{-3}$ is shown in green, and the threshold for heavy pollution, 150 $\mu g\,m^{-3}$, is shown in red.

aerosol module with eight aerosol size bins (Zaveri & Peters 1999, Zaveri et al. 2008). We use meteorological fields from the European Centre for Medium-Range Weather Forecasts (ECMWF), and anthropogenic emissions from the Multi-resolution Emission Inventory for China (MEIC) appropriate for 2014. Further details of the model configuration and evaluation over North China are provided in a previous study where we explored emission controls in Beijing during the Asia-Pacific Economic Cooperation (APEC) summit in November 2014 (Ansari et al. 2019a). In this previous study we demonstrated that the model reproduces the magnitude and variation of key pollutants over Beijing well, and showed that while national air quality standards were met during the APEC summit, they would have been greatly exceeded under the same emission controls if the summit had been held in October when the weather was less favourable (Ansari et al. 2019a). Formulation of effective short-term emission control policies therefore needs to account for the important role played by meteorological processes. In this study we focus on the same October-November period in 2014 and investigate the key source sectors and regions responsible for short-term pollution episodes during a range of meteorological conditions.

Figure 4.1 shows hourly and daily mean simulated $PM_{2.5}$ concentrations for Beijing at the end of October 2014, the period just before APEC emission controls were implemented. In the last 15 days of October, only three days meet the daily national Class 2 air quality standard of 24 h average $PM_{2.5}$ concentration less than 75 $\mu g\,m^{-3}$ (Air Quality Index, AQI = 100), and eight days exceed the higher threshold for heavy pollution of 150 $\mu g\,m^{-3}$ (AQI=200). Reducing the 24 h average $PM_{2.5}$ concentration below 75 $\mu g\,m^{-3}$ over the entire period would require strict, carefully tailored emission reductions across multiple sectors and regions that are timed to provide maximum benefit during the heaviest pollution episodes.

The APEC emission controls were implemented in two stages; an initial phase (APEC 1) that covered Beijing and some western districts of Hebei province including Baoding, Lang-

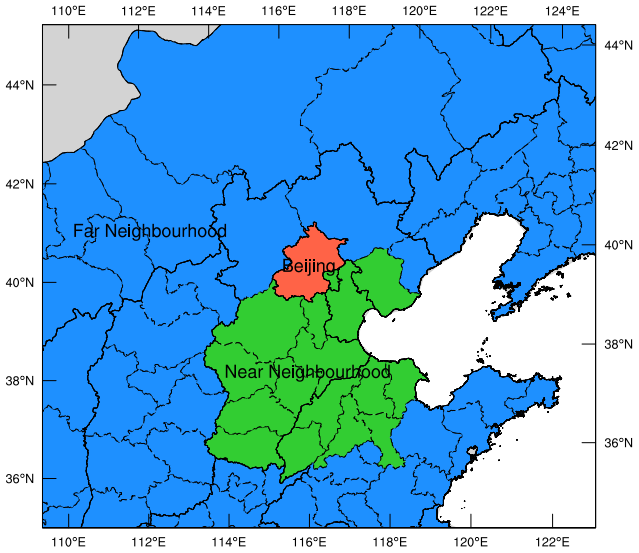

Figure 4.2: North China region (model domain 2) showing emission control regions used in this study.

fang, Shijiazhuang, Xingtai and Handan, and a second more stringent phase (APEC2) that additionally covered Tianjin, Tangshan, Cangzhou, Hengshui, Dezhou, Binzhou, Dongying, Jinan, Liaocheng and Zibo. In this study we consider three broad regions of control: local emissions from Beijing, Near-Neighbourhood emissions from the North China Plain and Far-Neighbourhood emissions from surrounding provinces (see figure 4.2). The Near-Neighbourhood region used here is defined to match the APEC2 control region described above. Since we have shown that applying APEC controls over this period was not sufficient to meet healthy air quality standards (Ansari et al. 2019a), we consider a Far-Neighbourhood region which covers parts of Shanxi, Shaanxi, Shandong, Henan, Inner Mongolia, Liaoning and Jilin provinces.

A number of measurement and modelling studies have investigated source apportionment of air pollution in Beijing. Most measurement studies have used the Positive Matrix Factorization (PMF) technique which effectively attributes $PM_{2.5}$ to different emission sectors but does not provide the district-based regional contributions critical for policymaking (Zhang et al. 2013, Zíková et al. 2016, Shang et al. 2018). Li et al. (2015) performed a comprehensive modelling study using the PSAT emissions-tagging approach in the CAMx model at 36 km resolution to generate district-based source contributions. However, the emissions-tagging technique does not apportion secondary aerosols, a major part of $PM_{2.5}$ loading in Beijing, to any specific emission source. Recently, Chen et al. (2019) used the CAMx-PSAT technique at 12 km resolution to calculate source contributions from districts included in the Chinese government's "2+26" regional emission control strategy, but they do not include the effect of surrounding regions in their analysis, which may be needed

to formulate successful emission control policy in unfavourable meteorological conditions. Moreover, none of these studies provide information about the temporal contribution of different sources which is important in the context of short-term emergency control measures. Matsui et al. (2009) provided some preliminary information on the temporal nature of source contribution from different regions. They found that primary aerosols in Beijing are affected by emissions within 100 km in the previous 24 h and secondary aerosols over Beijing are affected by emission sources within 500 km in the previous 3 days. However, a more detailed understanding of the temporal nature of regionally-resolved sectoral source contributions under a range of meteorological conditions is required to aid robust short-term emission control policymaking for Beijing.

With the aim of improving short-term emission reduction policies, we investigate the temporal contributions from different emission sectors and regions by conducting a range of different simulation experiments described below:

Experiment 1 (1-day pulses, 60 runs): In order to investigate the temporal nature of source contributions from different regions, we reduced anthropogenic emissions across all major sectors to APEC levels but just for the first day of simulation and conducted 5–day long runs with twenty different starting days to cover a range of different meteorological regimes. Three sets of these twenty runs were conducted where the emissions were reduced for (i) Beijing only, (ii) near-neighbourhood only, and (iii) far-neighbourhood only. This is described in section 4.4. See Table C.1 in the supplement for a list.

Experiment 2 (Zero-out, 14 runs): In order to quantify sectoral and regional source contributions, we conducted fourteen 11-day long runs including a baseline run, twelve runs where one of the twelve emission parameters (4 sectors for 3 regions) were reduced to zero continuously for the entire period, and one run where all twelve emission parameters were switched-off together. This is described in section 4.5. See Table C.3 in the supplement for a list.

Experiment 3 (Perturbation, 60 runs): In order to assess non-linear effects of combined sectoral controls, we conducted sixty 11-day long runs similar to experiment 2 but with different scalings of 0–120% across the twelve emission parameters (4 sectors for 3 regions) for each run instead of switching-off (zeroing-out) just one parameter. See Table C.4 in the supplement for a list. These runs were used to train a Gaussian Process Emulator which was then utilized to perform further 10,000 perturbation runs to obtain sensitivity indices for each of the twelve emission parameters and to build emission-concentration response-surfaces for Beijing. This is described in section 4.6.

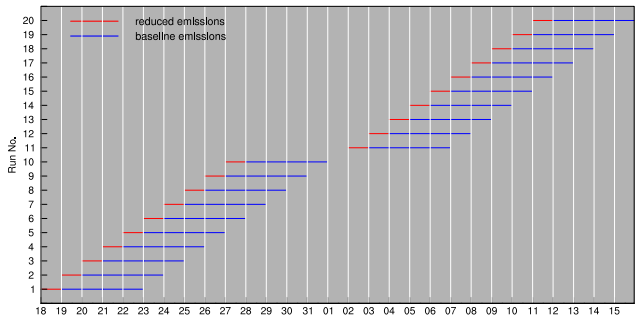

Figure 4.3: Schematic showing the start and end dates of each pulse run. These runs were performed for each of the three regions of control. The dates are from 12 October to 15 November.

4.4 Temporal response to emission controls

To ensure good air quality, regional short-term emission controls have been implemented for high-profile events in Beijing over the past decade, including the 2008 Olympics, the 2014 APEC meeting, and the 2015 China Victory Day parade. These controls resulted in improved air quality, although for all three events the successful outcomes were greatly helped by favourable meteorological conditions (Yang et al. 2011, Liang et al. 2017). In each case, emission controls were initiated substantially before the event: 18 days before for the Olympic games in 2008 (Gao et al. 2011, Yang et al. 2011), 7 days before for the APEC meeting in 2014 (Zhang et al. 2016a, Sun et al. 2016b) and 14 days before for the Victory Parade in 2015 (Liang et al. 2017, Zhao et al. 2016). This period allowed emission controls to take effect and existing pollution to be swept away, but the optimal timing for controls that balances improvements in air quality against the economic and social costs of implementing them remains unclear. To resolve this, it is important to understand how pollution from previous days and different regions builds up under different meteorological conditions and to determine the persistence of pollution from a single day of emissions.

We consider three regions of control: Beijing, Near-Neighbourhood and Far-Neighbourhood (Figure 4.2) and conducted sixty 5-day long model runs, twenty for each region, with emission reductions for the first day of simulation only and baseline emissions for the following four days as shown in figure 4.3). We applied emission reductions following those implemented during the APEC summit period: 40–50% for Beijing and 30–35% for surrounding districts (see Ansari et al. 2019a). The timing of the model runs was selected to cover a range of different meteorological conditions and includes a polluted period in mid to late October (10 days) and a cleaner period in early to mid November (also 10 days in length). The difference in simulated $PM_{2.5}$ values between each model run and the baseline run gives the contribution from a specific day over subsequent days.

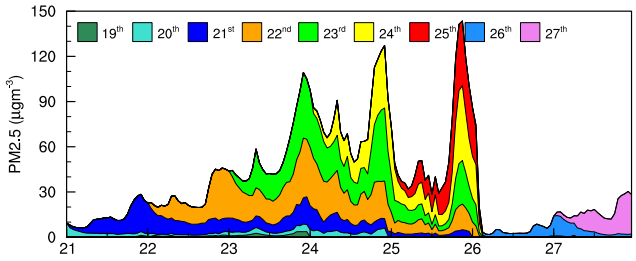

Figure 4.4: Contribution of one-day emission reductions on successive days to $PM_{2.5}$ in Beijing in October 2014.

Figure 4.4 shows the contribution of one-day emission reductions across all three regions on successive days to $PM_{2.5}$ in Beijing for 21–27 October 2014. While emission cuts on a given day make a substantial contribution to $PM_{2.5}$ on that day, the benefits often extend to a number of subsequent days due to the meteorological conditions and timescales for transport. The most polluted days (e.g., 24 and 25 October) show the accumulated contributions to $PM_{2.5}$ from as much as five days previously. Under clean, northwesterly winds, the pollution is swept away over the North China Plain, and the resulting clean days are dominated by fresh pollution from the same day, as occurs on 26 October. The daily contributions vary substantially in magnitude as well as timing, and pollution levels are typically higher at nighttime when the Planetary Boundary Layer (PBL) is more stable.

To gain insight into how meteorological processes affect the timescales for transport from different regions, we explore the contributions from Beijing, Near-Neighbourhood and Far-Neighbourhood regions separately. Figure 4.5 presents the contributions to $PM_{2.5}$ in Beijing from 1-day emission reductions relative to the day of control for the three different source regions over the two periods (20 days) considered here. Contributions from Beijing sources affect $PM_{2.5}$ in Beijing immediately and typically last 1–2 days, with peak contributions ranging from 8–43 $\mu g\,m^{-3}$ (median value 21 $\mu g\,m^{-3}$) and occurring towards the end of the day of emissions control. Contributions from the near-neighbourhood region are delayed somewhat and typically extend until the third day. The contributions are generally smaller than those from Beijing sources and and are greatest on the second day. Contributions from the far-neighbourhood region are even more spread-out and are further delayed in time, with very little contribution over Beijing on the day of control. The contributions are greater in the two days following controls, reflecting the timescales for transport, and can persist for as much as five days. The right hand panels in figure 4.5 show 24 h average contributions from each of the three source regions and highlight the variability in the contributions from these regions under meteorological conditions over all 20 simulations. The highest hourly contribution from Beijing controls (43 $\mu g\,m^{-3}$) occurs

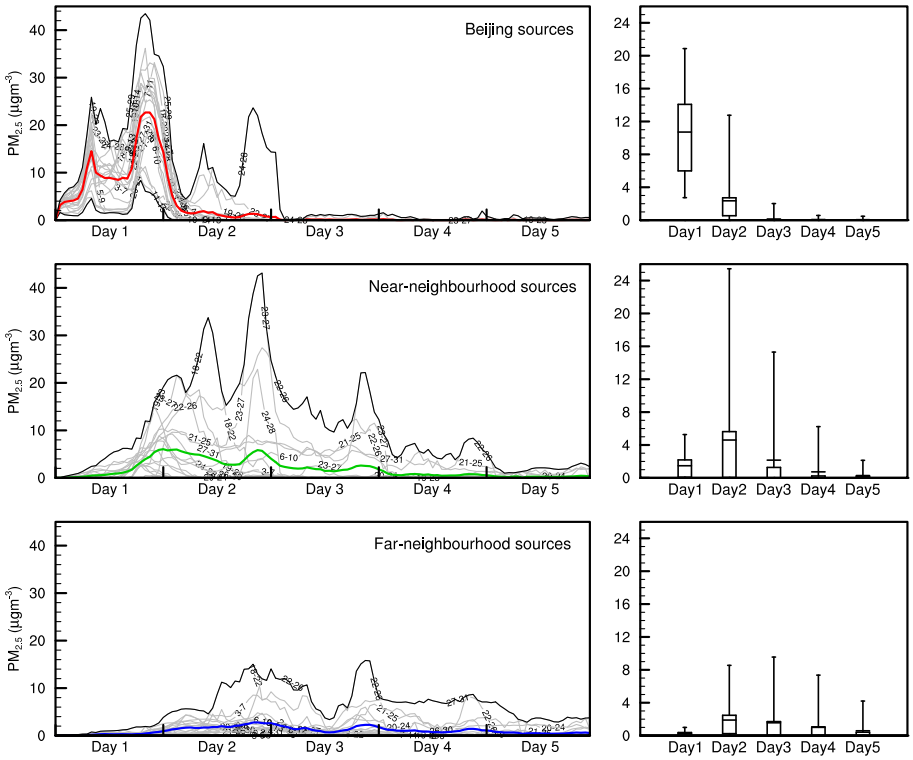

Figure 4.5: Hourly (left) and daily (right) contributions to $PM_{2.5}$ in Beijing due to one-day emission cuts in the Beijing (top), Near-Neighbourhood (middle) and Far-Neighbourhood (bottom) source regions. The contribution of individual days is shown in grey, mean contributions are coloured, and maximum and minimum contributions are shown in black. Boxplots (right) show hourly the mean, 25th/75th percentiles, and maximum/minimum contributions across all runs each day.

for emissions on 25 October, which is one of the most polluted days during the study period (see figure 4.1). The highest hourly contribution from near-neighbourhood controls is similar in magnitude (also 43 $\mu g\,m^{-3}$) occurs from the 23–27 October run where two of the most polluted days (24 and 25 October) are the second and third days subsequent to the emission reduction day, and the highest hourly peak contribution from far-neighbourhood pulses comes from the 22–26 October run where the most polluted days (24 and 25 October) are the third and fourth days subsequent to the emission emission reduction day.

To characterize the source contributions for each simulation, we calculate the peak contribution, the timing of the peak, the integrated contribution and the duration of the contribution (see Table C.2 in the supplementary material). For 5 of the 10 cases in October, the more polluted period, the highest integrated contribution comes from Beijing sources while near-neighbourhood sources dominated 4 cases and far-neighbourhood sources only 1 case. For the cleaner November period, the highest integrated contributions are from Beijing sources for 9 of the 10 cases, and far-neighbourhood sources made a

greater contribution than near-neighbourhood sources for 8 of the 10 cases. Highest peak contributions came from Beijing sources for 6 out of 10 cases in October and for all 10 cases in November. However near-neighbourhood sources also made a major contribution on polluted days. Far-neighbourhood sources showed higher or equal peaks as compared to near-neighbourhood sources for 7 out of 10 cases in November, however unlike the integrated contributions they were significantly smaller than the Beijing peaks. The greatest contributions from Beijing sources occur in late afternoon or early evening of the day of control, reflecting the accumulation of pollutants, rush hour traffic sources, and increased PBL stability in the evening. Peak contributions from near-neighbourhood sources occur in the morning to afternoon of the second day, while those from far-neighbourhood sources are more uniformly distributed over time and can occur anytime between the third and fourth day. The duration of contributions from Beijing sources never extends beyond the second day whereas contributions from near- and far-neighbourhood may extend to the fifth day. To test the persistence of contributions beyond the fifth day, we extended far-neighbourhood pulse runs to 8 days but their contributions became negligible beyond the fifth day.

While the temporal contributions from each region show clear mean behaviour, they also show significant variability. This is due to differing meteorological conditions for each day. To understand the effect of meteorology on the temporal contributions, we investigate the relationship between peak and integrated contributions with meteorological parameters such as daily average wind speed and direction on each day of the simulations. Some key relationships are shown in Figure 4.6. We find that peak contributions from Beijing sources show a clear negative correlation (r-value of -0.74) with average wind speed in Beijing on the day of emission control. This is as expected, and reflects the greater build up of pollution under more stagnant conditions. The wind speed on subsequent days did not show a strong correlation with the contributions from Beijing or neighbourhood sources. The integrated contribution from all three source regions was higher when the wind was blowing from the south. This reflects the fact that the strongest emission sources lie over the North China Plain south of Beijing. Lower integrated contributions were seen during southerly winds when the wind speed was higher. It is noteworthy that over these periods wind speeds were generally lower when coming from the south, supporting the build-up of pollution as well as bring pollutants from the highest emission regions.

Overall, it is clear that local emission controls in Beijing provide an immediate but typically relatively short-lived benefit to air quality in the city, with the magnitude of the benefit dependent on whether stagnant meteorological conditions with low wind speed

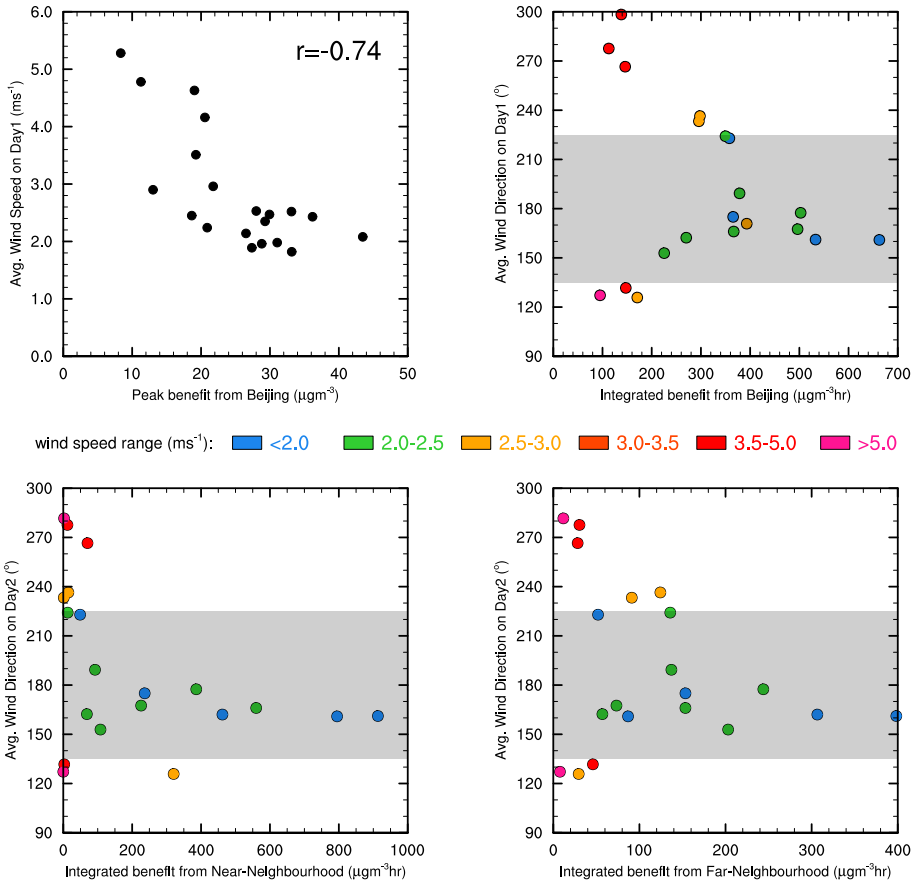

Figure 4.6: Effect of meteorology on peak and integrated contributions from the three regions of control. (a) Peak benefit from Beijing sources vs average wind speed on day 1, (b) integrated benefit from Beijing vs average wind direction on day 1, and integrated benefits from (c) Near-Neighbourhood and (d) Far-neighbourhood sources vs average wind direction on day 2. The shaded area highlights southerly winds.

are present. Regional emission controls over the North China Plain generally lead to smaller benefits which start later and last longer, although the contribution may rival those from local emissions under weak, southerly winds. More distant regions may also make a contribution under these conditions, although these typically take a number of days to build up. These results suggest that avoiding major pollution episodes in Beijing requires control of local emissions one or two days in advance, control of near-neighbourhood emissions two to three days in advance, and control of far-neighbourhood emissions three to four days in advance.

4.5 Sectoral emission controls

An understanding of contributions from individual sectors (industry, transport, residential and power plants) from different regions is also important to inform successful short-term

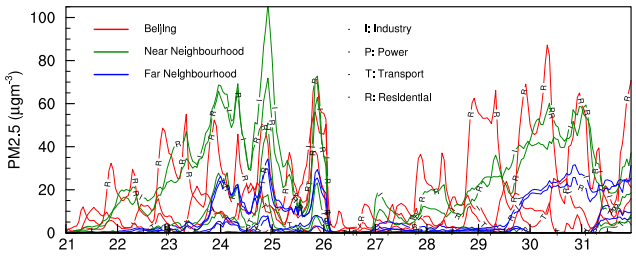

Figure 4.7: Contribution of each sector in each emission region to $PM_{2.5}$ in Beijing. The emission sectors include residential (R), industrial (I), power (P) and transport (T) sources.

emission control policies. To determine the impact of each source sector in each different region, we conduct model simulations where one of the twelve emission sources (4 sectors over 3 regions) was removed in turn for the entire simulation period (21–31 October). The difference of each of these runs from the baseline run yields an estimate of the contributions of the source considered. We also conducted an additional run with all twelve emission sources removed to provide an estimate of the background contribution from sources outside the regions considered here.

The October simulation period is characterised by two distinct pollution episodes: 21–25 October (episode 1) and 26–30 October (episode 2). During each episode the total $PM_{2.5}$ over Beijing builds up over a five-day period and peaks on the fifth day. Figure 4.7 shows hourly time-series of contributions from each emission source. In general, residential and industrial sectors make much greater contributions than the power and transport sectors. The Beijing emission sources show a more pronounced diurnal variation than the regional sources. This is because the Beijing plume is still fresh and contains the diurnal signal of local emissions whereas regional plumes are transported to Beijing over longer distances and are better mixed, losing this diurnal signal through dispersion. All sources show a build up during the two episodes, but the rate of this increase is high for Beijing sources, low for near-neighbourhood sources and lower still for far-neighbourhood sources. Far-neighbourhood contributions show a much delayed increase compared with those from Beijing and Near-Neighbourhood sources, highlighting that 3–4 days of stagnation over Beijing are needed before Far-Neighbourhood sources make a substantial contribution. This is consistent with our findings on the temporal response to emission changes in Section 4.4. It is interesting to note that the source contributions do not peak at the same time, and therefore the maximum concentrations of $PM_{2.5}$ do not reflect the maximum contributions from each source. Figure 4.7 reveals the anatomy of the two $PM_{2.5}$ episodes shown in Figure 4.1 and shows that episode 1 was dominated by regional pollution, particularly industry, residential and transport emissions from near-neighbourhood sources, while episode 2 had greatest

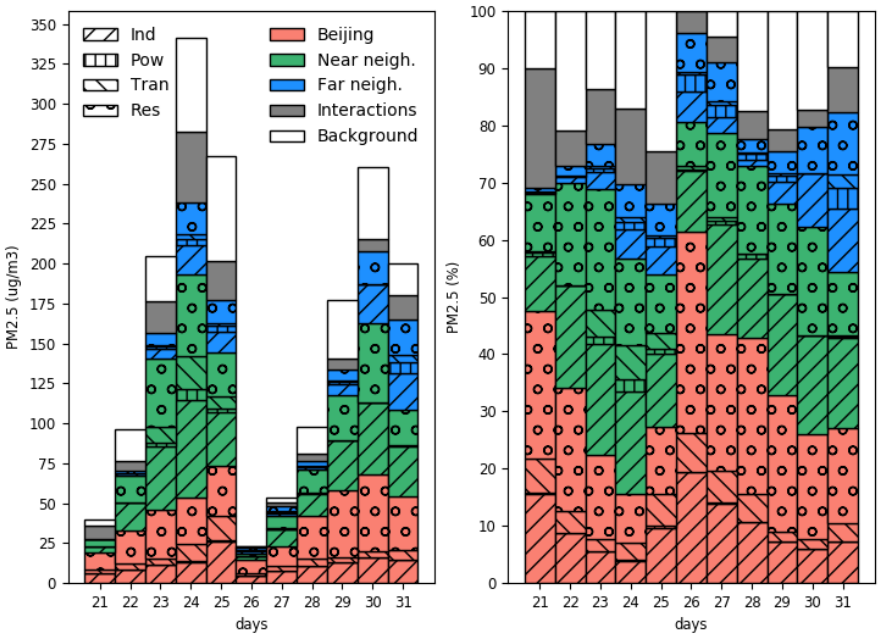

Figure 4.8: Absolute (left) and relative (right) contributions to daily mean $PM_{2.5}$ obtained by removing one emission sector from one region at a time. The three regions are shown in different colours and the four sectors are shown with distinct patterns. Contribution from other sources is shown in white and contributions due to interactions between emission sectors is shown in grey.

influence from local residential emissions which exceeded the contributions from regional emissions. This is because episode 1 experienced stronger southwesterly winds during 23–24 October ($4\,m\,s^{-1}$) that brought $PM_{2.5}$ from high-emission sources south of Beijing enabling greater accumulation over the city before it was swept away by the clean northeasterly winds the next day. Episode 2 experienced weak southeasterly winds during 29–30 October ($2\,m\,s^{-1}$) which did not bring as much $PM_{2.5}$ from neighbouring sources but allowed local emissions to build up under calmer conditions. See Figure C.1 in the supplement for more details on the meteorological conditions during the simulation period.

Figure 4.8 presents absolute and relative contributions to daily mean $PM_{2.5}$ in Beijing from the twelve emission sources along with those from the background sources. For each day, the total height of all stacked bars represents the baseline levels. The size of each of 12 coloured bars was calculated by subtracting the daily mean $PM_{2.5}$ concentrations of each sectoral sensitivity run from the baseline values. The white bars were calculated by subtracting $PM_{2.5}$ values of the sensitivity run where all 12 sectors were removed together from the baseline values. The remainder was attributed as "interactions", shown in grey bars which can be interpreted as the extra reductions in $PM_{2.5}$ concentrations due to combined reduction of various emission sectors compared to the added reductions

from individual reduction of each sector. The major contributions are from Beijing and Near-Neighbourhood sources on most days, which make up an average of 35% and 32% respectively. However, Far-Neighbourhood sources also show significant contributions (up to 28%) on more polluted days. The two episodes have slightly different characteristics: as noted above, the 24 October episode was more greatly affected by near-neighbourhood emissions while the 30 October showed a greater influence from local residential emissions. The spatial distribution of 24 h average $PM_{2.5}$ for the two days is shown in Figure 4.9 and confirms this finding. It is interesting to note the differences between these two pollution episodes just five days apart, which emphasises the importance of meteorological processes in governing the source contributions. It is worth noting that local sources are proportionally smallest on polluted days (and largest on clean days).

The contributions of key sources, including background sources build up consistently over the course of each pollution episode. The relative contribution of background sources is slightly higher during the first episode (17%) as compared to that for the second episode (12%). This is likely because, for the first few days, the white bars must also include contribution from the 12 known sources (coloured bars) from previous days before the start date of controls. After about five days, the white bars show only background contribution because we know from experiment 1 that at this point all contribution from the 12 sources are from days within the simulation period, i.e., after the controls began and therefore they are included in the blue, green and red bars.

A sizeable portion of $PM_{2.5}$, denoted as "Interactions" in the figure, remains unattributed to the 12 emission sources or to background, and this reflects non-linear model responses, particularly in the formation of secondary aerosols. Removal of individual sources independently does not account for the interactions between gas-phase precursors from different sectors or regions that drive secondary aerosol formation, and the contribution to total aerosol may thus be underestimated (Zhao et al. 2017). The grey bars show a notably different behaviour from that of other sources, for example, some cleaner days have higher contributions from interactions (e.g., 23 October) than do more polluted days (30 October). On further analysis, the interaction contributions were found to be highly correlated to near-neighbourhood power and transport sectors. In general, the days which have higher contributions from transport and power sectors (not necessarily highest total concentrations) show bigger grey bars. Power and transportation sectors are major sources of SO_2 and NO_2 respectively and this nonlinear behaviour can be explained by the competition between SO_2 and NO_2 in the presence of ammonia to form sulphate and nitrate aerosols. For instance, if a particular day has significant contributions from power and transport sector,

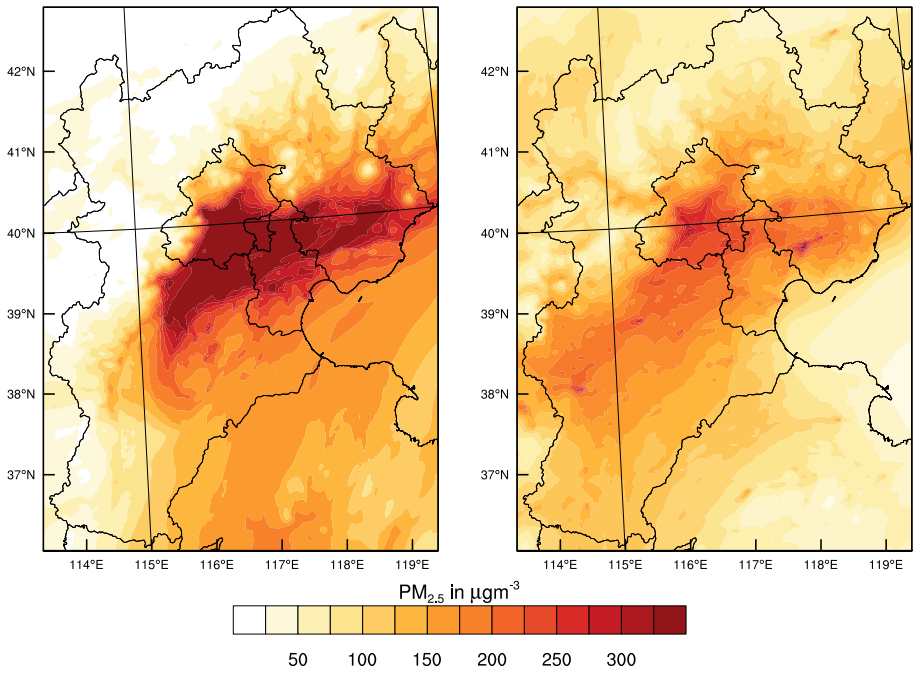

Figure 4.9: 24 h average $PM_{2.5}$ over the study region for 24 October (left) and 30 October (right) episodes showing regional and local accumulation respectively.

reducing power sector emissions alone will reduce SO_2 and therefore $(NH_4)_2SO_4$ thereby freeing up ammonia gas which may then react with NO_2 to form NH_4NO_3 with little change in total $PM_{2.5}$ concentrations, thereby offsetting the benefits of emission reduction. On the other hand, if both power and transportation sectors are controlled together, there may not be enough NO_2 available to react with the freed ammonia, leading to a more efficient PM reduction. However, if power and transportation sectors have small contributions for a particular day, this nonlinear chemistry will not have a significant effect.

To check the robustness of the attribution approaches used here and gain further insight into secondary aerosol responses, we compare the cumulative contributions from one-day controls across all sectors with those from continuous controls on individual sectors. We scale the contributions from individual sectors by 45% for Beijing sources and by 35% for regional sources to match the emission reductions used in the one-day control runs described in Section **??**. A comparison of the cumulative contributions to $PM_{2.5}$ in Beijing from the one-day pulses against those from the continuous controls from each of three regions is shown in Figure 4.10, and the total contributions from all three regions combined is shown in Figure 4.11.

Figure 4.10 shows the composition of contributions from the three source regions in two different ways: as a cumulative of successive one-day controls and as a cumulative of each emission sector. The left hand panels demonstrate that the cleaner days had predominantly

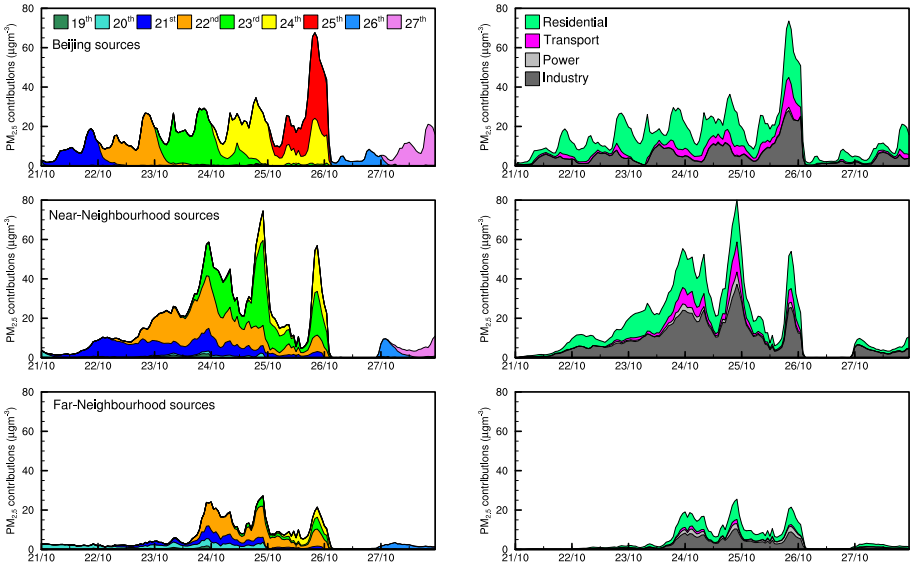

Figure 4.10: Contributions of one-day emission controls (left) and continuous controls (right). Contributions from continuous reductions of each sector (at 100%) were scaled down to match the 30–50% reductions used for the one-day controls.

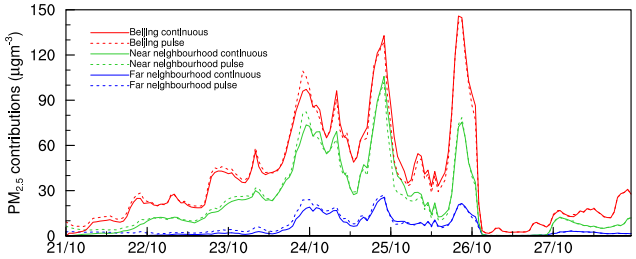

Figure 4.11: Comparison of cumulative contributions from successive one-day pulses and from continuous controls. Contributions from continuous removal of each sector (100% reductions) were scaled down to match one-day controls (30–50% reductions) similar to APEC levels.

local contribution from the same day while the polluted days are formed of accumulated contribution from the previous day for local sources, from up to three days before for near-neighbourhood sources, and from up to four days before for far-neighbourhood sources. In fact, there's no contribution of current day emissions from far-neighbourhood sources. The right hand panels show the region-wise contributions broken into sectors. Industry and residential sectors dominate for all three source regions. Contributions from all three regions show a different, and slow, build-up profile towards the polluted days followed by rapid and almost simultaneous reductions. This behaviour denotes the partly chemical nature of build-up through secondary aerosol production (slower), and on the contrary the physical nature of regional clean-up.

The cumulative contributions of different sources based on one-day emission controls are

very similar to those from the continuous sectoral controls, see Figure 4.10, demonstrating that the two approaches give comparable responses. This lends confidence in our separate attribution of the temporal and sectoral contributions to $PM_{2.5}$ in Beijing.

4.6 Integrated source contributions

To assess the nonlinear response of secondary aerosols towards primary emissions from different sectors, generally a large number of model runs are required with distinct perturbations across all emission sectors. Ideally, if we conduct thousands of model runs with different perturbations across all known primary emission sectors, it would be possible to derive a sensitivity index for each emission sector towards the pollutant of interest, here $PM_{2.5}$ including its secondary mass. This sensitivity index for a sector would be computed to reflect the response of $PM_{2.5}$ towards change in the given sector, averaged over all possible ranges of all other sectors. Such a sensitivity index provides richer information than one-at-a-time local sensitivity index as it reflects the importance of a given parameter in relation with various magnitudes of other parameters rather than independent of them, and helps us in identifying the most influential parameter. Such sensitivity indices are called Global Sensitivity Indices or GSIs (see Dellino & Meloni 2008). However, the thousands of model runs required to generate such indices are not practical given the high computational cost of running a fully coupled high-resolution atmospheric chemical transport model.

Gaussian Process Emulation is an attractive technique to circumvent the large number of model runs required and still derive GSIs. An emulator is a statistical model that mimics the input-output relationship of an expensive simulator, here, the WRF-Chem model. If we are confident that the emulator is accurate, then we can compute GSIs from the outputs of the emulator instead of the simulator (Ryan et al. 2018). The number of model runs required to build an accurate emulator is far less than the number of runs required to obtain reliable GSIs directly from the model. Here, we built daily Gaussian Process emulators using the DICE-Kriging package in R (Roustant et al. 2012) which relate daily mean $PM_{2.5}$ in Beijing for each day to the twelve emission parameters (four sectors across three regions) considered in this study.

To design the model training runs, we use maximin Latin Hypercube sampling, following (Lee et al. 2011), to assign 60 distinct sets of scalings in the range 0–120% to each of the 12 emission sources (see sections C.1 and C.2 in the supplementary material for a brief description of Gaussian process emulation and Latin Hypercube sampling, and Table C.4 for the scalings used). We performed new model simulations for each of these conditions

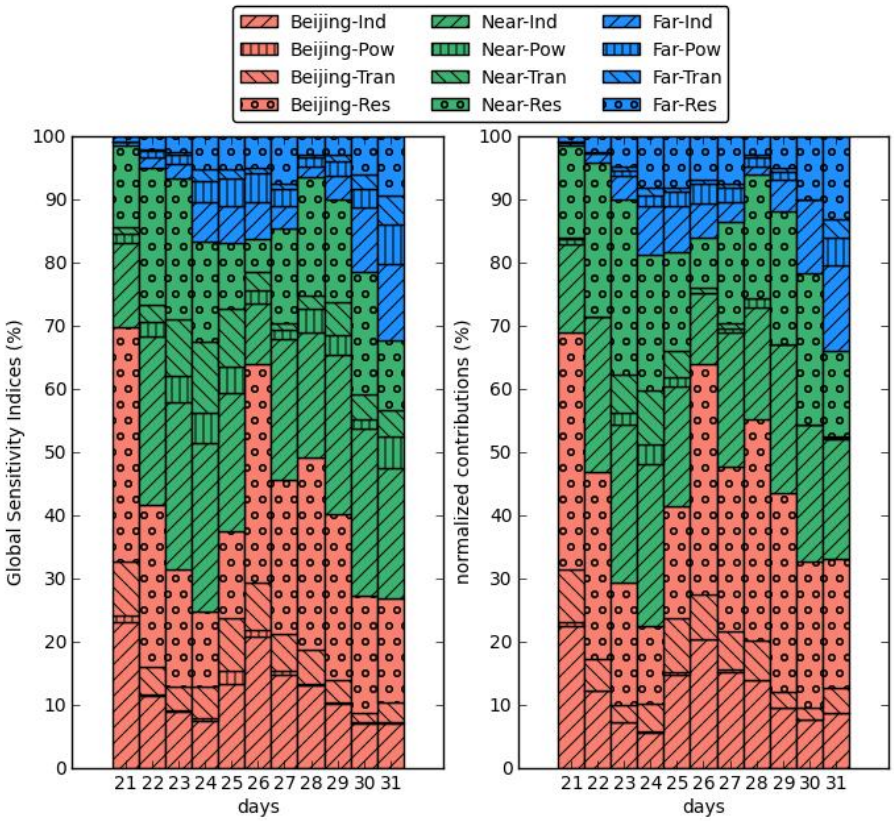

Figure 4.12: A comparison between daily global sensitivity indices for the 12 emission parameters based on Gaussian process emulation (left) and normalized contributions obtained from one-at-a-time sensitivity runs.

for the 11-day period 21–31 October and built 11 corresponding emulators to predict daily mean $PM_{2.5}$ in Beijing for each day using model output. The 11 daily emulators are validated using a leave-one-out method where all 11 emulators are successively rebuilt sixty times using 59 of the model outputs and are tested against the remaining one. This gives a correlation coefficient of 0.9996 (see Figure C.2) indicating that the emulators reproduce the model results well.

We conducted 10,000 sensitivity runs with the emulators to calculate the Global Sensitivity Indices for each of the twelve emission parameters. Figure 4.12 presents a comparison of GSIs obtained from emulation and normalized contributions of each emission parameter from one-at-a-time zero-out runs for all 11 days. We see that the local emissions dominate $PM_{2.5}$ pollution in Beijing on the cleaner days whereas, they become much less important on the polluted days which are dominated by Near-Neighbourhood emissions and to a lesser extent, Far-Neighbourhood emissions. Residential and Industry remain the two most important emission sectors for controlling $PM_{2.5}$ levels in Beijing.

While the sensitivity indices and contributions look very similar on a regional level,

there are some notable differences between sectors. In general, power and transport sectors have higher sensitivity than contributions. This means that while power and transport sectors are not likely to reduce $PM_{2.5}$ levels in Beijing significantly if they are controlled alone, they might have a larger effect when controlled along with other sectors (especially with each other). This kind of non-linear behaviour can be explained by the precursor chemistry that forms $PM_{2.5}$ in Beijing. A large part of $PM_{2.5}$ during these episodes was composed of secondary inorganic aerosols, mainly NH_4NO_3 and NH_4SO_4 (see Ansari et al. 2019a). Power plants are a major source of SO_2 and transport is a major source of NO_2. Reducing only SO_2, through power sector, may lead NH_3 to bind with free NO_2 thereby forming NH_4NO_3. Similarly, reducing only NO_2, through transport sector, may lead NH_3 to bind with free SO_2, forming NH_4SO_4 and thereby not reducing total $PM_{2.5}$ concentration (see Seinfeld & Pandis 2006). However, when both power and transport sectors are reduced together, their individual effect will be more significant–and this is reflected in the sensitivity indices.

Concentration response surfaces were developed for daily average $PM_{2.5}$ in Beijing for each day of the training runs (21–31 October) using computationally efficient Gaussian process emulation. Figure 4.13 presents response surfaces for some key combinations of emission sources for 24 October, the day with highest $PM_{2.5}$ concentrations. Panels (a-c) show $PM_{2.5}$ response to changes in key sectors from all source regions. Panel a highlights that transport sector is more efficient than power sector in reducing total $PM_{2.5}$ over Beijing; 80% reduction in transport results in a drop of 30 $\mu g\,m^{-3}$ (from 343 $\mu g\,m^{-3}$ down to 313 $\mu g\,m^{-3}$) as compared to a drop of only 16 $\mu g\,m^{-3}$ for the same reduction in power sector. The nonlinearity of $PM_{2.5}$ response is also worth noting. For example, reducing the transport sector by 60% (from 100% to 40% strength) when the power sector is at its full strength reduces $PM_{2.5}$ by 20 $\mu g\,m^{-3}$ (343 to 323) while the same reduction in transport sector when the power sector is only at its 20% strength reduces $PM_{2.5}$ by 27 $\mu g\,m^{-3}$ (327 to 300). The more dominant sector from panel a is then compared against residential sector in panel b and the more dominant sector in panel b is compared against industry sector in panel c. Industry turns out to be the most dominant sector, showing highest gradient of $PM_{2.5}$, as shown in panel c and is therefore the most dominant of all sectors.

Panels d and e show response surfaces for different source regions with all sectors combined. Based on $PM_{2.5}$ gradient, panel d highlights that Near Neighbourhood is more dominant than Beijing and panel e highlights that it is also more dominant than Far Neighbourhood. So panels (a-e) establish that industry is the most dominant emission sector overall and Near Neighbourhood is the most dominant source region. To further

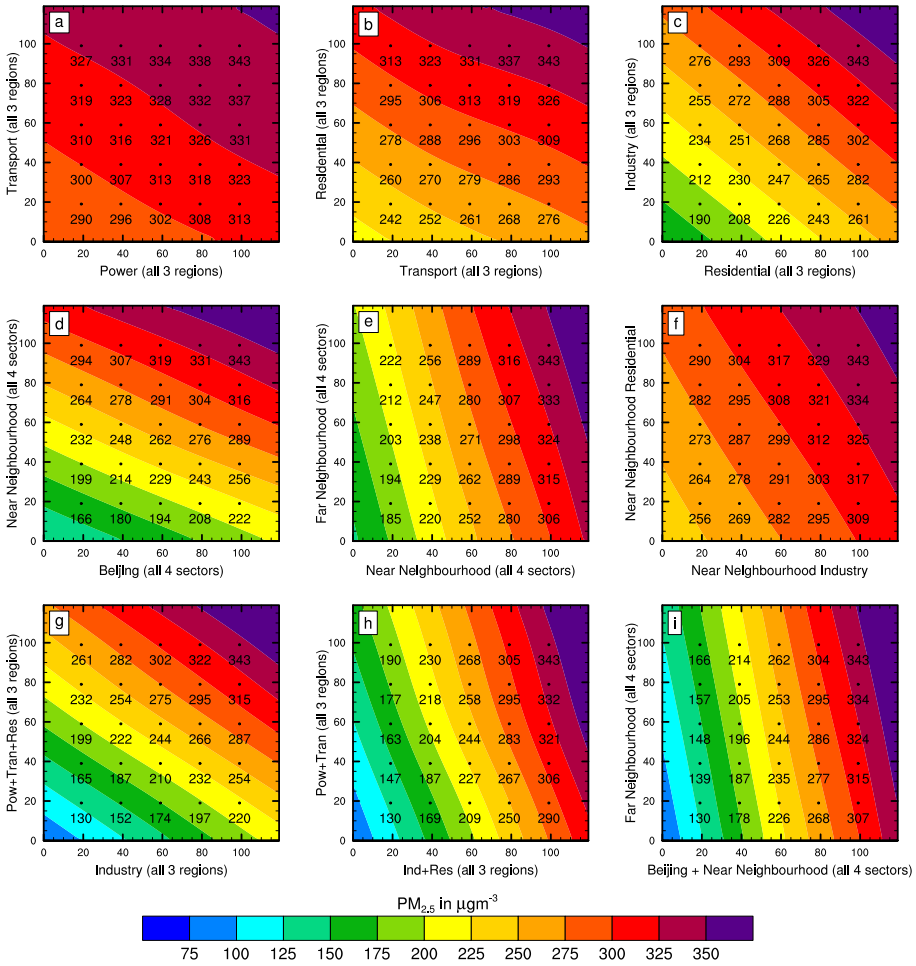

Figure 4.13: Response of daily average $PM_{2.5}$ concentrations in Beijing to changes in sectoral and regional emissions. Axes show the scaling applied to the relevant source (in %) starting on 21 October; contours show the corresponding daily mean $PM_{2.5}$ in Beijing on 24 October (concentrations at 20% intervals are labelled).

investigate the most dominant sector within the most dominant source region, a response surface for Near Neighbourhood Industry versus Near Neighbourhood Residential sectors was developed and is shown in panelf. Near Neighbourhood Industry turns out to be the most dominant individual sector of all the 12 emission parameters considered, leading to a drop of 53 $\mu g\,m^{-3}$ in $PM_{2.5}$ over Beijing for a 80% reduction.

While panels (a-f) highlight the most important emission sectors and source regions for $PM_{2.5}$ control in Beijing, they also show that even 80% reduction of up to 8 out of the 12 emission parameters cannot reduce the $PM_{2.5}$ in Beijing to safe levels. Therefore, three new response surfaces were developed which include reductions across all 12 parameters in various combinations. Three such response surfaces are shown in panels (g-i) which present reductions across the 12 parameters in three different combinations. Panels (g-i) show a substantial drop of 213 $\mu g\,m^{-3}$ in $PM_{2.5}$ levels (from 343 $\mu g\,m^{-3}$ down to 130 $\mu g\,m^{-3}$) if

Table 4.1: Policy options for controlling $PM_{2.5}$ in Beijing

Daily mean $PM_{2.5}$ reduction needed ($\mu g\,m^{-3}$)	Policy recommendation
up to 25	60% reduction across residential and industry sectors for Beijing
26–50	80% reduction across all sectors for Beijing
51–75	50% reduction across all sectors for Beijing and Near-Neighbourhood or, 80% reduction across all sectors for Beijing and 40% reduction across industry in Near- and Far-Neighbourhood or, 80% reduction across industry for all three regions
76–100	60% reduction across all sectors for Beijing and Near-Neighbourhood or, 80% reduction across all sectors for Beijing and 60% reduction across industry for Near- and Far-Neighbourhood
101–125	70% reduction across all sectors for Beijing and Near-Neighbourhood or, 60% reduction across all sectors for all three regions
126–150	80% reduction across all sectors for Beijing and Near-Neighbourhood or, 70% reduction across all sectors for all three regions
151–175	80% reduction across all sectors for all three regions
more than 175	90% reduction across all sectors for all three regions

all 12 parameters are reduced simultaneously by 80%. However, it still does not meet the healthy air quality standard of daily average $PM_{2.5}$ concentrations less than or equal to $75\,\mu g\,m^{-3}$. Meeting this stringent target would require complete control of all emission sectors for all three regions (Figure 4.13 first column) which would bring down the levels to $79\,\mu g\,m^{-3}$. To further reduce the $PM_{2.5}$ concentrations on 24 October, the controls should start one or two days earlier than 21 October, as demonstrated in section 4.4. Nonetheless, these response surfaces provide us with a variety of different emission reduction choices to reduce $PM_{2.5}$ over Beijing in order to meet the healthy air quality target, without the need to run the computationally expensive simulations.

Table 4.1 presents some policy recommendations for pollution episodes of various intensities based on the drop in daily average $PM_{2.5}$ needed. For less polluted episodes of daily mean $PM_{2.5}$ concentrations up to $125\,\mu g\,m^{-3}$, the air quality target can be met by controlling local emissions only, although stringently. For episodes of moderate intensities (daily average $PM_{2.5}$ of 126–$225\,\mu g\,m^{-3}$) stringent controls within the Near-neighbourhood region can meet the standards, whereas for highly polluted episodes (daily average $PM_{2.5}$ of more than $225\,\mu g\,m^{-3}$), all emission sectors within the entire Far-Neighbourhood region need to be controlled. The response surfaces developed here can serve as a guide to prioritizing the more important emission parameters over others, enabling formulation of efficient and effective short-term emission reduction policies for Beijing.

4.7 Conclusions

In this study we provide critical understanding of source contributions for improvement of short-term emission control policies in terms of sectoral and regional selection of emissions and the timing of control for two PM pollution episodes in Beijing using a state-of-the-art numerical atmospheric chemical transport model WRF-Chem and a statistical model trained by it. We split the north China region into three regions of control: Beijing, near-neighbourhood and far-neighbourhood. We found that the effects of local emission controls in Beijing on a given day last until the next day, near-regional controls last until two to three, and far-regional controls up to four days. We found through model sensitivity studies that near-regional industry and residential sectors are major sources of $PM_{2.5}$ pollution in Beijing and further developed a fast metamodel based on Gaussian process emulation to improve source attribution estimates. We finally developed emission-concentration response surfaces for $PM_{2.5}$ in Beijing to serve as a quick guide for better formulating short-term emission control policies without the need of running computationally expensive numerical models.

Results of this study are derived from model simulations over a limited period in October-November 2014, and therefore care must be taken to apply these results over a different period or season. The response surfaces developed here can nonetheless serve as a valuable guide in policy formulation for Beijing for winter period. More generally, these methods can be utilized to build an extensive framework for policy formulation and improvement for other seasons as well as other cities around the world.

APPENDIX C

Supplementary material for chapter 4

This appendix presents the supplementary material of the manuscript prepared for submission in Atmospheric Chemistry and Physics. The tables C.1, C.3 and C.4 briefly describe the runs performed for experiments 1,2 and 3 respectively. Table C.2 presents some key statistics about temporal contributions from each source region. Figure C.1 shows time-series of local and regional average wind speed and direction to facilitate interpretation of results. Figure C.2 shows a scatterplot of simulated versus emulated daily mean $PM_{2.5}$ concentration in Beijing for 60 different sets of emulators trained on 59 sets of model output leaving out one set for validation.

C.1 Gaussian process emulation

In statistics, Gaussian process emulator is a type of statistical model that is used in contexts where the problem is to make maximum use of the outputs of a complicated (often non-random) computer-based simulation model. Each run of the simulation model is computationally expensive and each run is based on many different controlling inputs. The variation of the outputs of the simulation model is expected to vary reasonably smoothly with the inputs, but in an unknown way. The overall analysis involves two models: the simulation model, or "simulator", and the statistical model, or "emulator", which notionally emulates the unknown outputs from the simulator. The Gaussian process emulator model treats the problem from the viewpoint of Bayesian statistics. In this approach, even though the output of the simulation model is fixed for any given set of inputs, the actual outputs are unknown unless the simulator is run with those inputs, and hence can be made the

subject of a Bayesian analysis (O'Hagan 2006). The main element of the Gaussian process emulator is that it models the outputs as a Gaussian process on a space that is defined by the model inputs. The emulator includes a description of the correlation or covariance of the outputs, which enables the model to encompass the idea that differences in the output will be small if there are only small differences in the inputs. In such a framework, the uncertainty does not refer to an actual random phenomenon, but to a partially observed deterministic phenomenon. One often refers to the latter kind of uncertainty as epistemic, whereas the former one is called aleatory (Helton & Davis 2003). Gaussian process emulation has been successfully used for global sensitivity analysis in atmospheric chemical transport models (Lee et al. 2012, Ryan et al. 2018).

C.2 Latin hypercube sampling

Latin Hypercube Sampling (LHS) is a way of generating random samples of parameter values. It is widely used in Monte Carlo simulation, because it can drastically reduce the number of runs necessary to achieve a reasonably accurate result. The whole purpose of LHS is to capture the probability distribution with less number of samples and it is done by stratifying the probability distribution into equal intervals and choosing random samples from each stratification (Loh 1996, Helton & Davis 2003). LHS is based on the Latin square design, which has a single sample in each stratification. In the context of statistical sampling, a square grid containing sample positions is a Latin Square if and only if there is only one sample in each row and each column. A "hypercube" is a cube with more than three dimensions; the Latin square is extended to sample from multiple dimensions and multiple hyperplanes.

Table C.1: List of pulse runs for the three source regions. These runs were part of experiment 1.

Span	**Beijing**	**Near-Neigh.**	**Far-Neigh.**
18–22 Oct	Run 1	Run 21	Run 41
19–23 Oct	Run 2	Run 22	Run 42
20–24 Oct	Run 3	Run 23	Run 43
21–25 Oct	Run 4	Run 24	Run 44
22–26 Oct	Run 5	Run 25	Run 45
23–27 Oct	Run 6	Run 26	Run 46
24–28 Oct	Run 7	Run 27	Run 47
25–29 Oct	Run 8	Run 28	Run 48
26–30 Oct	Run 9	Run 29	Run 49
27–31 Oct	Run 10	Run 30	Run 50
2–6 Nov	Run 11	Run 31	Run 51
3–7 Nov	Run 12	Run 32	Run 52
4–8 Nov	Run 13	Run 33	Run 53
5–9 Nov	Run 14	Run 34	Run 54
6–10 Nov	Run 15	Run 35	Run 55
7–11 Nov	Run 16	Run 36	Run 56
8–12 Nov	Run 17	Run 37	Run 57
9–13 Nov	Run 18	Run 38	Run 58
10–14 Nov	Run 19	Run 39	Run 59
11–15 Nov	Run 20	Run 40	Run 60

Each run is 5-day long with APEC-level controls on Day 1 but no controls for Day 2–Day 5

Table C.2: Statistical metrics of 1-day pulses of emission cuts for various regions

Start/End	Peak Benefit ($\mu g\,m^{-3}$)			Time to reach peak benefit (hours)			Length of benefits (hours)			Integrated benefit ($\mu g\,m^{-3}$ hours)		
	Beijing	Near	Far	Beijing	Near	Far	Beijing	Near	Far	Beijing	Near	Far
Polluted period												
18–22 Oct	33.12	33.73	15.03	16	30	46	28	44	61	393.1	386.07	243.89
19–23 Oct	29.93	21.61	1.93	14	24	31	35	36	44	502.67	320.45	29.49
20–24 Oct	13.03	5.76	3.76	12	21	103	23	116	117	170.65	108	203.02
21–25 Oct	18.65	11.52	6.63	16	33	79	33	101	93	225.37	560.02	153.42
22–26 Oct	26.52	27.4	15.82	15	39	58	34	93	95	366.64	913.39	398.29
23–27 Oct	28.81	43.12	6	15	36	61	40	71	72	532.95	794.94	86.81
24–28 Oct	31.05	22.86	5.48	14	37	38	48	48	49	662.57	226.01	73.35
25–29 Oct	43.47	0.62	1.27	14	103	19	24	66	49	496.45	0.00	7.75
26–30 Oct	8.34	9.25	3.12	13	34	105	25	45	50	95.1	68.58	57
27–31 Oct	20.89	10.31	8.19	17	33	82	30	91	101	270.17	462.06	306.6
Clean period												
2–6 Nov	19.04	0.25	2.63	14	33	37	25	30	74	138.22	1.45	91.16
3–7 Nov	21.76	4.68	8.53	13	28	40	35	49	55	295.85	92.23	137.14
4–8 Nov	29.29	7.78	4.38	16	21	34	26	28	34	378.48	70.37	28.29
5–9 Nov	20.56	0.34	2.84	12	91	87	23	119	99	146.15	2.83	45.98
6–10 Nov	19.25	8.8	4.01	13	58	38	26	74	77	147.34	236.41	153.45
7–11 Nov	33.16	3.23	1.77	17	17	44	33	28	105	365.47	48.94	51.97
8–12 Nov	27.37	2.75	4.43	13	20	37	25	24	99	357.81	14.77	124.34
9–13 Nov	28.01	2.6	5.65	13	28	35	29	79	69	298.03	12.81	135.82
10–14 Nov	36.18	3.11	3.1	14	14	20	24	69	31	349.86	12.12	30.4
11–15 Nov	11.27	0.71	1.19	12	30	15	22	119	46	112.8	2.31	11.68

3 sets of simulations corresponding to the 3 regions were performed for each 5-day slot. Emissions were reduced only on the first day of each simulation. Benefits were calculated by substracting hourly $PM_{2.5}$ values of each run from the baseline run. A 24-hour running average was applied on the absolute benefits time-series to calculate reliable peak timings.

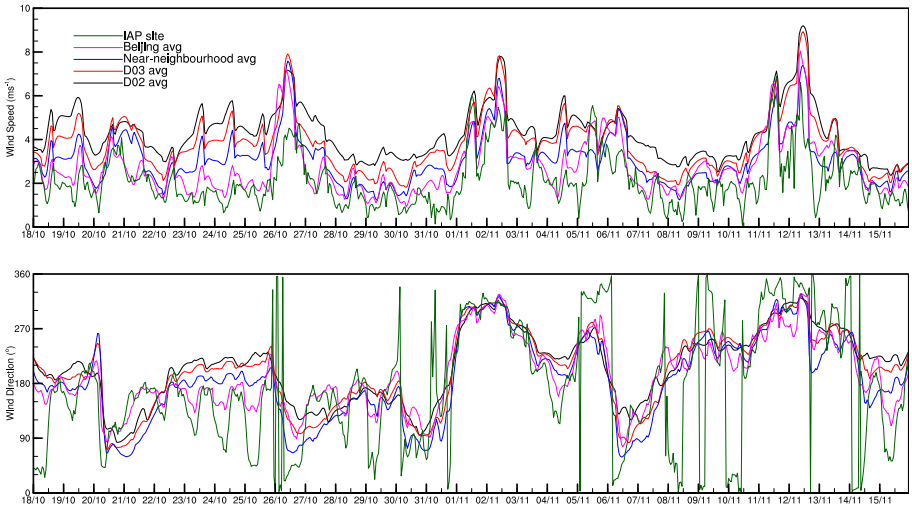

Figure C.1: Hourly wind speed and direction averaged over various regions.

Table C.3: List of runs part of experiment 2 where one of the emission sectors was removed.

Run no.	**Switched-off Emissions**
Run 1	Beijing Industry
Run 2	Beijing Power
Run 3	Beijing Transport
Run 4	Beijing Residential
Run 5	Near-Neighbourhood Industry
Run 6	Near-Neighbourhood Power
Run 7	Near-Neighbourhood Transport
Run 8	Near-Neighbourhood Residential
Run 9	Far-Neighbourhood Industry
Run 10	Far-Neighbourhood Power
Run 11	Far-Neighbourhood Transport
Run 12	Far-Neighbourhood Residential
Run 13	All of the above

Table C.4: Perturbations across the 12 emission parameters ranging from 0–1.2 for the 60 runs

Run No.	Beijing Industry	Beijing Power	Beijing Tranport	Beijing Residential	Near Industry	Near Power	Near Tranport	Near Residential	Far Industry	Far Power	Far Tranport	Far Residential
1	0.730	1.055	0.620	0.509	0.907	0.280	0.974	0.150	0.505	0.992	0.128	0.602
2	0.949	0.923	1.020	0.255	0.420	0.040	1.149	1.028	0.574	0.160	1.061	0.055
3	0.101	0.322	0.669	0.225	0.161	1.051	0.684	0.047	0.095	0.204	0.434	0.686
4	0.594	0.164	0.206	0.061	1.062	0.199	0.829	0.077	0.365	0.690	0.512	0.771
5	0.042	0.945	1.185	0.993	0.414	0.141	0.887	0.400	1.094	1.177	0.539	1.084
6	0.247	1.013	0.176	1.139	1.094	1.175	0.451	0.990	0.943	0.387	0.191	0.810
7	0.322	0.416	0.688	0.498	1.135	0.309	0.983	0.352	0.875	0.959	0.173	1.189
8	0.009	0.789	0.709	0.527	0.920	0.229	0.049	0.637	0.841	1.139	0.768	1.136
9	0.658	0.457	0.798	0.378	0.460	0.734	0.790	0.948	1.159	0.522	0.660	1.160
10	0.274	0.536	0.094	0.029	0.094	0.572	0.847	0.681	0.748	0.711	0.994	0.369
11	0.536	0.668	0.727	0.900	0.034	0.758	1.185	1.058	0.661	0.021	0.267	0.542
12	0.845	1.137	0.255	0.479	0.265	0.540	0.352	0.473	0.980	0.403	0.970	0.333
13	0.411	0.372	1.076	0.676	0.869	0.670	0.674	0.857	0.265	1.069	0.340	0.745
14	0.786	0.593	0.144	0.558	1.104	0.386	0.136	0.715	1.182	0.816	0.086	1.180
15	0.511	0.516	0.517	0.682	0.392	0.866	0.616	0.793	0.017	0.622	0.898	0.073
16	1.043	0.061	0.559	1.004	0.970	0.209	0.491	0.617	0.547	0.483	0.077	0.507
17	0.027	0.118	0.871	0.581	0.055	1.025	0.750	1.151	0.438	0.932	0.231	0.171
18	0.442	0.850	0.185	0.601	0.281	0.544	1.100	0.219	1.020	0.276	1.195	0.262
19	0.567	0.764	0.607	0.818	0.073	0.422	0.027	0.442	0.308	0.659	1.111	0.673
20	1.193	0.882	0.314	0.433	1.162	0.376	0.420	0.025	0.905	0.433	1.059	1.049
21	0.695	0.997	1.165	0.771	0.138	1.018	1.047	0.739	0.713	0.789	1.096	0.450
22	1.032	0.714	0.108	0.154	0.204	1.193	0.236	0.162	1.120	0.352	0.709	0.910
23	0.097	0.193	0.849	0.972	0.530	0.408	0.012	0.820	0.400	1.198	1.022	0.526
24	0.176	0.907	0.943	0.107	0.672	0.653	0.410	0.262	0.188	0.745	0.026	0.213
25	0.619	1.101	0.373	0.338	0.319	0.681	0.264	0.898	0.036	0.587	0.149	0.186
26	0.500	0.825	0.432	0.736	0.324	0.764	0.517	1.139	0.823	0.905	1.017	0.561
27	0.977	0.488	0.776	1.093	1.017	0.883	1.134	0.974	0.412	0.139	0.638	0.233
28	0.806	0.300	0.990	1.080	1.052	0.906	1.018	0.577	1.122	0.224	0.616	0.825
29	1.174	0.093	0.835	0.178	0.799	0.090	0.090	0.300	0.072	0.002	0.295	0.582
30	0.310	1.161	0.584	0.705	1.035	0.446	0.730	1.095	0.352	0.826	0.939	0.418
31	0.399	1.195	1.151	0.564	0.888	0.472	0.205	1.186	0.465	0.193	0.445	0.248
32	0.998	0.462	0.534	0.850	0.563	0.964	0.873	1.102	0.137	0.861	0.251	0.659
33	0.422	0.750	0.815	1.169	0.621	0.923	1.175	0.091	0.584	0.459	0.866	1.010
34	0.376	0.730	0.914	0.647	0.518	1.141	0.717	0.380	0.680	0.380	0.205	0.111
35	1.004	0.387	0.754	0.888	0.836	1.093	0.158	0.656	0.460	0.555	1.138	0.629
36	0.868	0.046	0.461	1.052	0.843	0.835	0.108	0.194	0.888	0.083	0.686	0.032
37	1.103	0.602	0.064	1.021	0.643	0.595	0.560	0.400	0.162	0.109	0.757	0.982
38	0.135	0.012	0.966	0.310	0.990	0.811	1.062	0.921	0.339	0.257	0.003	0.010
39	1.070	0.639	0.269	1.107	0.682	1.061	0.761	0.498	0.769	1.112	0.473	0.347
40	0.839	0.243	0.481	0.865	0.224	0.984	1.106	0.915	0.732	0.053	0.948	0.462
41	1.149	0.153	0.231	0.285	0.114	1.132	0.536	0.813	0.118	1.036	0.919	1.036
42	0.471	0.878	0.574	1.183	0.734	0.629	0.364	0.424	0.793	0.890	1.175	0.392
43	0.181	0.660	1.125	0.082	0.243	0.007	0.912	0.013	0.220	0.564	0.860	1.115
44	0.287	1.159	0.649	0.260	1.155	0.792	0.311	0.244	0.298	0.294	0.586	0.785
45	0.710	0.134	0.413	0.942	0.149	0.077	0.937	0.559	0.818	0.853	0.802	0.140
46	0.741	0.542	1.091	0.448	0.610	0.340	0.199	0.331	0.057	0.612	1.144	0.292
47	0.671	0.340	1.106	0.793	0.808	1.103	0.079	0.315	0.156	1.047	0.568	0.895
48	0.776	1.072	0.932	0.635	0.186	0.117	0.654	0.865	0.980	1.006	0.786	0.428
49	0.552	0.204	0.007	0.921	0.717	0.266	0.477	1.066	1.179	0.317	0.542	0.974
50	0.905	0.817	0.322	0.833	0.376	0.351	0.396	0.511	0.625	0.331	0.051	1.061
51	0.077	0.425	0.046	0.211	0.585	0.958	0.168	0.763	0.922	0.737	0.491	0.848
52	0.893	0.233	0.022	0.418	0.751	0.509	0.952	1.017	0.610	0.469	0.312	0.952
53	0.156	0.034	1.060	0.181	0.341	0.480	0.816	0.596	1.060	0.960	0.827	0.726
54	1.086	0.564	0.400	0.047	0.007	0.242	0.291	0.536	0.485	1.090	0.113	0.152
55	0.239	0.264	0.356	0.747	1.190	0.851	0.324	0.676	0.534	0.080	0.647	0.300
56	0.213	1.040	0.889	0.398	0.480	0.704	0.584	0.116	1.034	0.771	0.405	0.497
57	0.342	0.973	0.458	0.136	0.774	0.169	0.626	1.169	0.210	0.661	0.329	0.936
58	0.637	0.315	1.017	0.358	0.459	0.135	0.241	0.757	0.645	1.159	0.389	0.719
59	0.934	0.698	0.137	1.151	0.543	0.027	0.540	0.133	0.252	0.152	0.726	0.097
60	1.123	1.082	0.280	0.004	0.945	0.601	1.031	0.236	1.042	0.510	0.380	0.865

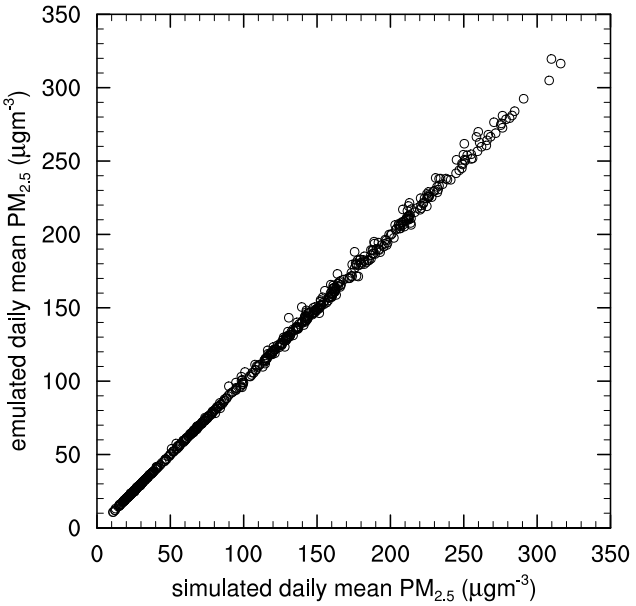

Figure C.2: Correlation plot showing simulated versus emulated daily mean $PM_{2.5}$ in Beijing. The plot contains results for sixty different sets of 11 daily emulators (21–31 October) built by training with all but one set of model output which they are validated against. A total of 60x11 datapoints are shown.

CHAPTER 5

Developing a dynamic modelling framework to inform short-term air pollution emission controls

Tabish Umar Ansari[1], Oliver Wild[1] and Andrew Jarvis[1]

[1]Lancaster Environment Centre, Lancaster University, Lancaster, UK

(Manuscript in preparation)

Author contributions: TUA, OW, and AJ designed this study. TUA performed the model simulations and analysis. TUA and OW prepared the manuscript, with input from AJ.

5.1 Abstract

Despite the implementation of long-term action plans to curb air pollution, Beijing continues to experience severe winter haze days. Additional short-term emergency measures are needed to prevent high levels of fine particulate matter. Here we present, for the first time, a dynamic emissions scaling framework DESMoRF that uses a state-of-the-art atmospheric chemical transport model WRF-Chem at high-resolution over Northern China and Beijing to identify optimal emission controls across major emission sectors in order to mitigate a forthcoming pollution episode in Beijing. The reductions are optimized across industry, power plants, transportation and residential sectors for Beijing, neighbouring provinces, and farther provinces based on their contribution to $PM_{2.5}$ in Beijing. We demonstrate three different implementations of DESMoRF based on one-day, three-day and four-day

forecasts. This approach can be used for other polluted regions of the world and has tremendous potential to be extended into a multi-faceted air quality policy guidance and implementation system.

5.2 Introduction

Air pollution episodes are a major problem in many cities around the world damaging health and well-being of the local population (Brimblecombe 2017, Anderson 1999). In recent decades, severe winter haze episodes characterized by very high values of fine particulate matter ($PM_{2.5}$) have become a high-profile problem particularly in China(Guo et al. 2014, Dang & Liao 2019, An et al. 2019). Reduction of emissions through change in industrial technology, and transition to cleaner fossil fuels (e.g., oil and gas instead of coal) is the only durable solution to the persistent menace of air pollution. However, such transition takes place slowly and does not immediately prevent air pollution episodes.

The Chinese government has implemented long-term pollution mitigation policies such as the *Action Plan on Prevention and Control of Air Pollution, APPCAP, 2013–2017* which set $PM_{2.5}$ targets for the city clusters of Beijing–Tianjin–Hebei and the Pearl and Yangtze Deltas. This action plan covered a wide variety of measures such as industrial restructuring, technology transformation, clean energy supply, change in economic policy, improving laws and regulations, regional cooperation, monitoring systems and public participation (McMullen-Laird et al. 2015). The APPCAP was followed by the *Three year Action Plan for Winning the Blue Sky War, 2018-2020* which covers a total of 338 cities and sets a standard of annual mean $PM_{2.5}$ of $35\,\mu g\,m^{-3}$.

While the implementation of these long term pollution mitigation policies has significantly reduced annual average $PM_{2.5}$ concentrations and mortality (Huang & Gao 2018), Beijing and its neighbourhood continues to experience heavy haze days with very high levels of $PM_{2.5}$ especially during the winter months (Dang & Liao 2019, Yu et al. 2018). Therefore, short-term controls are still needed to mitigate the worst episodes.

National policies for short-term control measures such as the *Clean Air Protection during Mega Events* and *Air Pollution Warning and Protection Measures* have been introduced by the Ministry of Ecology and Environment of China (Li et al. 2019) and have been successfully implemented during major events including the 2008 Beijing Olympics; the 2010 Guangzhou Asian Games; the 2014 Asia-Pacific Economic Cooperation forum (APEC); 2014 Summer Youth Olympics in Nanjing; and the 2015 China Victory Day Parade. Several observational studies have reported an improvement in air quality during these events

(Wang et al. 2014c, Tao et al. 2015, Wang et al. 2015, Miettinen et al. 2019, Ren et al. 2019) while modelling studies have evaluated the effectiveness of these emission controls (Streets et al. 2008, Liu et al. 2013, Ansari et al. 2019a, Wang et al. 2017a). These short-term controls have typically been successful in reducing $PM_{2.5}$ concentrations but were greatly aided by favourable meteorology (Zhang et al. 2016a, Gao et al. 2017) and may not be effective under more stagnant weather conditions. Ansari et al. (2019a) studied a five week period in October-November 2014 during which 15 days did not meet the healthy air quality criteria of 24h average $PM_{2.5}$ less than 75 $\mu g\,m^{-3}$ (henceforth, AQ criteria) and demonstrated that while implementation of emission controls similar to APEC-controls would bring the pollutant levels down, still 13 days (about 30% of the time) would not meet the standards, highlighting the need for more stringent controls.

Even as significant knowledge has been gained from past experience of these real-world experiments of short- and long-term emission controls, there is still need for a framework to inform short-term controls–ideally to identify controls that are no stricter (and more expensive) than needed to meet the AQ criteria on a continuous basis. Limited studies (e.g., Yu et al. 2018, Li et al. 2019) have attempted to identify optimal short-term controls through model simulations but have not developed an automatic emission prescription framework.

Here, we introduce an entirely new approach bringing ideas from system control theory together with air quality models for the first time to demonstrate an effective way to identify appropriate emission controls to mitigate major episodes: the *Dynamic Emissions Scaling Model Running Framework (DESMoRF)*. DESMoRF performs air quality forecasts on a daily basis to determine if a major pollution episode is forthcoming, calculates appropriate emission reduction needed based on pre-defined model pollutant response surfaces (see chapter 4), and applies these controls in the model so that the AQ standards are met.

A brief description of the model and the study period is presented in section 5.3. A description of the approach is presented in section 5.4 and its three different implementations are presented in sections 5.5, 5.6 and 5.7. Section 5.8 provides further discussions and implications and future outlook.

5.3 Model configuration and study period

We use a well-tested configuration of the WRF-Chem model version 3.7.1 as developed in our previous studies (Ansari et al. 2019a,b) to simulate air pollution over China focusing on to Beijing at 3 km horizontal resolution for the October 2014 period. We use the

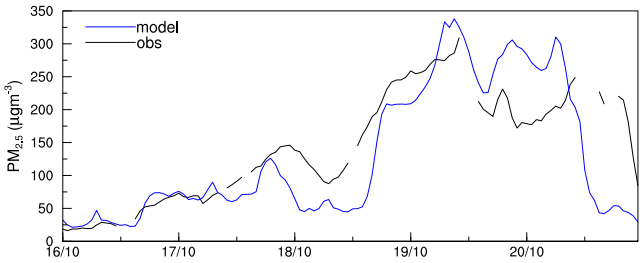

Figure 5.1: Simulated and observed hourly $PM_{2.5}$ concentrations averaged over 12 measurement stations in Beijing during 16–20 October 2014.

Multi-resolution Emission Inventory for China (MEIC) with base year 2010 modified for 2014 for anthropogenic emissions of NO_X, CO, NMVOCs, SO_2, NH_3, $PM_{2.5}$, PM_{10}, black carbon (BC) and organic carbon (OC) which are provided for four major emission sectors that include industrial sources, power plants, transportation sources, and residential cooking and heating (Li et al. 2017c). NH_3 is also provided for agricultural sources. While residential, transportation and agricultural emissions were supplied at surface, emissions from industries and power plants were supplied at various heights based on EMEP emissions (Bieser et al. 2011, Mailler et al. 2013). Biogenic emissions are provided based on online calculations within the model (MEGAN; Guenther et al. 2012) and hourly fire emissions are provided through the Fire Emissions INventory from NCAR (FINN; Wiedinmyer et al. 2011). We use the Carbon Bond Mechanism version Z (CBMZ) gas-phase chemistry scheme along with the Model for Simulating Aerosol Interactions and Chemistry (MOSAIC) sectional aerosol scheme with 8 size bins. Further details of the model configuration and a comprehensive meteorological and chemical evaluation are presented in Ansari et al. (2019a).

Strict short-term emission controls were implemented in Beijing and its neighbourhood at the beginning of November 2014 before and during the Asia-Pacific Economic Cooperation (APEC) summit which was held in Beijing from 10–12 November 2014 (Tang et al. 2015, Wen et al. 2016). The controls were largely successful in reducing $PM_{2.5}$ concentrations in Beijing during the meeting but favourable meteorology made a major contribution to this reduction (Zhang et al. 2016a, Gao et al. 2017) and the same controls would have been insufficient in meeting healthy air quality standards during the pre-APEC period (Ansari et al. 2019a). Here we focus on a five-day pollution episode during the extended polluted period at the end of October 2014 preceding the APEC summit (see Figure 5.1).

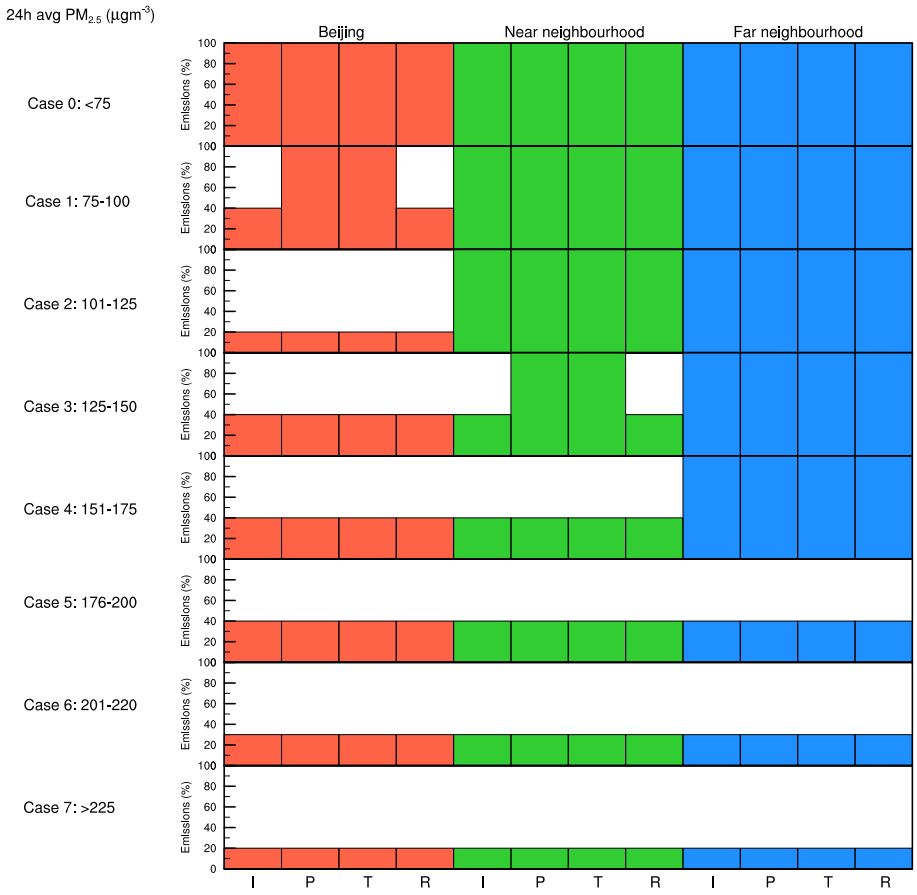

Figure 5.2: Emissions scalings needed for controlling $PM_{2.5}$ in Beijing. I, P, T and R refer to industry, power, transport and residential sectors respectively.

5.4 Methods

Figure 5.2 shows a simple emission reduction policy based on the response surface results as discussed in chapter 4. This policy framework is adopted in DESMoRF where emissions are reduced across industry, power, transport and residential sectors of three regions of control: Beijing, Near neighbourhood and Far neighbourhood (see Figure 4.2) based on the predicted daily mean $PM_{2.5}$ concentration in Beijing. Here, we have considered eight cases with different set of emission reductions across the twelve sectors. There are multiple ways to achieve a given target some of which are highlighted in Table 4.1, however we have prioritized the residential and industry sectors over others due to their higher contribution to $PM_{2.5}$ in Beijing. Similarly we have prioritized Beijing over Near neighbourhood which is prioritized over Far neighbourhood because local and near neighbourhood controls show quicker and higher peak reductions over Beijing (see Ansari et al. 2019b). For simplicity we use 10% reduction steps across each sector and a bracket of 25 $\mu g\, m^{-3}$ for each case. However, the same policy can also be implemented at a higher resolution: say, 300 cases

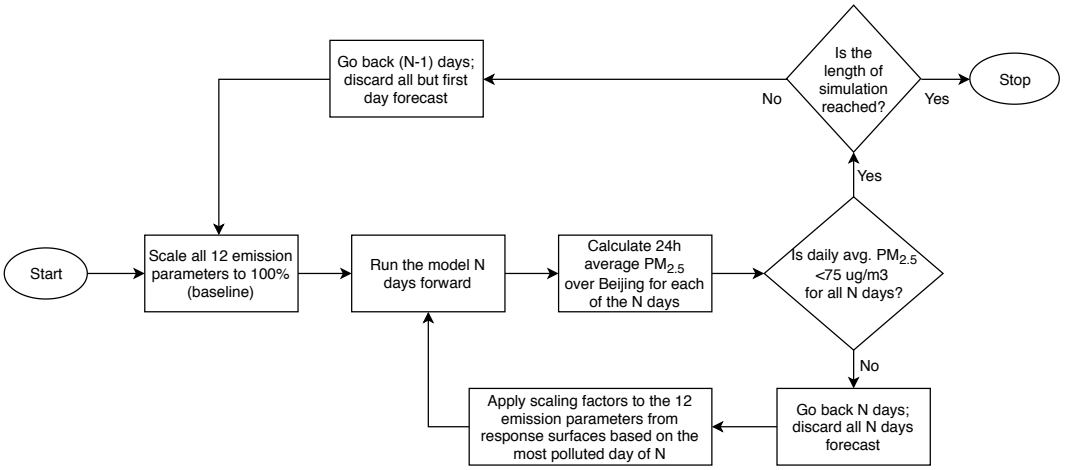

Figure 5.3: A simple flowchart of the dynamic emission controls run. Three cases (N=1,3,4) were tested.

based on $1\,\mu g\,m^{-3}$ change in predicted daily mean $PM_{2.5}$ and 1% reduction steps across each sector.

Figure 5.3 shows the general workflow of DESMoRF. It begins with a one day forecast with baseline emissions and calculates the daily mean $PM_{2.5}$ concentration for Beijing. If the forecasted $PM_{2.5}$ concentration meets the AQ criteria, the model forecasts the next day and repeats the same operations. If the AQ criteria is not met, emissions are reduced across the twelve emission sectors based on the emission reductions shown in Figure 5.2 and the model performs the forecast with the reduced emissions. It then moves to the next day and repeats the same procedure. Ultimately DESMoRF provides the prescribed emission reductions for each day of the simulation.

Since regional controls need three to four days to provide maximum reductions in $PM_{2.5}$ concentration at the receptor, as discussed in the previous chapter, controls based on a one-day forecast may not be sufficient to mitigate a next day episode. Therefore, we demonstrate additional implementations of DESMoRF where the reductions are applied over longer time periods (3-4 days) before the episode.

While such emission reductions can be tested by manually applying them to the model input and running the model for every pollution episode, it is desirable to have an automated system where the model runs ahead in time with baseline emissions, stops if the forecasted day violates the AQ criteria and reruns with reduced emissions until it meets it, then proceeds to the next day following the same rule, ultimately providing us with the requisite scalings for all 12 emission sectors and their optimal timing. DESMoRF performs all these operations without user intervention.

5.5 One-day forecast

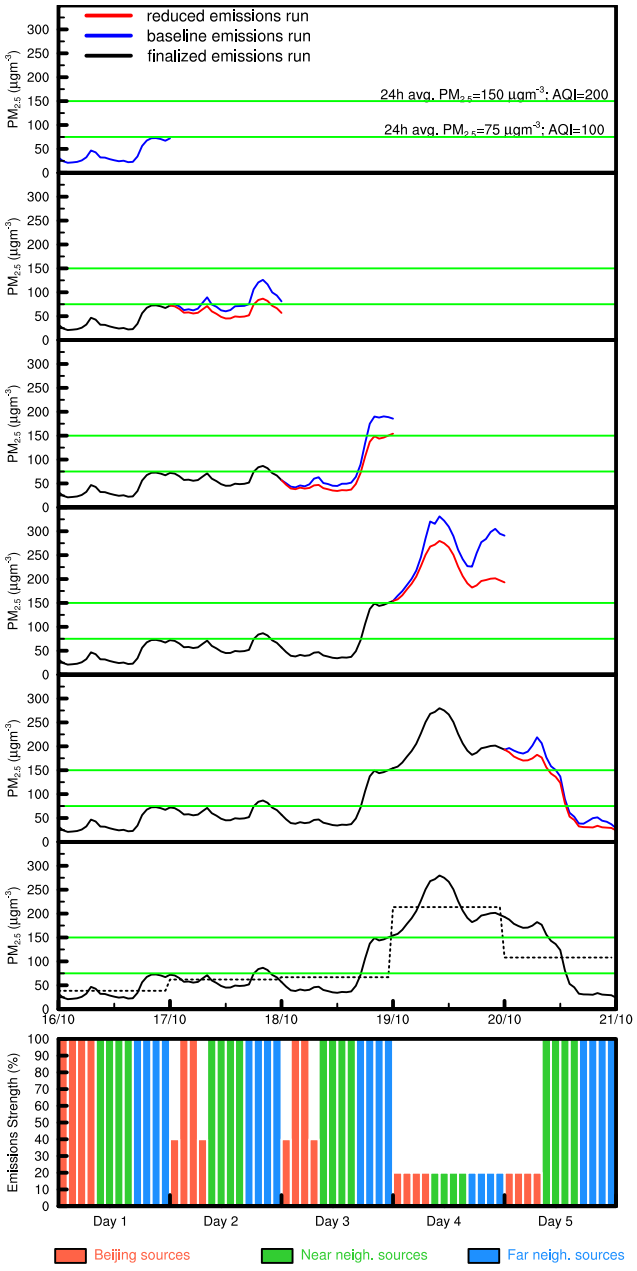

Figure 5.4: Simulated hourly $PM_{2.5}$ concentrations in Beijing with baseline and reduced emissions for 1 day ahead.

In this implementation, the model was run one day forward with baseline emissions for 16 October leading to a daily mean $PM_{2.5}$ concentration of 40 $\mu g\,m^{-3}$ (see Figure 5.4). Since this value is below the target value of 75 $\mu g\,m^{-3}$, the model run was continued for the next day with the same emissions and a daily mean $PM_{2.5}$ concentration of 80 $\mu g\,m^{-3}$ was obtained which violates the AQ criteria. The model output for 17 October is then discarded, emissions are scaled down as per Figure 5.2 and the model is run again for 17 October leading to a daily mean $PM_{2.5}$ concentration of 61 $\mu g\,m^{-3}$ which meets the AQ

criteria. The model is then advanced to 18 October with baseline emissions leading to a daily mean $PM_{2.5}$ concentration of 89 $\mu g\,m^{-3}$. The model is rerun for 18 October with scaled down emissions following the reductions identified for case 1 leading to a daily mean $PM_{2.5}$ concentration of 71 $\mu g\,m^{-3}$ (AQ criteria satisfied). From this point the model is run one day forward for 19 October with baseline emissions leading to a very high daily mean $PM_{2.5}$ concentration of 264 $\mu g\,m^{-3}$. Again, the model output for 19 October is deleted and the model is rerun with greatly reduced emissions (80% reduction across all parameters; case 7) leading to a daily mean $PM_{2.5}$ concentration of 215 $\mu g\,m^{-3}$. This shows that the reductions in Figure 5.2 are not sufficient if implemented just one day in advance of a major pollution episode. Nonetheless, the model run is carried on from this point for the next day with baseline emissions leading to a a daily mean $PM_{2.5}$ concentration of 116 $\mu g\,m^{-3}$ (case 3) which, again, was discarded and repeated with scaled down emissions for case 3 leading to a final daily mean $PM_{2.5}$ concentration of 101 $\mu g\,m^{-3}$ (lesser than 116 but still above the critical value of 75), again highlighting the inadequacy of just-in-time implementation of emission controls.

Figure 5.4 shows the predicted $PM_{2.5}$ concentrations in Beijing at each step along with the emissions scalings applied. The black line denotes the $PM_{2.5}$ concentrations corresponding to the finalized emission reductions for each day which are shown in the bottom most panel. Here, we demonstrated that dynamic emission controls can be applied online to generate feasible combinations of reductions that improve air quality but that applying controls one day in advance is insufficient to meet AQ standards.

5.6 Three-day forecasts

Here we implement the emission controls policy three days in advance. We start with a three day forward run with baseline emissions and gives us daily mean $PM_{2.5}$ concentrations of 40, 80 and 97 $\mu g\,m^{-3}$ for 16–18 October (see Figure 5.5). Since both 17 and 18 October fail to meet the AQ criteria, the model is rerun for 16–18 October with reduced emissions to meet the AQ criteria for the worst of the three days, i.e., 18 October (97 $\mu g\,m^{-3}$). Applying emission controls given by Case 1 leads to $PM_{2.5}$ concentrations of 32, 60 and 71 $\mu g\,m^{-3}$ for 16–18 October and all three days meet the criteria.

Now, the model output and corresponding emission reductions for 17 and 18 October are discarded. This is because although both these days meet the criteria with the current reductions, it is uncertain whether the pollutant levels on the next day would be low enough to be avoided by continuing these controls or implementing more stringent controls

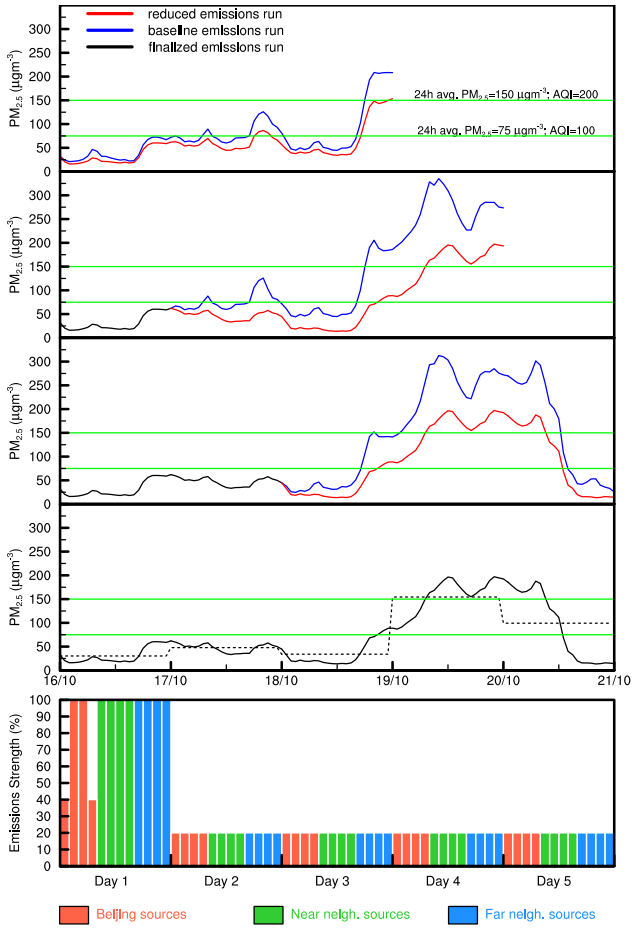

Figure 5.5: Simulated hourly $PM_{2.5}$ concentrations in Beijing with baseline and reduced emissions for 3 days ahead.

just one day in advance. In this framework, the possible more stringent controls need to start three days in advance so instead of preserving the emission reductions and model output for 16–18 October and starting the next forecast for 19 October, we only preserve the model output and reductions for 16 October (32 µg m^{-3}) and start the model from this point onwards again with baseline emissions for the next three days and obtain daily mean $PM_{2.5}$ concentrations of 77, 92 and 268 µg m^{-3} for 17–19 October. We then select the worst of the three cases, i.e. 268 µg m^{-3} (case 7) and scale the emissions accordingly. The model output for 17–19 October is then discarded and the model is rerun for these three days with reduced emissions (case 7) leading to new daily mean $PM_{2.5}$ concentrations of 47, 36 and 159 µg m^{-3} for 17–19 October. This shows that guided emission scalings are not able to reduce the $PM_{2.5}$ concentrations to desired levels, even when implemented three days in advance. However, the framework is continued to complete the five day simulation period.

The model output and corresponding reductions for 18 and 19 October are discarded while preserving 16 and 17 October results. The model is then run three day forward for 18–20 October with baseline emissions to obtain new daily mean $PM_{2.5}$ concentrations of

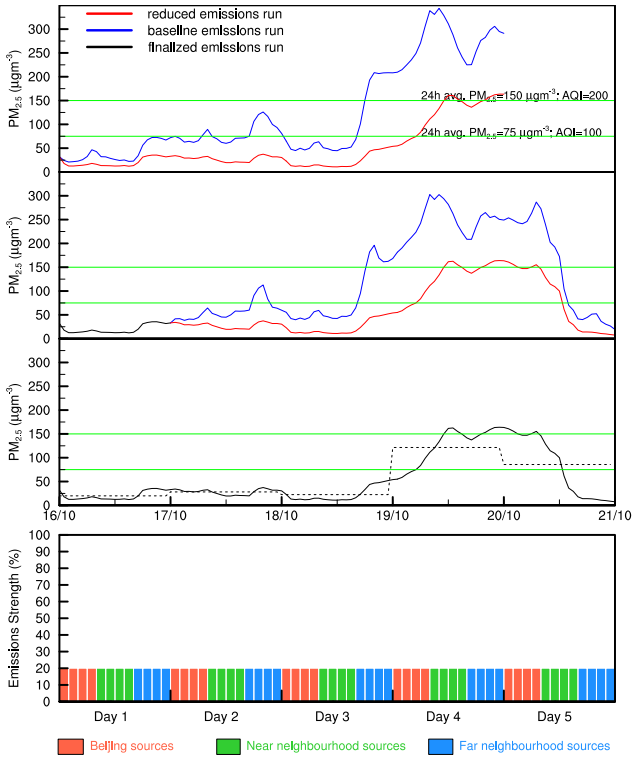

Figure 5.6: Simulated hourly $PM_{2.5}$ concentrations in Beijing with baseline and reduced emissions for 4 days ahead.

67, 248 and 151 µg m^{-3}. The highest of these concentrations (248 µg m^{-3}) is used to reduce emissions and the model output is discarded for all three days. The model is rerun with reduced emissions as per case 7 leading to new daily mean $PM_{2.5}$ concentrations of 36, 159 and 92 µg m^{-3} for 18–20 October. These results and corresponding emission reductions are preserved. Finally, we get the preserved output for all five days of the simulation period (32, 47, 36, 159 and 92 µg m^{-3}) and also their corresponding reductions. These are shown in Figure 5.5.

Here we demonstrate the flexibility of the dynamic emission control framework applied under different assumptions with three day long emission controls based on the worst of the three forecasted days. It shows that air quality can be improved greatly during episodes when emissions can be controlled up to three days in advance: a reduction in maximum daily mean $PM_{2.5}$ concentration from 274 to 159 µg m^{-3} and a reduction in peak hourly $PM_{2.5}$ concentration from 338 to 197 µg m^{-3}.

5.7 Four-day forecasts

In this implementation of DESMoRF, the emission reductions are identified based on the highest daily mean $PM_{2.5}$ in a four-day forecast. It begins by running the model four

days forward with baseline emissions to obtain daily mean $PM_{2.5}$ concentrations of 40, 80, 97 and 275 $\mu g\,m^{-3}$ for 16–19 October (see Figure 5.6). Emissions are reduced based on the most polluted of these days ,i.e., 19 October (275 $\mu g\,m^{-3}$) and the model is rerun with reduced emissions (case 7) for the same period. The next four-day forecast begins from the next day, 17 October and the emission reductions for 16 October are preserved from the previous run. This implementation takes fewer steps than one-day and three-day implementations to complete the five day simulation period. Each forecast step is shown in Figure 5.6 along with the finalised reductions (80% reductions across all 12 sectors for all five days continuously) and the resulting hourly and daily $PM_{2.5}$ concentrations (20, 28, 23, 126 and 79 $\mu g\,m^{-3}$).

Here, we get further improvement in air quality on all days as compared to the one-day and three-day implementations: a further drop in the daily mean $PM_{2.5}$ concentration on 19 October to 126 $\mu g\,m^{-3}$ which meets the secondary air quality criteria of 24 h average $PM_{2.5}$ concentration less than 150 $\mu g\,m^{-3}$ and a significant reduction in peak hourly $PM_{2.5}$ concentration from 338 to 164 $\mu g\,m^{-3}$. We did not implement the controls based on longer forecasts because the meteorology is increasingly uncertain beyond five days (Epstein 1987).

5.8 Discussion and conclusions

We have created a novel modelling framework based on dynamic emission scaling guided by emission-concentration response surfaces for Beijing developed earlier and demonstrated its three different implementations: one-day forecast, three-day forecast and four-day forecast. The framework works well and identifies the emission reductions needed for each day throughout the simulation period without the need for user intervention to stop and restart the model. It uses a state-of-the-art atmospheric chemical transport model WRF-Chem at a high resolution of 3 km and is first to utilize the temporal aspect of source contributions.

Although here we show the application of the approach over a five day period, it can be applied to much longer periods in hindcast mode to get a detailed understanding of source contributions as well as model behaviour. Here, for simplicity and to demonstrate the technique, we adopted a simple one-step process where the emission reduction was applied based on a policy which was informed by model behaviour over other episodes. However, the policy itself can be updated every time the model fails to meet the criteria on its implementation. Such an iterative method can lead to a robust policy and modelling framework and longer tests in hindcast mode along with availability of observations can improve the accuracy of the system.

This approach also has tremendous scope to be coupled with economic models in order to prioritize emission controls based on cost-benefit analysis and ease-of-implementability such that alternative policies can be used to achieve the same results. It can be actively used in air quality forecasting centres such as China National Environmental Monitoring Center (CNEMC) in Beijing and can also be extended to other polluted cities of the world.

CHAPTER 6

Conclusions

This research aimed at building better-informed approaches to urban air pollution control in Beijing. Short-term emission controls during the APEC summit of 2014, the most recent in Beijing at the time of the start of this research, were chosen for a comprehensive evaluation. The state-of-the-art online atmospheric chemical transport model WRF-Chem was tuned over China, zooming into Northern China and the North China Plain at a high resolution of 3 km. Model performance was evaluated against hourly observations from over 300 meteorological stations and over 1300 pollutant measurement stations across China for a 40 day period including the pre-APEC, APEC and post-APEC periods. Vertical representation of pollutants in the model was also evaluated against a host of meteorological and pollutant observations from tower measurements in Beijing city. Best-suited model parameters for physical and chemical representations were carefully selected based on a number of sensitivity studies. Sensitivity of model results to model resolution, emissions, and particularly boundary layer mixing were highlighted. The issue of underestimation of nighttime boundary layer mixing was circumvented by nudging the model using reanalysis data.

After comprehensive testing and tuning of both input parameters and model processes, a final version of the model was arrived at which was demonstrated to be a true-enough representation of the physical and chemical atmospheric processes governing air quality in Beijing and its regional neighbourhood. The model was then used to conduct *what-if* experiments: without emission controls during the APEC period and with emission controls during the pre-APEC period. It was found that the better air quality during APEC period

was largely due to favourable meteorology and also that the same emission controls would have been insufficient in achieving the same air quality a few weeks earlier: out of the 15 days which did not meet the national air quality standard of daily mean $PM_{2.5}$ less than $75\,\mu g\,m^{-3}$ without controls during the study period, only 2 days would meet the criteria on implementation of APEC-like controls.

With model results indicating that 45% reduction across all major emission sectors in Beijing and its neighbourhood would lead only to roughly 22% reduction in $PM_{2.5}$ concentrations over Beijing, and that much more stringent emission controls (85% reduction) would have been needed across these sectors for 10 days to mitigate major pollution episodes, the model was then utilized to investigate temporally-resolved regional contributions to $PM_{2.5}$ concentrations in Beijing, for multiple source regions including farther provinces not included in APEC controls. It was found that while reduction in local sources improves air quality in Beijing on the same day, sources in nearby provinces show their peak effect two to three days after the beginning of controls, and farther sources show peak effect in Beijing three to four days later. Local sources show higher and earlier peak contributions than regional sources. It was also found, quite surprisingly, that during milder episodes, the far-regional sources often contribute more than the near-regional sources to $PM_{2.5}$ levels in Beijing.

Furthermore, it was identified through simple one-at-a-time sensitivity studies and through statistical emulation that local and near-regional residential and industry sectors are major contributors to $PM_{2.5}$ pollution in Beijing. Contributions from four emission sectors of three source regions were quantified through these studies for diverse meteorological conditions. Computationally efficient statistical emulators built on training data from 60 perturbation model runs were used to create response surfaces which relate emission strength of a source (or a combination of sources) to the resulting $PM_{2.5}$ concentration in Beijing. These response surfaces can be used to identify the needed emission cuts across various sectors in order to mitigate a future pollution episode. Through their multi-dimensionality, the response surfaces provide different ways of reaching the same air quality goal.

Combining the findings about the temporal contributions as well as sectoral and regional contributions, a dynamic emissions scaling system was built which works in tandem with the model run, identifies the needed emission reductions based on the forecasted target and supplies the reduced emissions across four emission sectors over three source regions to the model in order to meet daily air quality standards. Three implementations of this automated framework (one-day forecast, three-day forecast and four-day forecast) were

demonstrated. The framework prescribes optimal emission controls through an iterative approach as the model runs forward in time. The preferential order in which different source regions are controlled to prevent the forthcoming air quality episode is informed by the findings of the temporal assessment of contributions based on the delay between the start of controls and their peak contributions to $PM_{2.5}$ levels in Beijing. Beijing sectors are controlled before near-neighbourhood sectors, which are controlled before far-neighbourhood sectors. Similarly, within a source region, industry and residential sectors are reduced first and others are additionally reduced only of air quality standards are still not met. The magnitude of reductions prescribed within the forecasting framework is based on the gradients of the various response surfaces developed earlier. The framework was tested over a new air quality episode over the same region. It works well and can be used operationally across air quality forecasting centres in Beijing and other cities.

The results of this work are subject to inevitable uncertainties both in the modelling system, including input parameters, and in observations. Some of the uncertainties in the model world were explored in section 3.5 and the sensitivity of model results to emissions, model resolution and boundary layer treatment in the model were discussed. Further improvements in modelling of secondary aerosol formation processes are needed to increase confidence in emissions scenario modelling. Dust treatment in the model also needs a more realistic representation in order to model other regions and periods where dust is a major issue. Explicit representation of parameterized processes such as convection and turbulence is also desirable. However, the success of the framework is independent of the model and can be applied despite the weaknesses in the modelling system. The use of Model Predictive Control can in fact help identify the deficiencies in the model and address them by incorporating new atmospheric processes.

The approach developed in this work has scope to be further modularized by including economic and practical considerations of emission controls. Very recently, Xing et al. (2019) have developed a module for least-cost control strategy optimization for meeting air quality goals for $PM_{2.5}$ and O_3 in the Beijing–Tianjin–Hebei region. They used the cost associated with control technology application to optimize their control policies. Tools are also available to calculate the economic value of health impacts resulting from changes in air quality ,e.g., the BenMap tool developed by USEPA (`https://www.epa.gov/benmap`). While such methods might be more relevant for longer-term control strategies, other considerations such as cost of implementation can be explored for short-term controls. Such economic and practical considerations can be incorporated into the approach developed in this work to achieve an automated least-cost control policy prescription system. The

framework is open-source and the atmospheric modelling community is invited to use it and implement it for other polluted regions of the world.

APPENDIX D

Model tuning

A lot of time and effort went in performing short sensitivity tests to select the best-suited model parameters such as the meteorological and chemical time steps, number of vertical levels in the model, location of model top, boundary layer schemes, realistic emissions, meteorological reanalyses, and nudging options in order to achieve a realistic simulation of air quality in Northern China and particularly in Beijing. Since it is computationally expensive to run a high-resolution nested air quality model, sensitivity tests were carried out to investigate the difference in output with shorter and longer time steps. To maintain numberical stability of the model, the meteorological time step in seconds has to be three to six times the grid size in km. Figure D.1 shows $PM_{2.5}$ concentrations from three runs with different combinations of meteorological and chemical time steps. It shows that increasing time steps leads to only minor differences between the simulated concentrations. In the interest of computational efficiency, a meteorological time step of 150 seconds and a chemical time step of 10 minutes was selected for further tests. Figure D.2 shows the simulated $PM_{2.5}$ concentrations for two different vertical resolutions of the model - with 31 and 51 levels and with chemical time steps of 10 minutes and 150 seconds. The aim of this experiment was to assess the difference in simulated concentrations with the computationally most intensive option versus the computationally cheapest option. The model configuration with 51 levels showed a smoother temporal profile of the simulated $PM_{2.5}$. Since increasing the model resolution to 51 levels meant a significant increase in computational time and model output size, 31 vertical levels were chosen. Further, a suitable model top of 50 hPa was selected based on realistic boundary layer height simulation (see,

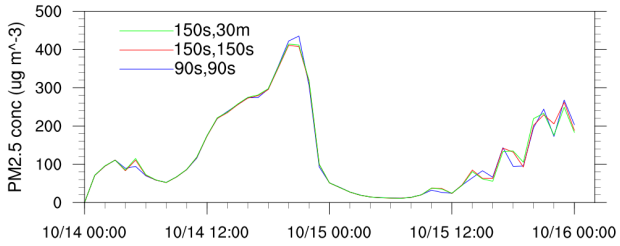

Figure D.1: Simulated $PM_{2.5}$ for various combinations of meteorological and chemical time steps. The legends denote meteorological time step value followed by chemical time step value. There are minor differences in predicted concentrations.

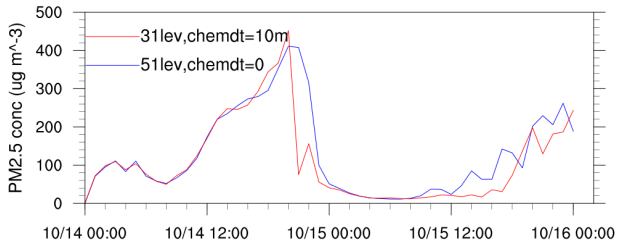

Figure D.2: Simulated $PM_{2.5}$ for different no. of vertical levels and chemical time steps. chemdt=0 means it is equal to meteorological time step, in this case, 150s.

Figure D.3).

A particular problem faced in the study was unrealistically high simulated concentrations of all pollutants during 21–25 Oct particularly due to unrealistically low nighttime boundary layer height. Several tests were performed to address this issue which are listed in table D.1 with results shown in figure D.4. 3D injection of emissions (as described earlier in section B.1), and nudging of key meteorological fields (temperature, moisture and winds) to reanalysis data reduced the bias and provided a more realistic simulation of $PM_{2.5}$ levels during this period. Ultimately, the YSU boundary layer scheme, 3D emission injection, grid nudging and 2-way nesting were selected.

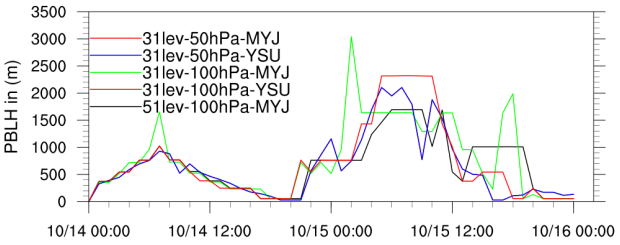

Figure D.3: Simulated boundary layer height for various combinations of model top, no. of vertical levels and boundary layer schemes.

Table D.1: Description of short sensitivity runs as shown in figure D.4

Run no.	PBL scheme	Grid nudging of met parameters	Vertical emission injection	Emission reduction	Urban canopy parameterization	Nesting	Top-down PBL mix
1	YSU	No	No	No	Off	2-way	No
2	YSU	Yes	Yes	No	Off	2-way	No
3	YSU	Yes	Yes	No	On	2-way	No
4	QNSE	No	Yes	No	On	2-way	No
5	QNSE	No	Yes	No	Off	2-way	No
6	QNSE	Yes	Yes	No	Off	2-way	No
7	YSU	Yes	Yes	Yes	Off	2-way	No
8	YSU	Yes	Yes	Yes	Off	1-way	No
9	YSU	Yes	Yes	Yes	Off	2-way	Yes

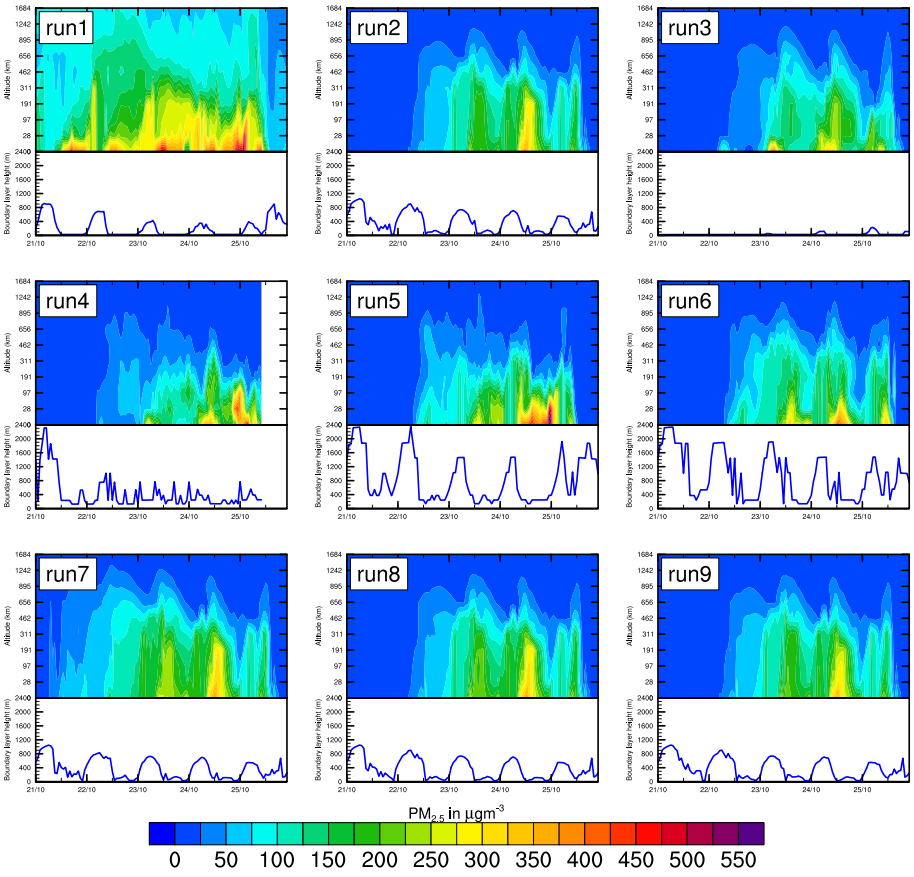

Figure D.4: Temporal evolution of simulated vertical distribution of $PM_{2.5}$ at IAP site and corresponding boundary layer height using various combinations of boundary layer schemes, emission injection heights, urban canopy parameterization and grid nudging of key meteorological parameters.

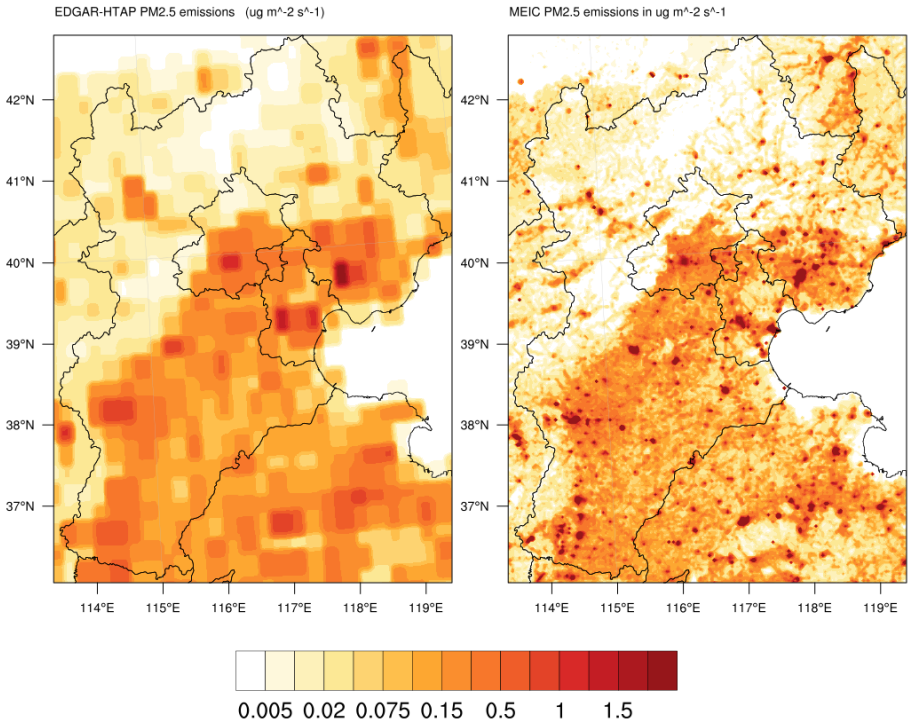

Figure D.5: A comparison between EDGAR-HTAP and MEIC emission inventories for $PM_{2.5}$ emissions over the inner domain. While the magnitudes are comparable, the spatial detail in MEIC is finer which provides an improved simulation of pollution over the region.

Bibliography

An, Z., Huang, R. J., Zhang, R., Tie, X., Li, G., Cao, J., Zhou, W., Shi, Z., Han, Y., Gu, Z. & Ji, Y. (2019), 'Severe haze in northern China: A synergy of anthropogenic emissions and atmospheric processes', *Proceedings of the National Academy of Sciences of the United States of America* **116**(18), 8657–8666.

Anderson, H. (2009), 'Air pollution and mortality: A history', *Atmospheric Environment* **43**(1), 142 – 152. Atmospheric Environment - Fifty Years of Endeavour.
URL: *http://www.sciencedirect.com/science/article/pii/S1352231008008558*

Anderson, H. R. (1999), 21 - health effects of air pollution episodes, *in* S. T. Holgate, J. M. Samet, H. S. Koren & R. L. Maynard, eds, 'Air Pollution and Health', Academic Press, London, pp. 461 – 482.
URL: *http://www.sciencedirect.com/science/article/pii/B978012352335850096X*

Ansari, T. U., Ojha, N., Chandrasekar, R., Balaji, C., Singh, N. & Gunthe, S. S. (2016), 'Competing impact of anthropogenic emissions and meteorology on the distribution of trace gases over Indian region', *Journal of Atmospheric Chemistry* .
URL: *http://link.springer.com/10.1007/s10874-016-9331-y*

Ansari, T. U., Valsan, A. E., Ojha, N., Ravikrishna, R., Narasimhan, B. & Gunthe, S. S. (2015), 'Model simulations of fungal spore distribution over the Indian region', *Atmospheric Environment* **122**, 552–560.

Ansari, T. U., Wild, O., Li, J., Yang, T., Xu, W., Sun, Y. & Wang, Z. (2019a), 'Effectiveness of short term air quality emission controls : A high-resolution model study of Beijing during the APEC period', *Atmos. Chem. Phys. Discuss.* (January), 1–29.
URL: *https://doi.org/10.5194/acp-2018-1173*

Ansari, T. U., Wild, O., Ryan, E., Chen, Y., Li, J. & Wang, Z. (2019b), Investigating the temporal, sectoral and regional contributions to air pollution in Beijing.

Banks, R. F., Tiana-Alsina, J., Baldasano, J. M., Rocadenbosch, F., Papayannis, A., Solomos, S. & Tzanis, C. G. (2016), 'Sensitivity of boundary-layer variables to PBL schemes in the WRF model based on surface meteorological observations, lidar, and radiosondes during the HygrA-CD campaign', *Atmospheric Research* **176–177**, 185–201.
URL: *http://www.sciencedirect.com/science/article/pii/S0169809516300412*

Batterman, S., Xu, L., Chen, F., Chen, F. & Zhong, X. (2016), 'Characteristics of PM2.5 concentrations across Beijing during 2013???2015', *Atmospheric Environment* **145**, 104–114.
URL: *http://dx.doi.org/10.1016/j.atmosenv.2016.08.060*

Bell, M. L. & Davis, D. L. (2001), 'Reassessment of the lethal london fog of 1952: novel indicators of acute and chronic consequences of acute exposure to air pollution.', *Environmental health perspectives* **109**(11), 389–94.

Bey, I., Jacob, D. J., Yantosca, R. M., Jennifer A. Logan, Field, B. D., Fiore, A. M., Li, Q., Liu, H. Y., Mickley, L. J., Schultz, M. G. & Field, B. D. (2001), 'Global modeling of tropospheric chemistry with assimilated meteorology: Model description and evaluation', *Journal of Geophysical Research: Atmospheres* **106**(D19), 23073–23095.

Bieser, J., Aulinger, A., Matthias, V., Quante, M. & Denier Van Der Gon, H. A. C. (2011), 'Vertical emission profiles for Europe based on plume rise calculations', *Environmental Pollution* **159**(10), 2935–2946.
URL: *http://dx.doi.org/10.1016/j.envpol.2011.04.030*

Brasseur, G. P. & Jacob, D. J. (2017), *Reviews*, Cambridge University Press, pp. ii–ii.

Brimblecombe, P. (2006), 'The clean air act after 50 years', *Weather* **61**(11), 311–314.
URL: *https://rmets.onlinelibrary.wiley.com/doi/abs/10.1256/wea.127.06*

Brimblecombe, P. (2017), *Air Pollution Episodes*, WORLD SCIENTIFIC (EUROPE).
URL: *https://www.worldscientific.com/doi/abs/10.1142/q0098*

Brimblecombe, P., Fenger, J., Hertel, O. & Palmgren, F. (1998), History of Urban Air Pollution, *in* 'Urban Air Pollution — European Aspects', Springer Netherlands, Dordrecht, pp. 7–20.

burden of disease, G. (2016), Global, regional, and national comparative risk assessment of behavioural, environmental and occupational, and metabolic risks or clusters of risks, 1990–2015: a systematic analysis for the global burden of disease study 2015, Technical report.

Burr, M. J. & Zhang, Y. (2011), 'Source apportionment of fine particulate matter over the eastern u.s. part i: source sensitivity simulations using cmaq with the brute force method', *Atmospheric Pollution Research* **2**(3), 300 – 317.
URL: *http://www.sciencedirect.com/science/article/pii/S1309104215304864*

CEPB: Chengdu Environmental Protection Bureau (2013). Accessed: 2019-03-05 (in Chinese).
URL: *http://www.cdepb.gov.cn*

Chang, D., Song, Y. & Liu, B. (2009), 'Visibility trends in six megacities in china 1973–2007', *Atmospheric Research* **94**(2), 161 – 167.
URL: *http://www.sciencedirect.com/science/article/pii/S0169809509001562*

Chang, X., Wang, S., Zhao, B., Cai, S. & Hao, J. (2018), 'Assessment of inter-city transport of particulate matter in the Beijing-Tianjin-Hebei region', *Atmospheric Chemistry and Physics* **18**(7), 4843–4858.

Chen, C., Sun, Y. L., Xu, W. Q., Du, W., Zhou, L. B., Han, T. T., Wang, Q. Q., Fu, P. Q., Wang, Z. F., Gao, Z. Q., Zhang, Q. & Worsnop, D. R. (2015b), 'Characteristics and sources of submicron aerosols above the urban canopy (260 m) in Beijing, China, during the 2014 APEC summit', *Atmospheric Chemistry and Physics* **15**(22), 12879–12895.
URL: *http://www.atmos-chem-phys.net/15/12879/2015/*

Chen, D., Li, Q., Stutz, J., Mao, Y., Zhang, L., Pikelnaya, O., Tsai, J. Y., Haman, C., Lefer, B., Rappenglück, B., Alvarez, S. L., Neuman, J. A., Flynn, J., Roberts, J. M., Nowak, J. B., de Gouw, J., Holloway, J., Wagner, N. L., Veres, P., Brown, S. S., Ryerson, T. B., Warneke, C. & Pollack, I. B. (2013a), 'WRF-Chem simulation of NOx and O3 in the L.A. basin during CalNex-2010', *Atmospheric Environment* **81**(x), 421–432.
URL: *http://linkinghub.elsevier.com/retrieve/pii/S1352231013006845*

Chen, D., Liu, Z., Fast, J. & Ban, J. (2016e), 'Simulations of sulfate-nitrate-ammonium (SNA) aerosols during the extreme haze events over northern China in October 2014', *Atmospheric Chemistry and Physics* **16**(16), 10707–10724.

Chen, F. & Dudhia, J. (2001), 'Coupling an Advanced Land Surface–Hydrology Model with the Penn State–NCAR MM5 Modeling System. Part II: Preliminary Model Validation', *Monthly Weather Review* **129**(4), 587–604.

Chen, H., Li, J., Ge, B., Yang, W., Wang, Z., Huang, S., Wang, Y., Yan, P., Li, J. & Zhu, L. (2015a), 'Modeling study of source contributions and emergency control effects during a severe haze episode over the Beijing-Tianjin-Hebei area', *Science China Chemistry* **58**(9), 1403–1415.
URL: *http://link.springer.com/10.1007/s11426-015-5458-y*

Chen, W., Yan, L. & Zhao, H. (2015c), 'Seasonal Variations of Atmospheric Pollution and Air Quality in Beijing', *Atmosphere* **6**(11), 1753–1770.
URL: *http://www.mdpi.com/2073-4433/6/11/1753*

Chen, X., Yang, W., Wang, Z., Li, J., Hu, M., An, J., Wu, Q., Wang, Z., Chen, H., Wei, Y., Du, H. & Wang, D. (2019a), 'Improving new particle formation simulation by coupling a volatility-basis set (VBS) organic aerosol module in NAQPMS+APM', *Atmospheric Environment* **204**(September 2018), 1–11.
URL: *https://doi.org/10.1016/j.atmosenv.2019.01.053*

Chen, Z., Chen, D., Cheng, N., Zhuang, Y., Kwan, M.-P., Chen, B., Zhao, B., Yang, L., Gao, B., Li, R. & Xu, B. (2019), 'Evaluating the Recent 2+26 Regional Strategy for Air Quality Improvement During Two Orange Air Pollution Alerts in Beijing: variations of PM2.5 concentrations, source apportionment, and the relative contribution of local emission and regional transport', *Atmospheric Chemistry and Physics* **19**, 1–24.

Chen, Z., Wang, J.-N., Ma, G.-X. & Zhang, Y.-S. (2013b), 'China tackles the health effects of air pollution', *The Lancet* **382**(9909), 1959–1960.

Chen, Z., Xu, B., Cai, J. & Gao, B. (2016), 'Understanding temporal patterns and characteristics of air quality in Beijing: A local and regional perspective', *Atmospheric Environment* **127**(December 2012), 303–315.
URL: *http://linkinghub.elsevier.com/retrieve/pii/S1352231015305793*

Cheng, J., Su, J., Cui, T., Li, X., Dong, X., Sun, F., Yang, Y., Tong, D., Zheng, Y., Li, J., Zhang, Q. & He, K. (2018), 'Dominant role of emission reduction in PM_{2.5} air quality improvement in Beijing during 2013–2017: a model-based decomposition analysis', *Atmospheric Chemistry and Physics Discussions* pp. 1–31.

Cheng, Y., Zheng, G., Wei, C., Mu, Q., Zheng, B., Wang, Z., Gao, M., Zhang, Q., He, K., Carmichael, G., Pöschl, U. & Su, H. (2016), 'Reactive nitrogen chemistry in aerosol water as a source of sulfate during haze events in China', *Science Advances* **2**(12), e1601530.

China Statistical Yearbook 2005, 2006 (n.d.).
URL: *http://www.stats.gov.cn/tjsj/ndsj/2006/indexeh.htm*

Clough, S. A., Shephard, M. W., Mlawer, E. J., Delamere, J. S., Iacono, M. J., Cady-Pereira, K., Boukabara, S. & Brown, P. D. (2005), 'Atmospheric radiative transfer modeling: A summary of the AER codes', *Journal of Quantitative Spectroscopy and Radiative Transfer* **91**(2), 233–244.

Crippa, P., Sullivan, R. C., Thota, A. & Pryor, S. C. (2017), 'The impact of resolution on meteorological, chemical and aerosol properties in regional simulations with WRF-Chem', *Atmospheric Chemistry and Physics* **17**(2), 1511–1528.
URL: *http://www.atmos-chem-phys.net/17/1511/2017/*

Dang, R. & Liao, H. (2019), 'Severe winter haze days in the Beijing-Tianjin-Hebei region from 1985–2017 and the roles of anthropogenic emissions and meteorological parameters', *Atmospheric Chemistry and Physics* **5**, 1–31.

Dellino, G. & Meloni, C., eds (2008), *Global Sensitivity Analysis*, John Wiley & Sons Ltd., The Atrium, Southern Gate, Chichester, West Sussex PO19 8SQ, England.

Di, Q., Dai, L., Wang, Y., Zanobetti, A., Choirat, C., Schwartz, J. D. & Dominici, F. (2017), 'Association of Short-term Exposure to Air Pollution With Mortality in Older AdultsAssociation of Short-term Exposure to Air Pollution With Mortality in Older AdultsAssociation of Short-term Exposure to Air Pollution With Mortality in Older Adults', *JAMA* **318**(24), 2446–2456.
URL: *https://dx.doi.org/10.1001/jama.2017.17923*

Emmons, L. K., Walters, S., Hess, P. G., Lamarque, J.-F., Pfister, G. G., Fillmore, D., Granier, C., Guenther, A., Kinnison, D., Laepple, T., Orlando, J., Tie, X., Tyndall, G., Wiedinmyer, C., Baughcum, S. L. & Kloster, S. (2010), 'Description and evaluation of the Model for Ozone and Related chemical Tracers, version 4 (MOZART-4)', *Geoscientific Model Development* **3**(1), 43–67.
URL: *http://www.geosci-model-dev.net/3/43/2010/*

Epstein, E. S. (1987), 'Long-Range Weather Prediction: Limits of Predictability and Beyond', *Weather and Forecasting* **3**(1), 69–75.

Fahey, K. M. & Pandis, S. N. (2003), 'Size-resolved aqueous-phase atmospheric chemistry in a three-dimensional chemical transport model', *Journal of Geophysical Research D: Atmospheres* **108**(22), 1–12.

Fast, J. D., Gustafson, W. I., Easter, R. C., Zaveri, R. A., Barnard, J. C., Chapman, E. G., Grell, G. A. & Peckham, S. E. (2006), 'Evolution of ozone, particulates, and aerosol direct radiative forcing in the vicinity of Houston using a fully coupled meteorology-chemistry-aerosol model', *Journal of Geophysical Research Atmospheres* **111**(21), 1–29.

Firket, J. (1931), 'Sur les causes des accidents survenus dans la vallée de la meuse, lors des brouillards de décembre 1930', *Bulletin de l'Académie, Royale de Médecine de Belgique* **11**, 683–741.
URL: *https://pubs.rsc.org/en/content/articlepdf/1936/tf/tf9363201192*

Flaounas, E., Kotroni, V., Lagouvardos, K., Klose, M. & Flamant, C. (2017), 'Sensitivity of the WRF-Chem (V3 . 6 . 1) model to different dust emission parametrisation : assessment in the broader Mediterranean region', pp. 2925–2945.

Gao, J., Peng, X., Chen, G., Xu, J., Shi, G.-L., Zhang, Y.-C. & Feng, Y.-C. (2016a), 'Insights into the chemical characterization and sources of PM2.5 in Beijing at a 1-h time resolution', *Science of The Total Environment* **542**, 162–171.
URL: *http://linkinghub.elsevier.com/retrieve/pii/S0048969715308986*

Gao, M., Carmichael, G. R., Saide, P. E., Lu, Z., Yu, M., Streets, D. G. & Wang, Z. (2016b), 'Response of winter fine particulate matter concentrations to emission and meteorology changes in North China', *Atmospheric Chemistry and Physics* **16**(18), 11837–11851.

Gao, M., Carmichael, G. R., Wang, Y., Saide, P. E., Yu, M., Xin, J., Liu, Z. & Wang, Z. (2015a), 'Modeling study of the 2010 regional haze event in the North China Plain', *Atmospheric Chemistry and Physics Discussions* **15**(16), 22781–22822.
URL: *http://www.atmos-chem-phys-discuss.net/15/22781/2015/*

Gao, M., Liu, Z., Wang, Y., Lu, X., Ji, D., Wang, L., Li, M., Wang, Z., Zhang, Q. & Carmichael, G. R. (2017), 'Distinguishing the roles of meteorology , emission control measures , regional transport , and co-benefits of reduced aerosol feedbacks in "APEC Blue"', *Atmospheric Environment* **167**, 476–486.
URL: *http://dx.doi.org/10.1016/j.atmosenv.2017.08.054*

Gao, Y., Liu, X., Zhao, C. & Zhang, M. (2011), 'Emission controls versus meteorological

conditions in determining aerosol concentrations in Beijing during the 2008 Olympic Games', *Atmospheric Chemistry and Physics* **11**(2007), 12437–12451.

Gao, Y., Zhang, M., Liu, Z., Wang, L., Wang, P., Xia, X., Tao, M. & Zhu, L. (2015b), 'Modeling the feedback between aerosol and meteorological variables in the atmospheric boundary layer during a severe fog-haze event over the North China Plain', *Atmospheric Chemistry and Physics* **15**(8), 4279–4295.

GEPB: Guangzhou Environmental Protection Bureau (2009). Accessed: 2019-03-05 (in Chinese).
URL: *http://www.gz.gov.cn/gzgov/s2812/200912/163197.shtml*

Grell, G. a., Peckham, S. E., Schmitz, R., McKeen, S. a., Frost, G., Skamarock, W. C. & Eder, B. (2005), 'Fully coupled "online" chemistry within the WRF model', *Atmospheric Environment* **39**(37), 6957–6975.

Guenther, A. B., Jiang, X., Heald, C. L., Sakulyanontvittaya, T., Duhl, T., Emmons, L. K. & Wang, X. (2012), 'The model of emissions of gases and aerosols from nature version 2.1 (MEGAN2.1): An extended and updated framework for modeling biogenic emissions', *Geoscientific Model Development* **5**(6), 1471–1492.

Guo, J., He, J., Liu, H., Miao, Y., Liu, H. & Zhai, P. (2016), 'Impact of various emission control schemes on air quality using WRF-Chem during APEC China 2014', *Atmospheric Environment* **140**, 311–319.
URL: *http://linkinghub.elsevier.com/retrieve/pii/S1352231016303934*

Guo, S., Hu, M., Zamora, M. L., Peng, J., Shang, D., Zheng, J., Du, Z., Wu, Z., Shao, M., Zeng, L., Molina, M. J. & Zhang, R. (2014), 'Elucidating severe urban haze formation in China', *Proceedings of the National Academy of Sciences* **111**(49), 17373–17378.
URL: *http://www.pnas.org/lookup/doi/10.1073/pnas.1419604111*

Han, X., Zhang, M., Zhu, L. & Skorokhod, A. (2016), 'Assessment of the impact of emissions reductions on air quality over north china plain', *Atmospheric Pollution Research* **7**(2), 249 – 259.
URL: *http://www.sciencedirect.com/science/article/pii/S1309104215000562*

He, H., Tie, X., Zhang, Q., Liu, X., Gao, Q., Li, X., Gao, Y., He, H., Cao, J., Han, S., Gao, Y., Li, X., Jia, X. C., Matsui, H., Koike, M., Kondo, Y., Takegawa, N., Kita, K., Miyazaki, Y., Hu, M., Chang, S. Y., Blake, D. R., Fast, J. D., Zaveri, R. A., Streets,

D. G., Zhang, Q. & Zhu, T. (2014), 'Analysis of the causes of heavy aerosol pollution in Beijing, China: A case study with the WRF-Chem model', *Journal of Geophysical Research Atmospheres* **114**(15), 32–40.
URL: *http://dx.doi.org/10.1016/j.atmosenv.2014.10.038 http://www.sciencedirect.com/science/article/pii/S1674200114001485*

Helton, J. C. & Davis, F. J. (2003), 'Latin hypercube sampling and the propagation of uncertainty in analyses of complex systems', *Reliability Engineering & System Safety* **81**(1), 23–69.
URL: *http://www.sciencedirect.com/science/article/pii/S0951832003000589*

Hoesly, R. M., Smith, S. J., Feng, L., Klimont, Z., Janssens-maenhout, G., Dawidowski, L., Kholod, N., Kurokawa, J.-i., Li, M., Liu, L. & Lu, Z. (2018), 'Historical (1750–2014) anthropogenic emissions of reactive gases and aerosols from the Community Emissions Data System (CEDS)', *Geoscientific Model Development* **11**, 369–408.

Hong, S.-Y., Noh, Y. & Dudhia, J. (2006), 'A New Vertical Diffusion Package with an Explicit Treatment of Entrainment Processes', *Monthly Weather Review* **134**(9), 2318–2341.

Hu, J., Wang, P., Ying, Q., Zhang, H., Chen, J., Ge, X., Li, X., Jiang, J., Wang, S., Zhang, J., Zhao, Y. & Zhang, Y. (2016), 'Modeling Biogenic and Anthropogenic Secondary Organic Aerosol in China', *Atmospheric Chemistry and Physics Discussions* **0**, 1–31.
URL: *http://www.atmos-chem-phys-discuss.net/acp-2016-687/*

Huang, D. & Gao, S. (2018), 'Impact of di ff erent reanalysis data on WRF dynamical downscaling over China', *Atmospheric Research* **200**(April 2017), 25–35.
URL: *http://dx.doi.org/10.1016/j.atmosres.2017.09.017*

Huang, R.-j., Wang, Y., Cao, J., Lin, C., Duan, J., Chen, Q., Li, Y., Gu, Y., Yan, J., Xu, W., Frohlich, R., Canonaco, F., Bozzetti, C., Ovadnevaite, J., Ceburnis, D., Canagaratna, M. R., Jayne, J., Worsnop, D. R., El-haddad, I., Prévôt, A. S. H. & Dowd, C. D. O. (2019), 'Primary emissions versus secondary formation of fine particulate matter in the most polluted city (Shijiazhuang) in North China', pp. 2283–2298.

Huang, X.-F., He, L.-Y., Xue, L., Sun, T.-L., Zeng, L.-W., Gong, Z.-H., Hu, M. & Zhu, T. (2012), 'Highly time-resolved chemical characterization of atmospheric fine particles during 2010 shanghai world expo', *Atmospheric Chemistry and Physics* **12**(11), 4897–

4907.
URL: *https://www.atmos-chem-phys.net/12/4897/2012/*

IPCC (2013), Climate Change 2013: The Physical Science Basis. Contribution of Working Group I to the Fifth Assessment Report of the Intergovernmental Panel on Climate Change, Technical report, Cambridge, United Kingdom and New York, NY, USA.
URL: *https://www.ipcc.ch/report/ar5/wg1/*

Jiantang, M., Weimin, Z., Yifan, X., Hongguang, X., Xianchun, X., Qiang, L., Jianhua, G., Jingping, Z., Zude, X., Xiaochao, L. & Laiyun, S. (2014), *China Statistical Yearbook*, september edn.

Kajino, M., Ueda, H., Han, Z., Kudo, R. & Inomata, Y. (2017), 'Synergy between air pollution and urban meteorological changes through aerosol-radiation-diffusion feedback–A case study of Beijing in January', *Atmospheric Environment* **171**(October), 98–110.
URL: *http://dx.doi.org/10.1016/j.atmosenv.2017.10.018*

Kang, Y., Liu, M., Song, Y., Huang, X., Yao, H., Cai, X., Zhang, H., Kang, L., Liu, X., Yan, X., He, H., Zhang, Q., Shao, M. & Zhu, T. (2016), 'High-resolution ammonia emissions inventories in China from 1980 to 2012', *Atmospheric Chemistry and Physics* **16**(4), 2043–2058.

Krotkov, N. A., McLinden, C. A., Li, C., Lamsal, L. N., Celarier, E. A., Marchenko, S. V., Swartz, W. H., Bucsela, E. J., Joiner, J., Duncan, B. N., Boersma, K. F., Veefkind, J. P., Levelt, P. F., Fioletov, V. E., Dickerson, R. R., He, H., Lu, Z. & Streets, D. G. (2016), 'Aura omi observations of regional so_2 and no_2 pollution changes from 2005 to 2015', *Atmospheric Chemistry and Physics* **16**(7), 4605–4629.
URL: *https://www.atmos-chem-phys.net/16/4605/2016/*

Kuik, F., Lauer, A., Churkina, G., Denier Van Der Gon, H. A., Fenner, D., Mar, K. A. & Butler, T. M. (2016), 'Air quality modelling in the Berlin-Brandenburg region using WRF-Chem v3.7.1: Sensitivity to resolution of model grid and input data', *Geoscientific Model Development* **9**(12), 4339–4363.

Laprise, R. (1992), 'The Euler Equations of motion with hydrostatic pressure as an independent variable', *Monthly Weather Review* **120**, 197–207.

Lary, D. J., Alavi, A. H., Gandomi, A. H. & Walker, A. L. (2016), 'Machine learning in geosciences and remote sensing', *Geoscience Frontiers* **7**(1), 3–10.
URL: *http://dx.doi.org/10.1016/j.gsf.2015.07.003*

Lee, H.-M., Park, R. J., Henze, D. K., Lee, S., Shim, C., Shin, H.-J., Moon, K.-J. & Woo, J.-H. (2017), 'Pm2.5 source attribution for seoul in may from 2009 to 2013 using geos-chem and its adjoint model', *Environmental Pollution* **221**, 377 – 384.
URL: *http://www.sciencedirect.com/science/article/pii/S0269749116324757*

Lee, L. A., Carslaw, K. S., Pringle, K. J. & Mann, G. W. (2012), 'Mapping the uncertainty in global CCN using emulation', *Atmospheric Chemistry and Physics* **12**(20), 9739–9751.
URL: *https://www.atmos-chem-phys.net/12/9739/2012/*

Lee, L. A., Carslaw, K. S., Pringle, K. J., Mann, G. W. & Spracklen, D. V. (2011), 'Emulation of a complex global aerosol model to quantify sensitivity to uncertain parameters', *Atmospheric Chemistry and Physics* **11**(23), 12253–12273.

Lelieveld, J., Evans, J. S., Fnais, M., Giannadaki, D. & Pozzer, A. (2015), 'The contribution of outdoor air pollution sources to premature mortality on a global scale.', *Nature* **525**(7569), 367–71.
URL: *http://www.ncbi.nlm.nih.gov/pubmed/26381985*

Li, G., Bei, N., Cao, J., Huang, R., Wu, J., Feng, T., Wang, Y., Liu, S., Zhang, Q., Tie, X. & Molina, L. (2017a), 'A Possible Pathway for Rapid Growth of Sulfate during Haze Days in China', *Atmospheric Chemistry and Physics* **17**, 3301–3316.
URL: *http://www.atmos-chem-phys-discuss.net/acp-2016-994/*

Li, J., Yang, W., Wang, Z., Chen, H., Hu, B., Li, J., Sun, Y. & Huang, Y. (2014), 'A modeling study of source-receptor relationships in atmospheric particulate matter over northeast asia', *Atmospheric Environment* **91**, 40–51.

Li, K., Li, J., Wang, W., Tong, S., Liggio, J. & Ge, M. (2017d), 'Evaluating the effectiveness of joint emission control policies on the reduction of ambient VOCs: Implications from observation during the 2014 APEC summit in suburban Beijing', *Atmospheric Environment* **164**, 117–127.
URL: *http://linkinghub.elsevier.com/retrieve/pii/S1352231017303709*

Li, L., Zhu, S., An, J., Zhou, M., Wang, H., Yan, R., Qiao, L., Huang, C., Tian, X., Shen, L., Avise, J. C. & Fu, J. S. (2019), 'Evaluation on the effect of regional joint control measures in changing photochemical transformation: A comprehensive study of the optimization scenario analysis', *Atmospheric Chemistry and Physics Discussions* pp. 1–38.

Li, M., Zhang, Q., Kurokawa, J. I., Woo, J. H., He, K., Lu, Z., Ohara, T., Song, Y., Streets, D. G., Carmichael, G. R., Cheng, Y., Hong, C., Huo, H., Jiang, X., Kang, S., Liu, F., Su, H. & Zheng, B. (2017c), 'MIX: A mosaic Asian anthropogenic emission inventory under the international collaboration framework of the MICS-Asia and HTAP', *Atmospheric Chemistry and Physics* **17**(2), 935–963.

Li, X., Zhang, Q., Zhang, Y., Zheng, B., Wang, K., Chen, Y., Wallington, T. J., Han, W., Shen, W., Zhang, X. & He, K. (2015), 'Source contributions of urban PM2.5 in the Beijing–Tianjin–Hebei region: Changes between 2006 and 2013 and relative impacts of emissions and meteorology', *Atmospheric Environment* **123**, 229–239.
URL: *http://linkinghub.elsevier.com/retrieve/pii/S1352231015304660*

Li, Y. J., Sun, Y., Zhang, Q., Li, X., Li, M., Zhou, Z. & Chan, C. K. (2017), 'Real-time chemical characterization of atmospheric particulate matter in China: A review', *Atmospheric Environment* **158**, 270–304.
URL: *http://dx.doi.org/10.1016/j.atmosenv.2017.02.027*

Liang, P., Zhu, T., Fang, Y., Li, Y., Han, Y., Wu, Y., Hu, M. & Wang, J. (2017), 'The Role of Meteorological Conditions and Pollution Control Strategies in Reducing Air Pollution in Beijing during APEC 2014 and Parade 2015', *Atmospheric Chemistry and Physics* **2014**(May), 1–62.
URL: *http://www.atmos-chem-phys-discuss.net/acp-2017-456/*

Lin, B. & Zhu, J. (2018), 'Changes in urban air quality during urbanization in china', *Journal of Cleaner Production* **188**, 312 – 321.
URL: *http://www.sciencedirect.com/science/article/pii/S0959652618309740*

Lin, Yuh-Lang, Richard D. Farley, H. D. O. (1983), 'Bulk Parameterization of the Snow Field in a Cloud Model', *Journal of Climate and Applied Meteorology* .

Liu, H., He, J., Guo, J., Miao, Y., Yin, J., Wang, Y., Xu, H., Liu, H., Yan, Y., Li, Y. & Zhai, P. (2017), 'The blue skies in Beijing during APEC 2014 : A quantitative assessment of emission control efficiency and meteorological influence', *Atmospheric Environment* **167**, 235–244.
URL: *http://dx.doi.org/10.1016/j.atmosenv.2017.08.032*

Liu, H., Liu, C., Xie, Z., Li, Y., Huang, X. & Wang, S. (2016c), 'OPEN A paradox for air pollution controlling in China revealed by " APEC Blue " and " Parade Blue "', *Nature*

Publishing Group (September), 1–13.
URL: *http://dx.doi.org/10.1038/srep34408*

Liu, H., Wang, X., Zhang, J., He, K., Wu, Y. & Xu, J. (2013), 'Emission controls and changes in air quality in guangzhou during the asian games', *Atmospheric Environment* **76**, 81 – 93. Improving Regional Air Quality over the Pearl River Delta and Hong Kong: from Science to Policy.
URL: *http://www.sciencedirect.com/science/article/pii/S1352231012007686*

Liu, J. & Diamond, J. (2005), 'China's environment and in a globalizing world.pdf', *Nature* **435**(June), 1179–1186.

Liu, T., Gong, S., Yu, M., Zhao, Q., Li, H., He, J., Zhang, J., Li, L., Wang, X., Li, S., Lu, Y., Du, H., Wang, Y., Zhou, C. & Liu, H. (2016d), 'Attributions of meteorological and emission factors to the 2015 winter severe haze pollution episodes in Northern China', *Atmospheric Chemistry and Physics* pp. 1–19.
URL: *http://www.atmos-chem-phys-discuss.net/acp-2016-798/*

Loh, W.-L. (1996), 'On latin hypercube sampling', *Ann. Statist.* **24**(5), 2058–2080.
URL: *https://doi.org/10.1214/aos/1069362310*

Luan, T., Guo, X., Guo, L. & Zhang, T. (2018), 'Quantifying the relationship between PM2.5 concentration, visibility and planetary boundary layer height for long-lasting haze and fog-haze mixed events in Beijing', *Atmospheric Chemistry and Physics* **18**(1), 203–225.

Luo, G. & Yu, F. (2011), 'Simulation of particle formation and number concentration over the Eastern United States with the WRF-Chem + APM model', *Atmospheric Chemistry and Physics* **11**(22), 11521–11533.
URL: *http://www.atmos-chem-phys.net/11/11521/2011/*

Ma, X., Sha, T., Wang, J., Jia, H. & Tian, R. (2018), 'Investigating impact of emission inventories on PM 2 . 5 simulations over North China Plain by WRF-Chem', *Atmospheric Environment* **195**(March), 125–140.
URL: *https://doi.org/10.1016/j.atmosenv.2018.09.058*

Mailler, S., Khvorostyanov, D. & Menut, L. (2013), 'Impact of the vertical emission profiles on background gas-phase pollution simulated from the EMEP emissions over Europe', *Atmospheric Chemistry and Physics* **13**(12), 5987–5998.

Matsui, H., Koike, M., Kondo, Y., Takegawa, N., Kita, K., Miyazaki, Y., Hu, M., Chang, S. Y., Blake, D. R., Fast, J. D., Zaveri, R. A., Streets, D. G., Zhang, Q. & Zhu, T. (2009), 'Spatial and temporal variations of aerosols around Beijing in summer 2006: Model evaluation and source apportionment', *Journal of Geophysical Research Atmospheres* **114**(15), 1–22.

McMullen-Laird, L., Zhao, X., Gong, M. & McMullen, S. J. (2015), 'Air pollution governance as a driver of recent climate policies in china', *Carbon & Climate Law Review* **9**(3), 243–255.
URL: *http://www.jstor.org/stable/26245325*

Meng, R., Zhao, F. R., Sun, K., Zhang, R., Huang, C., Yang, J., Müller, R. & Thenkabail, P. S. (2014), 'Analysis of the 2014 " APEC Blue " in Beijing Using More than One Decade of Satellite Observations: Lessons Learned from Radical Emission Control Measures', *Remote Sens* **7**, 15224–15243.
URL: *www.mdpi.com/journal/remotesensing*

Miettinen, M., Leskinen, A., Abbaszade, G., Orasche, J., Sainio, M., Mikkonen, S., Koponen, H., Rönkkö, T., Ruusunen, J., Kuuspalo, K., Tiitta, P., Jalava, P., Hao, L., Fang, D., Wang, Q., Gu, C., Zhao, Y., Michalke, B., Schnelle-Kreis, J., Lehtinen, K. E., Zimmermann, R., Komppula, M., Jokiniemi, J., Hirvonen, M.-R. & Sippula, O. (2019), 'Pm2.5 concentration and composition in the urban air of nanjing, china: Effects of emission control measures applied during the 2014 youth olympic games', *Science of The Total Environment* **652**, 1 – 18.
URL: *http://www.sciencedirect.com/science/article/pii/S0048969718340828*

Misenis, C. & Zhang, Y. (2010), 'An examination of sensitivity of WRF/Chem predictions to physical parameterizations, horizontal grid spacing, and nesting options', *Atmospheric Research* **97**(3), 315–334.
URL: *http://linkinghub.elsevier.com/retrieve/pii/S0169809510000992*

Mlawer, E. J., Taubman, S. J., Brown, P. D., Iacono, M. J. & Clough, S. a. (1997), 'Radiative transfer for inhomogeneous atmospheres: RRTM, a validated correlated-k model for the longwave', *Journal of Geophysical Research* **102**(D14), 16663.

Monin, A. & Obukhov, A. (1954), 'Basic laws of turbulent mixing in the surface layer of the atmosphere', *Contrib. Geophys. Inst. Acad. Sci. USSR* **24**(151), 163–187.

Morgenstern, O., Braesicke, P., Hurwitz, M. M., O'Connor, F. M., Bushell, A. C., Johnson, C. E. & Pyle, J. A. (2008), 'The world avoided by the montreal protocol', *Geophysical Research Letters* **35**(16).
URL: *https://agupubs.onlinelibrary.wiley.com/doi/abs/10.1029/2008GL034590*

Mu, Q., Lammel, G., Gencarelli, C. N., Hedgecock, I. M., Chen, Y., Pribylova, P., Teich, M., Zhang, Y., Zheng, G., van Pinxteren, D., Zhang, Q., Herrmann, H., Shiraiwa, M., Spichtinger, P., Su, H., Poschl, U. & Cheng, Y. (2017), 'Regional modelling of polycyclic aromatic hydrocarbons: Wrf-chem-pah model development and east asia case studies', *Atmospheric Chemistry and Physics* **17**(19), 12253–12267.
URL: *https://www.atmos-chem-phys.net/17/12253/2017/*

Ng, N. L., Herndon, S. C., Trimborn, A., Canagaratna, M. R., Croteau, P. L., Onasch, T. B., Sueper, D., Worsnop, D. R., Zhang, Q., Sun, Y. L. & Jayne, J. T. (2011), 'An Aerosol Chemical Speciation Monitor (ACSM) for Routine Monitoring of the Composition and Mass Concentrations of Ambient Aerosol', *Aerosol Science and Technology* **45**(7), 780–794.
URL: *https://doi.org/10.1080/02786826.2011.560211*

O'Hagan, A. (2006), 'Bayesian analysis of computer code outputs: A tutorial', *Reliability Engineering & System Safety* **91**(10), 1290–1300.
URL: *http://www.sciencedirect.com/science/article/pii/S0951832005002383*

Ooyama, K. V. N. (1990), 'Ooyama-philosophy.pdf', *Journal of the Atmospheric Sciences* .

Parrish, D. D., Singh, H. B., Molina, L. & Madronich, S. (2011), 'Air quality progress in north american megacities: A review', *Atmospheric Environment* **45**(39), 7015 – 7025.
URL: *http://www.sciencedirect.com/science/article/pii/S1352231011009915*

Pithani, P., Ghude, S. D., Prabhakaran, T., Karipot, A., Hazra, A. & Kulkarni, R. (2018), 'WRF model sensitivity to choice of PBL and microphysics parameterization for an advection fog event at Barkachha , rural site in the Indo-Gangetic basin , India', (Stull 1988).

Qi, J., Zheng, B., Li, M., Yu, F., Chen, C., Liu, F., Zhou, X., Yuan, J., Zhang, Q. & He, K. (2017), 'A high-resolution air pollutants emission inventory in 2013 for the', **170**, 156–168.

Ren, Y., Li, H., Meng, F., Wang, G., Zhang, H., Yang, T., Li, W., Ji, Y., Bi, F. & Wang, X. (2019), 'Impact of emission controls on air quality in beijing during the 2015 china victory day parade: Implication from organic aerosols', *Atmospheric Environment* **198**, 207 – 214.
URL: *http://www.sciencedirect.com/science/article/pii/S1352231018307593*

Roustant, O., Ginsbourger, D. & Deville, Y. (2012), 'Dicekriging, diceoptim: Two r packages for the analysis of computer experiments by kriging-based metamodeling and optimization', *Journal of Statistical Software, Articles* **51**(1), 1–55.
URL: *https://www.jstatsoft.org/v051/i01*

Ryan, E., Wild, O., Voulgarakis, A. & Lee, L. (2018), 'Fast sensitivity analysis methods for computationally expensive models with multi-dimensional output', *Geoscientific Model Development* **11**(8), 3131–3146.

Saide, P. E., Spak, S. N., Carmichael, G. R., Mena-Carrasco, M. a., Yang, Q., Howell, S., Leon, D. C., Snider, J. R., Bandy, a. R., Collett, J. L., Benedict, K. B., de Szoeke, S. P., Hawkins, L. N., Allen, G., Crawford, I., Crosier, J. & Springston, S. R. (2012), 'Evaluating WRF-Chem aerosol indirect effects in Southeast Pacific marine stratocumulus during VOCALS-REx', *Atmospheric Chemistry and Physics* **12**(6), 3045–3064.
URL: *http://www.atmos-chem-phys.net/12/3045/2012/*

Seigneur, C. & Saxena, P. (1988), 'A theoretical investigation of sulfate formation in clouds', *Atmospheric Environment (1967)* **22**(1), 101–115.

Seinfeld, J. & Pandis, S. (2006), *Atmospheric Chemistry and Physics: From Air Pollution to Climate Change*, Wiley.

SEPB: Shanghai Environmental Protection Bureau (2010). Accessed: 2019-03-05 (in Chinese).
URL: *http://www.sepb.gov.cn/fa/cms/shhj//shhj2272/shhj2159/2010/02/20671.htm*

Shang, X., Zhang, K., Meng, F., Wang, S., Lee, M., Suh, I., Kim, D., Jeon, K., Park, H., Wang, X. & Zhao, Y. (2018), 'Characteristics and source apportionment of fine haze aerosol in Beijing during the winter of 2013', *Atmospheric Chemistry and Physics* **18**(4), 2573–2584.

Shao, M., Tang, X., Zhang, Y. & Li, W. (2006), 'City clusters in China air and surface water.pdf', *Frontiers in Ecology and the Environment* **4**(7), 353–361.

Sharma, A., Ojha, N., Pozzer, A., Mar, K. A., Beig, G., Lelieveld, J. & Gunthe, S. S. (2016), 'WRF-Chem simulated surface ozone over South Asia during the pre-monsoon: Effects of emission inventories and chemical mechanisms', *Atmospheric Chemistry and Physics Discussions* pp. 1–37.
URL: *http://www.atmos-chem-phys-discuss.net/acp-2016-1083/*

Sheehan, P., Cheng, E., English, A. & Sun, F. (2014), 'Effects of air pollution control policies on PM2.5 pollution improvement in China from 2005 to 2017: a satellite based perspective', *Nature Climate Change* **4**, 306–309.

Skamarock, W. C. & Klemp, J. B. (2008), 'A time-split nonhydrostatic atmospheric model for weather research and forecasting applications', *Journal of Computational Physics* **227**, 3465–3485.

Skamarock, W. C., Klemp, J. B., Gill, D. O., Barker, D. M., Duda, M. G., Wang, W. & Powers, J. G. (2008), A Description of the Advanced Research WRF Version 3, Technical Report June.

State of Global Air (2018), Special report: State of global air 2018, Technical report, Health Effects Institute, Boston, MA.
URL: *https://www.stateofglobalair.org/sites/default/files/soga-2018-report.pdf*

Streets, D. G., Fu, J. S., Jang, C. J., Hao, J., He, K., Tang, X., Zhang, Y., Wang, Z., Li, Z., Zhang, Q., Wang, L., Wang, B. & Yu, C. (2008), 'Air quality during the 2008 Beijing Olympic Games', *Atmospheric Environment* **41**(2007), 480–492.

Strode, S. A., Ziemke, J. R., Oman, L. D., Lamsal, L. N., Olsen, M. A. & Liu, J. (2019), 'Global changes in the diurnal cycle of surface ozone', *Atmospheric Environment* **199**, 323 – 333.
URL: *http://www.sciencedirect.com/science/article/pii/S1352231018308008*

Sun, Y., Chen, C., Zhang, Y., Xu, W., Zhou, L., Cheng, X., Zheng, H., Ji, D., Li, J., Tang, X., Fu, P. & Wang, Z. (2016a), 'Rapid formation and evolution of an extreme haze episode in Northern China during winter 2015', *Sci Rep* **6**(January), 27151.
URL: *http://www.ncbi.nlm.nih.gov/pubmed/27243909*

Sun, Y., Wang, Z., Dong, H., Yang, T., Li, J., Pan, X., Chen, P. & Jayne, J. T. (2012), 'Characterization of summer organic and inorganic aerosols in Beijing, China with an Aerosol Chemical Speciation Monitor', *Atmospheric Environment* **51**, 250–259.
URL: *https://www.sciencedirect.com/science/article/pii/S1352231012000337*

Sun, Y., Wang, Z., Wild, O., Xu, W., Chen, C., Fu, P., Du, W., Zhou, L., Zhang, Q., Han, T., Wang, Q., Pan, X., Zheng, H., Li, J., Guo, X., Liu, J. & Worsnop, D. R. (2016b), '"APEC Blue": Secondary Aerosol Reductions from Emission Controls in Beijing', *Scientific Reports* **6**(November 2015), 20668.
URL: *http://www.nature.com/articles/srep20668*

Tang, G., Zhu, X., Hu, B., Xin, J., Wang, L., Münkel, C., Mao, G. & Wang, Y. (2015), 'Vertical variations of aerosols and the effects responded to the emission control: application of lidar ceilometer in Beijing during APEC, 2014', *Atmospheric Chemistry and Physics Discussions* **15**(9), 13173–13209.
URL: *http://www.atmos-chem-phys-discuss.net/15/13173/2015/*

Tao, J., Zhang, L., Cao, J. & Zhang, R. (2017), 'A review of current knowledge concerning PM 2.5 chemical composition , aerosol optical properties and their relationships across China', *Atmos. Chem. Phys* **17**, 9485–9518.

Tao, J., Zhang, L., Zhang, Z., Huang, R., Wu, Y., Zhang, R., Cao, J. & Zhang, Y. (2015), 'Control of pm2.5 in guangzhou during the 16th asian games period: Implication for hazy weather prevention', *Science of The Total Environment* **508**, 57 – 66.
URL: *http://www.sciencedirect.com/science/article/pii/S0048969714016684*

Tie, X., Zhang, Q., He, H., Cao, J., Han, S., Gao, Y., Li, X. & Jia, X. C. (2014), 'A budget analysis of the formation of haze in Beijing', *Atmospheric Environment* **100**, 25–36.
URL: *http://dx.doi.org/10.1016/j.atmosenv.2014.10.038*

Tsimpidi, A. P., Karydis, V. A. & Pandis, S. N. (2007), 'Response of inorganic fine particulate matter to emission changes of sulfur dioxide and ammonia: The eastern united states as a case study', *Journal of the Air & Waste Management Association* **57**(12), 1489–1498.
URL: *https://doi.org/10.3155/1047-3289.57.12.1489*

Urban Statistical Yearbook of China 2005, 2006 (n.d.).

Wang, G., Cheng, S., Wei, W., Yang, X., Wang, X., Jia, J., Lang, J. & Lv, Z. (2017a), 'Characteristics and emission-reduction measures evaluation of PM2.5during the two major events: APEC and Parade', *Science of the Total Environment* **595**, 81–92.
URL: *http://dx.doi.org/10.1016/j.scitotenv.2017.03.231*

Wang, H., Zhao, L., Xie, Y. & Hu, Q. (2016a), '"APEC blue"-The effects and implications of joint pollution prevention and control program', *Science of the Total Environment*

553, 429–438.
URL: *http://dx.doi.org/10.1016/j.scitotenv.2016.02.122*

Wang, L. T., Wei, Z., Yang, J., Zhang, Y., Zhang, F. F., Su, J., Meng, C. C. & Zhang, Q. (2014a), 'The 2013 severe haze over southern Hebei, China: model evaluation, source apportionment, and policy implications', *Atmospheric Chemistry and Physics* **14**(6), 3151–3173.
URL: *https://www.atmos-chem-phys.net/14/3151/2014/*

Wang, L., Wang, S., Zhang, L., Wang, Y., Zhang, Y., Nielsen, C., McElroy, M. B. & Hao, J. (2014b), 'Source apportionment of atmospheric mercury pollution in china using the geos-chem model', *Environmental Pollution* **190**, 166 – 175.
URL: *http://www.sciencedirect.com/science/article/pii/S026974911400102X*

Wang, Q., Huang, R. J., Cao, J., Tie, X., Shen, Z., Zhao, S., Han, Y., Li, G., Li, Z., Ni, H., Zhou, Y., Wang, M., Chen, Y. & Su, X. (2016b), 'Contribution of regional transport to the black carbon aerosol during winter haze period in Beijing', *Atmospheric Environment* **132**, 11–18.
URL: *http://dx.doi.org/10.1016/j.atmosenv.2016.02.031*

Wang, S., Gao, J., Zhang, Y., Zhang, J., Cha, F., Wang, T., Ren, C. & Wang, W. (2014c), 'Impact of emission control on regional air quality: An observational study of air pollutants before, during and after the beijing olympic games', *Journal of Environmental Sciences* **26**(1), 175 – 180.
URL: *http://www.sciencedirect.com/science/article/pii/S1001074213603952*

Wang, S., Zhao, M., Xing, J., Wu, Y., Zhou, Y., Lei, Y., He, K., Fu, L. & Hao, J. (2010a), 'Quantifying the air pollutants emission reduction during the 2008 olympic games in Beijing', *Environmental Science and Technology* **44**(7), 2490–2496.

Wang, X., Liang, X.-Z., Jiang, W., Tao, Z., Wang, J. X., Liu, H., Han, Z., Liu, S., Zhang, Y. & Grell, G. a. (2010b), 'WRF-Chem simulation of East Asian air quality: Sensitivity to temporal and vertical emissions distributions', *Atmospheric Environment* **44**(5), 660–669.
URL: *http://linkinghub.elsevier.com/retrieve/pii/S1352231009009558*

Wang, Y., Zhang, Y., Jay, J., Foy, B. D., Guo, B. & Zhang, Y. (2016c), 'Relative impact of emissions controls and meteorology on air pollution mitigation associated with the Asia-Pacific Economic Cooperation (APEC) conference in Beijing , China', *Science of*

the Total Environment **571**, 1467–1476.
URL: *http://dx.doi.org/10.1016/j.scitotenv.2016.06.215*

Wang, Z., Li, Y., Chen, T., Li, L., Liu, B., Zhang, D., Sun, F., Wei, Q., Jiang, L. & Pan, L. (2015), 'Changes in atmospheric composition during the 2014 APEC conference in Beijing', *Journal of Geophysical Research: Atmospheres* pp. 3510–3532.

Wang, Z., Pan, X., Uno, I., Li, J., Wang, Z., Chen, X., Fu, P., Yang, T., Kobayashi, H., Shimizu, A., Sugimoto, N. & Yamamoto, S. (2017b), 'Significant impacts of heterogeneous reactions on the chemical composition and mixing state of dust particles: A case study during dust events over northern China', *Atmospheric Environment* **159**, 83–91.
URL: *http://www.sciencedirect.com/science/article/pii/S1352231017302133*

WEI, Y., LI, J., WANG, Z.-F., CHEN, H.-S., WU, Q.-Z., LI, J.-J., WANG, Y.-L. & WANG, W. (2017), 'Trends of surface PM _{2.5} over Beijing–Tianjin–Hebei in 2013–2015 and their causes: emission controls vs. meteorological conditions', *Atmospheric and Oceanic Science Letters* **10**(4), 276–283.
URL: *https://www.tandfonline.com/doi/full/10.1080/16742834.2017.1315631*

Wen, W., Cheng, S., Chen, X., Wang, G. & Li, S. (2016), 'Impact of emission control on PM 2.5 and the chemical composition change in Beijing-Tianjin-Hebei during the APEC summit 2014', *Environmental Science and Pollution Research* **23**, 4509–4521.

Westervelt, D., Horowitz, L., Naik, V., Tai, A., Fiore, A. & Mauzerall, D. (2016), 'Quantifying PM2.5-meteorology sensitivities in a global climate model', *Atmospheric Environment* **142**, 43–56.
URL: *https://www.sciencedirect.com/science/article/pii/S135223101630560X*

WHO (2016), Ambient air pollution: A global assessment of exposure and burden of disease, Technical report, Department of Public Health, Environmental and Social Determinants of Health (PHE), World Health Organization, Avenue Appia 20, CH-1211, Geneva.
URL: *https://www.who.int/phe/publications/air-pollution-global-assessment/en/*

Wiedinmyer, C., Akagi, S. K., Yokelson, R. J., Emmons, L. K., Al-Saadi, J. a., Orlando, J. J. & Soja, a. J. (2011), 'The Fire INventory from NCAR (FINN): a high resolution global model to estimate the emissions from open burning', *Geoscientific Model Development* **4**(3), 625–641.
URL: *http://www.geosci-model-dev.net/4/625/2011/*

Wild, O., Prather, M. J., Akimoto, H., Sundet, J. K., Isaksen, I. S. A., Crawford, J. H., Davis, D. D., Avery, M. A., Kondo, Y., Sachse, G. W. & Sandholm, S. T. (2004), 'Chemical transport model ozone simulations for spring 2001 over the western pacific: Regional ozone production and its global impacts', *Journal of Geophysical Research: Atmospheres* **109**(D15).
URL: *https://agupubs.onlinelibrary.wiley.com/doi/abs/10.1029/2003JD004041*

Wild, O., Zhu, X. & Prather, M. J. (2000), 'Fast-J: Accurate simulation of in- and below-cloud photolysis in tropospheric chemical models', *Journal of Atmospheric Chemistry* **37**(3), 245–282.

WMO, U. . (2011), Integrated assessment of black carbon and tropospheric ozone, Technical report, UNON/publishing Services Section, Nairobi.
URL: *ISO 14001:2014*

Wong, D. C., Pleim, J., Mathur, R., Binkowski, F., Otte, T., Gilliam, R., Pouliot, G., Xiu, A., Young, J. O. & Kang, D. (2012), 'Wrf-cmaq two-way coupled system with aerosol feedback: software development and preliminary results', *Geoscientific Model Development* **5**(2), 299–312.
URL: *https://www.geosci-model-dev.net/5/299/2012/*

Xing, J., Zhang, F., Zhou, Y., Wang, S., Ding, D., Jang, C., Zhu, Y. & Hao, J. (2019), 'Least-cost control strategy optimization for air quality attainment of Beijing–Tianjin–Hebei region in China', *Journal of Environmental Management* **245**(March), 95–104.
URL: *https://doi.org/10.1016/j.jenvman.2019.05.022*

Xu, W., Liu, X., Liu, L., Dore, A. J., Tang, A., Lu, L., Wu, Q., Zhang, Y., Hao, T., Pan, Y., Chen, J. & Zhang, F. (2019), 'Impact of emission controls on air quality in Beijing during APEC 2014: Implications from water-soluble ions and carbonaceous aerosol in PM 2.5 and their precursors', *Atmospheric Environment* **210**(October 2018), 241–252.

Xu, W. Q., Sun, Y. L., Chen, C., Du, W., Han, T. T., Wang, Q. Q., Fu, P. Q., Wang, Z. F., Zhao, X. J., Zhou, L. B., Ji, D. S., Wang, P. C. & Worsnop, D. R. (2015), 'Aerosol composition, oxidation properties, and sources in Beijing: results from the 2014 Asia-Pacific Economic Cooperation summit study', *Atmospheric Chemistry and Physics* **15**(23), 13681–13698.
URL: *http://www.atmos-chem-phys.net/15/13681/2015/*

Xu, W., Song, W., Zhang, Y., Liu, X., Zhang, L., Zhao, Y., Liu, D., Tang, A., Yang, D., Wang, D., Wen, Z., Pan, Y., Fowler, D., Collett, J. L., Erisman, J. W., Goulding, K., Li, Y. & Zhang, F. (2017), 'Air quality improvement in a megacity: implications from 2015 Beijing Parade Blue pollution control actions', *Atmos. Chem. Phys* **17**, 31–46.
URL: *www.atmos-chem-phys.net/17/31/2017/*

Yahya, K., Glotfelty, T., Wang, K., Zhang, Y. & Nenes, A. (2017), 'Modeling regional air quality and climate : improving organic aerosol and aerosol activation processes in WRF/Chem version 3 .7 .1', *Geosci. Model Dev.* **10**, 2333–2363.

Yan, D., Lei, Y., Shi, Y., Zhu, Q., Li, L. & Zhang, Z. (2018), 'Evolution of the spatiotemporal pattern of PM2.5 concentrations in China – A case study from the Beijing-Tianjin-Hebei region', *Atmospheric Environment* **183**(July 2017), 225–233.

Yang, L., Wu, Y., Davis, J. M. & Hao, J. (2011), 'Estimating the effects of meteorology on PM2.5 reduction during the 2008 Summer Olympic Games in Beijing, China', *Frontiers of Environmental Science and Engineering in China* **5**(3), 331–341.

Yang, T., Wang, Z., Zhang, W., Gbaguidi, A., Sugimoto, N., Wang, X. & Matsui, I. (2017), 'Technical note : Boundary layer height determination from lidar for improving air pollution episode modeling: development of new algorithm and evaluation', *Atmos. Chem. Phys* **17**, 6215–6225.

Yu, S., Li, P., Wang, L., Wu, Y., Wang, S., Liu, K., Zhu, T., Zhang, Y., Hu, M., Zeng, L., Zhang, X., Cao, J., Alapaty, K., Wong, D. C., Pleim, J., Mathur, R., Rosenfeld, D. & Seinfeld, J. H. (2018), 'Mitigation of severe urban haze pollution by a precision air pollution control approach', *Scientific Reports* **8**(1), 1–11.
URL: *http://dx.doi.org/10.1038/s41598-018-26344-1*

Zaveri, R. a., Easter, R. C., Fast, J. D. & Peters, L. K. (2008), 'Model for Simulating Aerosol Interactions and Chemistry (MOSAIC)', *Journal of Geophysical Research* **113**(D13), D13204.
URL: *http://doi.wiley.com/10.1029/2007JD008782*

Zaveri, R. a. & Peters, L. K. (1999), 'A new lumped structure photochemical mechanism for large-scale applications', *Journal of Geophysical Research* **104**(D23), 30387.
URL: *http://doi.wiley.com/10.1029/1999JD900876*

Zhang, H., Cheng, S., Wang, X., Yao, S. & Zhu, F. (2018), 'Continuous monitoring, compositions analysis and the implication of regional transport for submicron and fine

aerosols in beijing, china', *Atmospheric Environment* **195**, 30 – 45.
URL: *http://www.sciencedirect.com/science/article/pii/S1352231018306435*

Zhang, H., Wang, S., Hao, J., Wang, X., Wang, S., Chai, F. & Li, M. (2015a), 'Air pollution and control action in Beijing', *Journal of Cleaner Production* **112**, 1519–1527.
URL: *http://linkinghub.elsevier.com/retrieve/pii/S0959652615004679*

Zhang, K., O'Donnell, D., Kazil, J., Stier, P., Kinne, S., Lohmann, U., Ferrachat, S., Croft, B., Quaas, J., Wan, H., Rast, S. & Feichter, J. (2012), 'The global aerosol-climate model echam-ham, version 2: sensitivity to improvements in process representations', *Atmospheric Chemistry and Physics* **12**(19), 8911–8949.
URL: *https://www.atmos-chem-phys.net/12/8911/2012/*

Zhang, L., Shao, J., Lu, X., Zhao, Y., Hu, Y., Henze, D. K., Liao, H., Gong, S. & Zhang, Q. (2016a), 'Sources and Processes Affecting Fine Particulate Matter Pollution over North China: An Adjoint Analysis of the Beijing APEC Period', *Environmental Science and Technology* **50**(16), 8731–8740.

Zhang, L., Wang, T., Lv, M. & Zhang, Q. (2015b), 'On the severe haze in Beijing during January 2013: Unraveling the effects of meteorological anomalies with WRF-Chem', *Atmospheric Environment* **104**(January 2013), 11–21.
URL: *http://www.sciencedirect.com/science/article/pii/S1352231015000023*

Zhang, R., Jing, J., Tao, J., Hsu, S.-C., Wang, G., Cao, J., Lee, C. S. L., Zhu, L., Chen, Z., Zhao, Y. & Shen, Z. (2013), 'Chemical characterization and source apportionment of PM2.5 in Beijing: seasonal perspective', *Atmospheric Chemistry and Physics* **13**(14), 7053–7074.
URL: *http://www.atmos-chem-phys.net/13/7053/2013/*

Zhang, R., Wang, G., Guo, S., Zamora, M. L., Ying, Q., Lin, Y., Wang, W., Hu, M. & Wang, Y. (2015c), 'Formation of Urban Fine Particulate Matter', *Chemical Reviews* **115**(10), 3803–3855.

Zhang, Y., Dubey, M. K., Olsen, S. C., Zheng, J. & Zhang, R. (2009), 'and Physics Comparisons of WRF / Chem simulations in Mexico City with ground-based RAMA measurements during the 2006-MILAGRO', pp. 3777–3798.

Zhang, Y., Zhang, X., Wang, L., Zhang, Q., Duan, F. & He, K. (2016b), 'Application of WRF/Chem over East Asia: Part I. Model evaluation and intercomparison with

MM5/CMAQ', *Atmospheric Environment* **124**, 285–300.
URL: *http://dx.doi.org/10.1016/j.atmosenv.2015.07.022*

Zhang, Z., Wang, W., Cheng, M., Liu, S., Xu, J., He, Y. & Meng, F. (2017), 'The contribution of residential coal combustion to PM2.5 pollution over China's Beijing-Tianjin-Hebei region in winter', *Atmospheric Environment* **159**, 147–161.
URL: *http://dx.doi.org/10.1016/j.atmosenv.2017.03.054*

Zhao, B., Wu, W., Wang, S., Xing, J., Chang, X., Liou, K.-n. & Jiang, J. H. (2017), 'A modeling study of the nonlinear response of fine particles to air pollutant emissions in the Beijing–Tianjin–Hebei region', *Atmos. Chem. Phys* **17**, 12031–12050.

Zhao, J., Du, W., Zhang, Y., Wang, Q., Chen, C., Xu, W., Han, T., Wang, Y., Fu, P., Wang, Z., Li, Z. & Sun, Y. (2016), 'Insights into aerosol chemistry during the 2015 China victory day parade: results from simultaneous measurements at ground level and 260 m in Beijing', *Atmospheric Chemistry and Physics Discussions* (September), 1–29.
URL: *http://www.atmos-chem-phys-discuss.net/acp-2016-695/*

Zheng, B., Tong, D., Li, M., Liu, F., Hong, C., Geng, G., Li, H., Li, X., Peng, L., Qi, J., Yan, L., Zhang, Y., Zhao, H., Zheng, Y., He, K. & Zhang, Q. (2018), 'Trends in China's anthropogenic emissions since 2010 as the consequence of clean air actions', *Atmospheric Chemistry and Physics Discussions* **2018**, 1–27.
URL: *https://www.atmos-chem-phys-discuss.net/acp-2018-374/*

Zhong, J., Zhang, X., Dong, Y., Wang, Y., Liu, C., Wang, J., Zhang, Y. & Che, H. (2018), 'Feedback effects of boundary-layer meteorological factors on cumulative explosive growth of PM2.5 during winter heavy pollution episodes in Beijing from 2013 to 2016', *Atmospheric Chemistry and Physics* **18**(1), 247–258.
URL: *https://www.atmos-chem-phys.net/18/247/2018/*

Zhong, M., Saikawa, E., Liu, Y., Naik, V., Horowitz, L. W., Takigawa, M., Zhao, Y., Lin, N. H. & Stone, E. A. (2016), 'Air quality modeling with WRF-Chem v3.5 in East Asia: Sensitivity to emissions and evaluation of simulated air quality', *Geoscientific Model Development* **9**(3), 1201–1218.

Zhou, Y., Cheng, S., Lang, J., Chen, D., Zhao, B., Liu, C., Xu, R. & Li, T. (2015), 'A comprehensive ammonia emission inventory with high-resolution and its evaluation in

the Beijing-Tianjin-Hebei (BTH) region, China', *Atmospheric Environment* **106**, 305–317.
URL: *http://dx.doi.org/10.1016/j.atmosenv.2015.01.069*

Zhou, Y., Wang, Q., Huang, R., Liu, S., Tie, X., Su, X., Niu, X., Zhao, Z., Ni, H., Wang, M., Zhang, Y. & Cao, J. (2017), 'Optical Properties of Aerosols and Implications for Radiative Effects in Beijing During the Asia-Pacific Economic Cooperation Summit 2014', *Journal of Geophysical Research: Atmospheres* **122**(18), 10,119–10,132.

Zhou, Y., Wu, Y., Yang, L., Fu, L., He, K., Wang, S., Hao, J., Chen, J. & Li, C. (2010), 'The impact of transportation control measures on emission reductions during the 2008 olympic games in beijing, china', *Atmospheric Environment* **44**(3), 285 – 293.
URL: *http://www.sciencedirect.com/science/article/pii/S1352231009009157*

Zíková, N., Wang, Y., Yang, F., Li, X., Tian, M. & Hopke, P. K. (2016), 'On the source contribution to Beijing PM2.5 concentrations', *Atmospheric Environment* **134**, 84–95.